New breakwater of Genoa

Application of a vine-copula model in probabilistic design

Master Thesis

Menno van Dam

Delft University of Technology

TU Delft

New breakwater of Genoa

Application of a vine-copula model in probabilistic design

by

Menno van Dam

Instructors:	A. Antonini, O. Morales Napoles, E. Ragno
Institution:	Delft University of Technology
Place:	Faculty of Civil Engineering, Delft
Project Duration:	July, 2021 - May, 2022

Cover Image: A storm hitting the lighthouse in Porthcawl. Image by Marcus Woodbridge.

TU Delft

Preface

With the advent of this thesis, my studies in Delft will come to an end. The last 6.5 years have been a tremendously important time for me. I've learned an incredible amount and I feel like I've also really grown as a person. I began my studies in Delft in September of 2015 with the Bachelor of Civil Engineering. Adapting to the hectic lifestyle of a student wasn't easy, and at times overwhelming. Yet looking back now I can only feel glad that I've faced this challenge and, with the realization of this thesis, will have overcome.

This work couldn't be completed without the support of my thesis committee. First of all, I'd like to thank Alessandro for introducing me to this topic and helping me with every step on the way. I was always positively surprised by your quick and elaborate responses whenever I had a question or wished to show you something. You were always available to have a chat on the current state of affairs and give me a few (sometimes a lot) pointers to show me the right direction. You allowed me plenty of freedom yet also gave critical feedback when something was not up to standards. This only made it more satisfying to see you content with my progress. Secondly, I'd like to thank Oswaldo for his enthusiasm and suggestions regarding vine-copulas and dependence modelling which gave my work more depth. This inspired me to improve and gave me the feeling that I was really contributing something to a bigger picture. Lastly, I'd like to thank Elisa for her wonderful support and detailed feedback on my work. She didn't shy away from explaining difficult topics to me and giving me advice on how to proceed and improve. The support, feedback and ideas of all of you have been really valuable to me.

Of course, I'd also like to thank my friends for supporting me throughout this process. I am particularly grateful for the help I received from my friends Pim, Pepijn and Nigel, without whom I am sure my work would've been of lesser quality. Whenever I got stuck at a particular subject, I could discuss the problem with them and together we'd be able to find a solution. Working alone on a project as large as this one is difficult, especially in the solitary times of the corona pandemic. It is easy to keep dwelling in the same thought-process and make mistakes. Sometimes, simply discussing a topic with another person may provide a different perspective or insight needed to find the solution. I still fondly remember the 'copula borrel' I had with Pepijn and Nigel, where we finally solved the mystery of the vine-copula. Throughout my whole time as a student, Pim has always been available to help me, and the master thesis was no exception. Pim was actually the one that suggested me to make contact with Alessandro about this thesis topic. We worked on our theses during the same time period, and were able to share plenty of ideas and discussions that I feel like have greatly benefited us both. I always really enjoyed working together with Pim and I cherish the happy expectation that we will continue to do so in the future.

Lastly, I'd like to thank my mom, dad and brother. My whole life they've taught me the value of education and gave me plenty of support and motivation to continue, especially during the times where I struggled. Without their encouragement, I am certain I wouldn't have gotten even half as far as I have today. I am also really grateful for the unconditional love of my two dogs, Amigo and Baila.

Now, I am ready to leave the student life behind me, and to face the challenges of the life as a hydraulic engineer.

Menno van Dam
Delft, April 2022

Summary

The authorities of the Port of Genoa have requested the construction of a new vertical breakwater for the Sampierdarena canal, as well as the subsequent demolition of part of the existing breakwater. The reason for this project is the need to expand the size of the canal, in order to allow larger vessels to safely use it. A choice is made for a vertical-type breakwater, i.e. a concrete caisson placed on top of a rubble mound foundation. The main goal of this thesis is to provide a preliminary probabilistic design of a cross-section of the new breakwater at the port of Genoa.

In an effort to reach these goals, two main research questions are posed:

1) How can the extreme wave climate characteristics for Genoa be modelled?

2) What does a preliminary cross-sectional probabilistic design of the new breakwater in Genoa look like?

First of all, data of the wave and wind climate was needed. Buoy data was only available for La Spezia and Capo Mele, neither of which were close enough to the point of interest. Supplementary data of the region was supplied by the wave climate model WavewatchIII. This data contained a non-negligible bias, particularly in the highest waves, that needed to be corrected first. The bias of WavewatchIII was corrected by applying quantile mapping, specifically the QUANT method. This involves fitting a spline function through the differences in exceedance distribution functions of the observed data and modelled data. This spline function was added to the model data to correct it. Overall, quantile mapping proved very effective in correcting the biases. It was found that QM gave better results for larger datasets. In addition, the records used for the model and observed data ought to be of comparable length. The data for Offshore Genoa was obtained by taking a weighted average of the correction splines based on the distance between Capo Mele, La Spezia and the point of interest. This was based on the assumption that WavewatchIII has a similar bias on a regional level.

Extreme values are of special interest for design, as these are the occurrences that put the greatest load on a structure. Extremes should be independent occurrences, which means they follow approximately a Poisson distribution. The extremes were obtained by applying the Peak over Threshold method to the data. This method requires a selection of a threshold and a timelag to define what counts as an extreme. The threshold is univariate by nature, and as such could only be applied to a single variable. The wave height was chosen as the dominant wave climate characteristic. The timelag was selected at 1 day, while the threshold was defined at the 99^{th} quantile, which measured 3.31 meters. This yielded a total of 243 extreme wave heights, roughly 6 per year on average. Wave and wind characteristics concomitant to the extreme wave heights were taken to obtain the multivariate extreme wave data.

Dependence modelling was performed to be able to realistically simulate the correlations between the extreme values. A vine-based approach was taken to achieve this goal. A vine-copula is a structure of bivariate copulas, allowing for larger flexibility in higher-dimensional systems. Five wave climate variables were of interest: the wave height, wave period, wave direction, wind speed and wind direction. Vine-copula modelling is done in MATLAB with a custom toolbox called MATVines[18]. All possible regular vines were obtained by permuting the six equivalence classes for 5 nodes. 13 different copula types and all 480 possible 5-node regular vines were fitted on the extreme wave data. The best vine-copula was selected based on the lowest AIC value. Validation of the vine-copula model was done through NRMSEs and the sum of the absolute differences in correlation coefficients. This provided favorable results, indicating the model was a good fit of the data.

Offshore waves were transformed to onshore waves by applying SWAN. Normally, SWAN requires manual input, which wasn't practical in this case. A MATLAB loop-function was made to automate this process. Goda's method[27] was used for determining the wave-induced loads on the vertical breakwater. 10 failure modes were considered in total: shoreward sliding, seaward sliding, shoreward

overturning, seaward overturning, bearing failure, toe stability, berm stability, bottom scour, wave overtopping and wave transmission. Various pieces of literature were consulted for defining these failure modes, namely *Random Seas and Design of Maritime Structures*[27], the *Coastal Engineering Manual*[23], the *Rock Manual*[16][17] and the *EurOtop Manual*[40]. This established the foundation for defining the limit-state functions to be used in a Monte-Carlo simulation.

The *PIANC*[19] was consulted for determining appropriate probabilities of failure and the design working life of the structure according to the Italian Guidelines[55]. Three limit-states were established: ULS, RLS and SLS, and pertinent failure modes were assigned to these. The design probabilities of failure over the 50-year design working lifetime of the structure for each limit-state were selected at 15%, 30% and 50% respectively. Limit-state functions were assembled for 10 failure modes. Several probability distributions were applied to the most important variables in the limit-state functions, in addition to the wave and wind variables which were generated by the vine-copula. Reliability factors were introduced to account for the uncertainty of Goda's method. A Monte-Carlo simulation was built in MATLAB using parallel computing to speed-up the process. This made it possible to iterate several breakwater designs in a relatively short amount of time. Using the Monte-Carlo simulation, several dozen designs were tested in an iterative matter in order to find an optimized design. It was found that the addition of a bullnose significantly reduced the overtopping quantities, allowing the crest height to be reduced by 2 meters. In order to reduce the weight of the structure, a prefabricated concrete crown was placed on the top of the caisson. The width of the caisson was increased by 3 meters on either side by applying a bottom slab. The proposed preliminary cross-sectional design as can be seen in figure 1 fulfilled all design criteria.

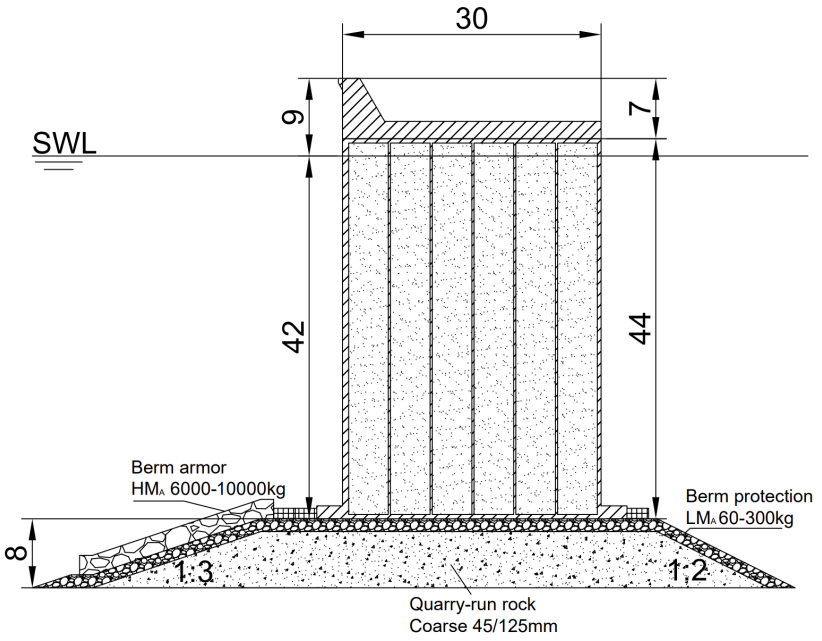

Figure 1: Overview of the proposed design.

The importance of dependence modelling was analyzed by comparing its performance to that of an independent model. The independent model was obtained by fitting univariate distributions on each of the variables based on the lowest AIC value. It was found that the independent data contained more scattering, as well as larger extreme values in general. The scattering meant that certain combinations of variables were present that weren't representative of the original data used for fitting. Using the independent data as input for the Monte-Carlo simulation returned significantly higher probabilities of failure for all failure modes. Ignoring correlations meant that a more expensive design is needed to get the same probabilities of failure. However, the resulting structure would actually be over-designed, as the independent data contains (combinations of) loads that will not occur in reality. Therefore, it can be concluded that correlations between wave and wind characteristics shouldn't be neglected in probabilistic design.

Contents

Preface i

Summary ii

Nomenclature vi

List of Figures ix

List of Tables xi

1 Introduction 1
- 1.1 Reason for the works . . . 1
- 1.2 Aim . . . 2
- 1.3 Methodology . . . 3
- 1.4 Structure . . . 3

2 Bias correction 5
- 2.1 Preliminary wave climate analysis . . . 5
- 2.2 QUANT method . . . 6

3 Extreme value analysis 9
- 3.1 Peak over threshold method . . . 9
- 3.2 Characteristics of extreme waves . . . 12

4 Multivariate modelling 14
- 4.1 Copulas & Vine-copulas . . . 14
- 4.2 Vine-copula modelling in MATVines . . . 17
- 4.3 Vine-copula model validation . . . 21

5 Loads & failure 23
- 5.1 Vertical breakwaters . . . 23
- 5.2 Onshore waves . . . 24
- 5.3 Wave-induced pressure . . . 26
- 5.4 Water level . . . 30
- 5.5 Overview of the failure modes . . . 31

6 Probabilistic design 39
- 6.1 Placement of the new breakwater . . . 39
- 6.2 Probabilistic design procedure . . . 40
- 6.3 Design proposal . . . 47

7 Effect of dependence modelling 51
- 7.1 Independent model . . . 51
- 7.2 Performance evaluation . . . 53

8 Discussion 55
- 8.1 WavewatchIII for wave climate data . . . 55
- 8.2 Multivariate modelling . . . 55
- 8.3 1-Dimensional bathymetry in SWAN . . . 56
- 8.4 Failure modes considered . . . 57
- 8.5 Reliability of the design equations . . . 57

9 Conclusion & Recommendations 58
- 9.1 Conclusion . . . 58
- 9.2 Recommendations . . . 60

References **63**

A Preliminary Wave Climate Analysis **64**
A.1 Data selection . . . 64
A.2 Wave characteristics . . . 66

B Quantile Mapping **70**

C Extreme value analysis of La Spezia and Capo Mele **73**
C.1 La Spezia . . . 73
C.2 Capo Mele . . . 74

D SWAN loop matlab code **77**

E Monte-Carlo simulation MATLAB code **80**
E.1 MC_Main . . . 80
E.2 MC_Hmax . . . 83
E.3 MC_Weight . . . 84
E.4 MC_GodaPressure . . . 84
E.5 MC_WaveTroughPressure . . . 86
E.6 MC_BearingCapacity . . . 87
E.7 MC_ToeProtection . . . 87
E.8 MC_BermProtection . . . 88
E.9 MC_BedProtection . . . 88
E.10 MC_Overtopping . . . 89
E.11 MC_Transmission . . . 90

F Preliminary Monte-Carlo runs **92**
F.1 Bullnose . . . 92
F.2 Bottom slab . . . 95
F.3 Rubble mound height . . . 97
F.4 Concrete crown . . . 99

Nomenclature

Abbreviations

Abbreviation	Definition
1D	1-Dimensional
2D	2-Dimensional
AIC	Akaike Information Criterion
BIC	Bayesian Information Criterion
BC	Bearing Capacity
C-vine	Canonical Vine
cr	critical
CDF	Cumulative Distribution Function
DI	Dispersion Index
D-vine	Drawable vine
EDF	Exceedance Distribution Function
EVA	Extreme Value Analysis
GEV	Generalized Extreme Value
GPD	Generalized Pareto Distribution
LB	Lower Bound
LL	Log-Likelihood
MC	Monte-Carlo
	Mass Center
MM	Multivariate Model
MRL	Mean Residual Life
MSc	Master of Science
MWL	Mean Water Level
NRMSE	Normalized Root-Mean-Square-Error
PDF	Probability Distribution Function
PoT	Peak over Threshold
QM	Quantile Mapping
RLS	Repairable Limit-State
RMSE	Root-Mean-Square-Error
R-vine	Regular vine
SC	Safety Class
SF	Safety Factor
SLS	Servicability Limit-State
STD	Standard Deviation
SW	South-West
SWAN	Simulating WAves Onshore
SWL	Still Water Level
th	threshold
UB	Upper Bound
ULS	Ultimate Limit-State
VC	Vine-Copula
wc	Wave Crest
wt	Wave Trough

Symbols

Symbol	Definition	Unit
b	Width of toe protection block	[m]
B	Caisson width	[m]
B_M	Berm width	[m]
c	Wave propagation speed	[m/s]
c_f	Bed friction coefficient	
C	Chézy coefficient	[$m^{½}$/s]
C_2	Drag coefficient for wind set-up/down	[-]
d	Wet caisson height	[m]
d_{n50}	Nominal grain diameter	[m]
Dir	Mean wave direction	[○]
Dir_0	Deepwater wave direction	[○]
g	Gravitational acceleration	[m/s^2]
h	Water depth	[m]
h'	Water depth at the berm of the structure	[m]
h_c	Crest height	[m]
h_s	Water depth at a distance of 5 H_s of the structure	[m]
h_{tide}	Tidal water level difference	[m]
H_0	Deepwater wave height	[m]
H_{max}	Maximum wave height	[m]
H_s	Significant wave height	[m]
H_t	Transmitted wave height	[m]
$H_{t,cr}$	Critical transmitted wave height	[m]
k	GPD shape parameter	[-]
k_r	Nikuradse bed roughness	[m]
K_1	Lunar diurnal tidal constituent	[m]
K_s	Shoaling coefficient	[-]
K_t	Transmission coefficient	[-]
l	Length of toe protection block	[m]
L	Wave length	[m]
	Structure design working lifetime	[yr]
L_0	Deepwater wave length	[m]
$M2$	Principal lunar semidiurnal tidal constituent	[m]
$M_{P_{wc}}$	Largest moment exerted by wave crest	[Nm]
$M_{P_{wt}}$	Largest moment exerted by wave trough	[Nm]
M_U	Largest moment exerted by uplift force	[Nm]
N_s	Number of storms per year	[-]
	Stability number for berm protection	[-]
p_{bc}	Bearing capacity	[Pa]
p_e	Largest bearing pressure	[Pa]
p_u	Uplift pressure	[Pa]
P_{ex}	Probability of exceedance	[-]
P_f	Probability of failure	[-]
$P_{f,yr}$	Probability of failure in 1 year	[-]
$P_{f,L}$	Probability of failure over lifetime	[-]
P_{wc}	Pressure force exerted by wave crest	[N]
P_{wt}	Pressure force exerted by wave trough	[N]
q	Overtopping discharge	[m^3/s]
q_{cr}	Critical overtopping discharge	[m^3/s]
R	Resistance	[-]
	Return period	[yr]
R_c	Crest height	[m]
s_{wt}	Arm of wave trough pressure force	[m]

Symbol	Definition	Unit
S	Sollicitation	[-]
	Wind set-up/down	[m]
S_2	Principal solar semidiurnal tidal constituent	[m]
S_r	Ratio of ρ_r to specific weight of seawater	[-]
t	Time	[s]
	Horizontal distance between MC and caisson toe	[m]
	Thickness of toe protection block	[m]
t_{cr}	Critical toe thickness	[m]
t_e	Arm of bearing pressure	[m]
T_p	Peak wave period	[s]
T_0	Deepwater wave period	[s]
u	Wind speed	[m/s]
u_{*b}	Shear velocity at bed	[m/s]
u_{*c}	Critical shear velocity	[m/s]
U	Uplift force	[N]
w_{spd}	Wind speed at 10m	[m/s]
w_{dir}	Wind direction	[○]
W	Weight of caisson	[kg]
	Weight of berm armor	[kg]
W_{cr}	Critical berm armor weight	[kg]
W_e	Submerged weight of caisson	[kg]
Z	Limit-state	[-]
α	GPD shape parameter	[-]
	Slope	[○]
α_s	Kimura coefficient for the effect of the slope	[-]
β	GPD scale parameter	[-]
	Wave angle of incidence	[○]
γ	GPD location parameter	[-]
γ_{Goda}	Goda safety factor	[-]
Δ	Relative density between grains and water	[-]
μ	Mean	[-]
	Friction coefficient between concrete and rubble	[-]
ν^*	Elevation to which wave pressure is exerted	[m]
ρ	Density	[kg/m^3]
ρ_c	Density of concrete	[kg/m^3]
ρ_r	Density of rubble rocks	[kg/m^3]
ρ_s	Density of seawater	[kg/m^3]
σ	Standard deviation	[-]
τ	Correction factor for local rapid flow around corners	[-]
Ψ_c	Shields stability parameter [-]	
$\mathcal{L}$	Log-likelihood	[-]

List of Figures

1 Overview of the proposed design. . . . iii

1.1 One of the several solutions proposed for the new breakwater, and the layout considered in this thesis. . . . 1
1.2 Reader's Guide. . . . 4

2.1 Locations of the three datapoints[29]. . . . 5
2.2 Visual explanation of the QUANT method. . . . 7
2.3 A direct comparison of the wave height at La Spezia and Capo Mele. . . . 7

3.1 The directions relevant for design. . . . 10
3.2 The Extremal Index for the considered thresholds over a varying timelag. . . . 11
3.3 The mean residual life plot and the GPD shape- and scale parameter stability plot. . . . 11
3.4 The dispersion index plot. . . . 12
3.5 The GPD curve fitted through the extreme values found using the PoT method. . . . 12
3.6 Plotmatrix of the extremes. . . . 13

4.1 An example of a graphical representation of all trees inside a vine of 5 nodes, specifically a D-vine. . . . 15
4.2 The 4 trees that compose the D-vine seen in figure 4.1. . . . 15
4.3 Example of a C-vine (Canonical vine) with 5 nodes. . . . 15
4.4 How the matrix representing a D-vine can be assembled. . . . 18
4.5 The five tree-equivalent regular vines for 5 nodes[45]. All 5-node regular vines are equivalent to one of these. . . . 19
4.6 Two D-vines created by permutation of the labelling of the trees. While these two vines are different permutations, they are functionally the same vine as they mirror each other perfectly, and thus will produce the same vine-copula model. . . . 20
4.7 Boxplot of the AIC values per tree-equivalent vine. . . . 20
4.8 The vine-copula with the lowest AIC, which was chosen as the best fitting model. It is vine V10, a C-vine corresponding to a permutation of matrix A_C. . . . 21
4.9 Plot-matrices comparing the extreme values to data generated with the vine-copula model. 21

5.1 Example cross-section of a vertical breakwater. Figure is based upon the Onahama Port Offshore Breakwater, Japan[27]. . . . 23
5.2 Above: 1-dimensional bottom profile used as input for SWAN. Below: Bathymetry of the Gulf of Genoa[1]. . . . 25
5.3 Plot-matrices of the ofshore and onshore wave characteristics. . . . 26
5.4 Boxplots comparing the wave characteristics between offshore and onshore. . . . 26
5.5 Illustration of the breakwater during different phases of wave attack. . . . 27
5.6 Simplified cross-section of a vertical breakwater. . . . 27
5.7 The wave pressure distribution against a vertical breakwater, as proposed by Goda[27]. 28
5.8 Illustration of the wave-induced pressure under the wave trough according to Goda's theory[27]. . . . 30
5.10 The fault tree of the new breakwater at the port of Genoa. . . . 32
5.11 Illustrations of all failure modes considered in design. . . . 32
5.12 Bearing pressure distribution and its two constituents: the weight and the uplifting pressure. 33
5.13 Toe protection for a vertical breakwater. . . . 34
5.14 Design of the toe protection blocks. Graph and table are from the Coastal Engineering Manual, VI-5-53[23]. . . . 34
5.15 Illustration of the berm protection. . . . 35

5.16 Orbital motions induced by propagating waves. 36
5.17 Simplified diagram of Shields parameter. Graph by Van Rijn[50]. 37
5.18 Illustration of the occurrence of wave overtopping. 37
5.19 Illustration of the occurrence of wave transmission. 38

6.1 Overview of the plans for the new breakwater and the cross-section of interest. 39
6.2 Left: Example distributions of an resistance R, load S and resulting limit-state Z. Right: Example of many realizations of R and S. 42
6.3 Goda's survey for a number of breakwaters[27]. 45
6.4 Overview of the proposed design. 47
6.5 Scatterplots of all 10 failure modes. 50
6.6 Stability of the probability of failure for the three limit-states. 50

7.1 Plotmatrix comparison between offshore independent data and vine-copula data. 52
7.2 Comparison between independent data and vine-copula data after applying SWAN. . . . 53
7.3 Boxplot comparing the onshore vine-copula model with the onshore independent model. 53
7.4 Scatterplots of all 10 failure modes. 54

A.1 Locations of the three datapoints[29]. 64
A.2 A time-series of the wave height data collected at points 1 and 2, La Spezia (left), Capo Mele (right). 65
A.3 Plotmatrix of La Spezia and Capo Mele. 67
A.4 The Western Mediterranean Sea[29]. 68
A.5 Wave rose signifying the directional frequency and height of the waves. Made with Wind Rose by Daniel Pereira[20]. 68
A.6 Wind rose signifying the directional frequency and speed of the wind. Made with Wind Rose by Daniel Pereira[20]. 68
A.7 Bathymetry of the Gulf of Genoa. 69

B.1 The Exceedance Distribution Functions (EDF) of the data. 70
B.2 A direct comparison of the hindcast data and the measured data of the buoys. 71
B.3 The hindcast data for Offshore Genoa. 72

C.1 Left: The Extremal Index for the considered thresholds over a varying time lag. Right: The Mean Residual Life plot. 73
C.2 Left: The GPD shape- and scale parameter stability plot. Right: The Dispersion Index plot. 74
C.3 Left: PoT method applied to the time-series. Right: The GPD curve fitted through the extreme values. 74
C.4 Left: The Extremal Index for the considered thresholds over a varying time lag. Right: The Mean Residual Life plot. 75
C.5 Left: The GPD shape- and scale parameter stability plot. Right: The Dispersion Index plot. 75
C.6 Left: PoT method applied to the time-series. Right: The GPD curve fitted through the extreme values. 76

F.1 Scatterplots of all 10 failure modes for the same breakwater design as proposed in figure 6.4, but without the bullnose. 92
F.2 Results for no bullnose and a freeboard of 10 meters. 93
F.3 Results for no bullnose and a freeboard of 11 meters. 94
F.4 Results for a bottom slab adding 2.5 meters width. 95
F.5 Results for a bottom slab adding 2 meters width. 96
F.6 Results for a rubble mound of 10 meters high. 97
F.7 Results for a rubble mound of 12 meters high. 98
F.8 Results for no concrete crown. 99

List of Tables

2.1 The RMSE values of WavewatchIII data compared to the respective buoy records, both before and after applying the correction. . . . 8

3.1 The seven different thresholds considered for the Peak over Threshold method. . . . 10
3.2 Fitting parameters for the Generalized Pareto Distribution function. . . . 13
3.3 The predicted wave heights per return period based on a GPD fit through the extreme wave heights. . . . 13

4.1 The amount of possible vines increases rapidly when more variables are introduced. . . . 16
4.2 The 13 copula families available in MATVines. . . . 17
4.3 The average NRMSE between the corrected WavewatchIII hindcast data and the data generated using a fitted vine-copula. . . . 22
4.4 Correlation matrix of the original dataset. . . . 22
4.5 Correlation matrix of the generated dataset. . . . 22

6.1 Italian Guidelines[55] for safety classes and design working life, as stated in the PIANC[19]. 40
6.2 Italian Guidelines[55] for maximum probability of admissible damage Pf in the period of working life, as stated in the PIANC[19]. . . . 41
6.3 Probabilities and return periods for various limit-states. . . . 42
6.4 The maximum wave height at which port facilities and operations remain safe[39]. . . . 44
6.5 General limits for overtopping for property behind the defence in the EuroTop Manual[40]. 44
6.6 Comparison between the Goda method and measured values, from Van der Meer *et al.* (1994)[41]. . . . 45
6.7 Distributions of every stochastic parameter for the Monte-Carlo simulation. . . . 46
6.8 Materials and weight per meter width of the design proposal. . . . 47
6.9 Results of 150.000 Monte-Carlo runs. . . . 49

7.1 Distributions and parameters of the independent model. The fitting was done using *fitmethis*[24]. . . . 51
7.2 The NRMSEs between the extreme data and data generated using the independent model. 52
7.3 Results of 150.000 Monte-Carlo runs. . . . 54

A.1 The wave data used in this project, for locations 1 (La Spezia), 2 (Capo Mele) and 3 (Offshore Genoa). . . . 65

C.1 The thresholds considered the La Spezia buoy record. . . . 73
C.2 The predicted wave heights per return period based on an extreme value GPD fit. . . . 74
C.3 The thresholds considered for the Capo Mele buoy record. . . . 75
C.4 The predicted wave heights per return period based on an extreme value GPD fit. . . . 76

F.1 Results of 150.000 Monte-Carlo runs for no bullnose. . . . 93
F.2 Results of 150.000 Monte-Carlo runs for no bullnose and +1 meter of freeboard. . . . 94
F.3 Results of 150.000 Monte-Carlo runs for no bullnose and +2 meters of freeboard. . . . 94
F.4 Results of 150.000 Monte-Carlo runs for a bottom slab adding 2.5 meters width. . . . 95
F.5 Results of 150.000 Monte-Carlo runs for a bottom slab adding 2 meters width. . . . 96
F.6 Results of 150.000 Monte-Carlo runs for a rubble mound of 10 meters high. . . . 97
F.7 Results of 150.000 Monte-Carlo runs for a rubble mound of 12 meters high. . . . 98
F.8 Results of 150.000 Monte-Carlo runs for no concrete crown. . . . 99

1 Introduction

1.1. Reason for the works

The authorities of the Port of Genoa have requested the construction of a new vertical breakwater for the Sampierdarena canal, as well as the subsequent demolition of part of the existing breakwater. The reason for this project is the need to expand the size of the canal, in order to allow larger vessels to safely use it. Currently ships of the old *Panamax* size category, with lengths up to 300 meters, can use the port. The expansion should allow container ships with lengths between 400 and 450 meters to utilize the port. To achieve this, a new breakwater will be constructed 200 meters further offshore than the current one. This would easily double the size of the current Sampierdarena canal, which means it will be more than enough to comply with current needs as well as possible future increases in ship size. Because of the large depth and the space required for vessels to navigate within the port, a choice is made for a vertical-type breakwater. This is a tall upright structure placed on a foundation to spread its weight on the seabed, i.e. a concrete caisson placed on top of a rubble mound foundation.

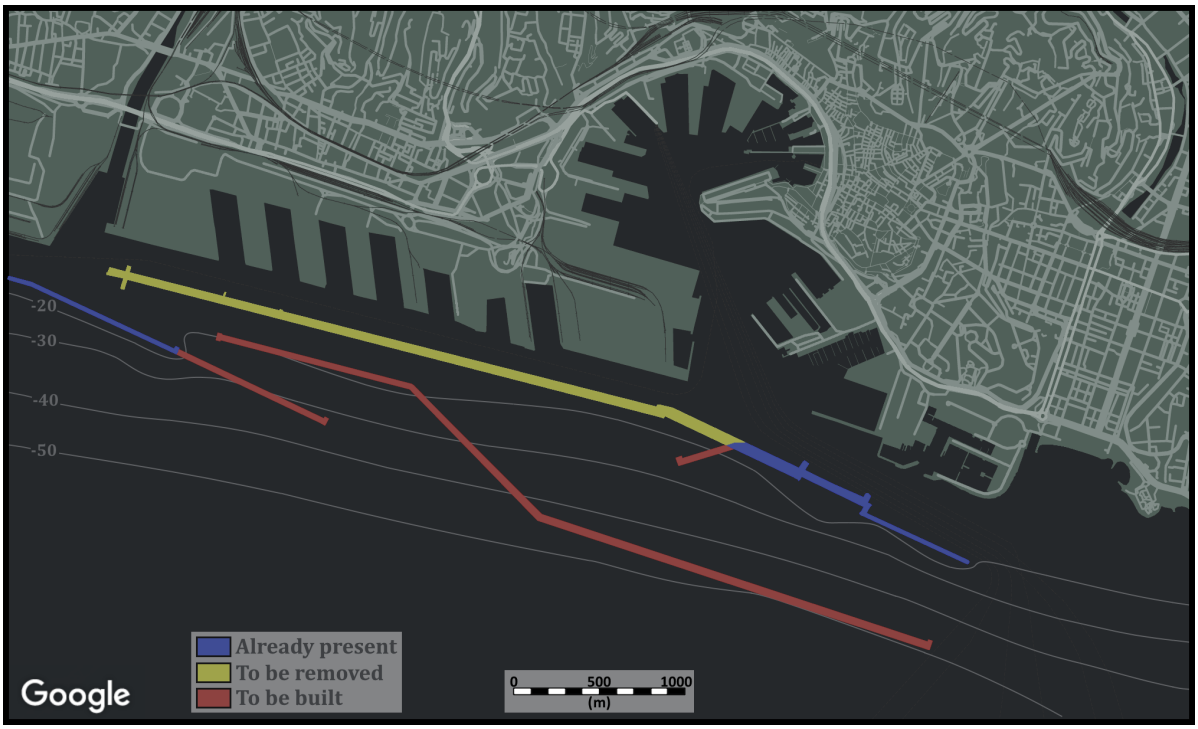

Figure 1.1: One of the several solutions proposed for the new breakwater, and the layout considered in this thesis.

Such a project brings with it a whole range of engineering challenges. A breakwater has only one

main function: to prevent excessive port agitation, while still allowing ships to enter it with as little inconvenience as possible. In order to fulfil its function, the structure should also be able to withstand the loads that it may experience during its lifetime, without being over-designed. The main source of loads acting on a breakwater comes from wave-attack. This is not a constant load as waves change continuously and irregularly. They could approach from various angles with various sizes. During a storm, the waves will be much larger than normal. No single wave can represent an entire wave climate. How does one design against such a fickle opponent? That is the core focus of this thesis.

Probabilistic design is not yet widespread in Italy. Probabilistic design involves the usage of probability distributions for design parameters, as opposed to a single extreme value. Deterministic design methods are often favored due to their simplicity. Though easy to use, deterministic design relies on a large number of assumptions and safety factors which could lead to an over- or underestimation of the design loads. As the world changes and becomes more complex, the question arises whether this way of design is still sufficient. The decision between these design methods can have enormous consequences. An overestimation of the loads could lead to a design that is more expensive than it should be. An underestimation of the loads could lead to failure of the structure. At the balance between these points is a theoretically 'optimal' design.

1.2. Aim

The main goal of this thesis is to provide a preliminary design of the new breakwater of the port of Genoa. This will be done fully probabilistically through a Monte-Carlo simulation, which will make it possible to calculate the probability of failure for a design. This makes it possible to iterate design choices to find an optimized design. The design will focus on a single cross-section of the breakwater. For this purpose, it is first necessary to define the relevant loads and failure modes.

This simulation will require a number of input values, notably wave climate characteristics. A way to generate representative values for the wave climate will be vital to obtain accurate results. Wave climates are complex systems with correlations between variables. Vine-copulas is a fairly new way of performing multivariate modelling. It takes into account the correlations between variables by forming a structure of bivariate copulas. The effect of accounting the inter-dependencies between variables will be analysed through a comparison with an independent model. The multivariate model will be fitted on extremes, as these are most important for design. Extreme wave characteristics will be obtained by applying the Peak over Threshold method on wave data. However, there is only limited measurement data available in the Gulf of Genoa. The solution will come in the form of a numerical model called WavewatchIII. The bias of this model will have to be corrected prior.

In an effort to reach these goals, two main research questions are posed:

1) How can the extreme wave climate characteristics for Genoa be modelled?

2) What does a preliminary cross-sectional probabilistic design of the new breakwater in Genoa look like?

These research questions split the project into two parts: question 1 focuses on the statistical part, while question 2 focuses on the engineering part. Since these are rather broad questions, they are further divided into smaller sub-questions that are easier to answer.

Research question 1 breaks down into the following four sub-questions:

- *1.1: How can the bias of the hindcast model be corrected?*
- *1.2: How can the extreme wave characteristics be defined?*
- *1.3: How can the dependence between extreme wave climate characteristics be modelled?*
- *1.4: What is the effect of accounting the dependencies between wave climate variables?*

Research question 2 breaks down into the following three sub-questions:

- *2.1: How can the relevant loads and failure modes be identified and defined?*
- *2.2: How can the failure modes be verified in a fully probabilistic approach?*
- *2.3: What design measures result in a cross-sectional design with an acceptable probability of failure?*

By the end of this thesis, elaborate answers will have been given to all of these questions.

1.3. Methodology

The starting point for this project is the data that is going to be used. As stated before, wave measurements inside the Gulf of Genoa are limited. As a solution, data from the wave hindcast model WavewatchIII, *WAVE-height, WATer depth and Current Hindcasting*, will be utilized instead. WavewatchIII is a third generation numerical model that simulates global ocean waves. It was developed at NOAA/NCEP, *National Oceanic and Atmospheric Administration / National Centers for Enviromental Prediction*, and has been verified and applied on numerous research projects. It is a vital source of data for a project such as this where little long-term data is readily available. However, Wavewatch is known to contain biases. It particularly tends to underestimate the highest waves in the wave spectrum[15], which are also the waves most important for design. This will be solved through quantile mapping, which is a bias correction method. Quantile mapping involves analyzing the differences in exceedance distribution functions between a model and observed data. The data for Offshore Genoa may be obtained by looking at WavewatchII's biases at nearby locations.

For the purpose of design, only extreme wave characteristics are of interest. The definition of what constitutes as 'extreme' isn't immediately clear. The extreme data will be obtained by applying the Peak over Threshold method on the data. This involves selecting an appropriate threshold for wave heights and timelag. Wave and wind characteristics concomitant to the extreme wave heights will provide a multivariate dataset of the extreme waves. The multivariability of the extreme wave and wind data can be of great importance to the design. Five variables are of interest: wave height, wave period, wave direction, wind speed and wind direction. To uphold the dependencies between these variables, a multivariate model of the extreme waves will be developed. This will be done through a vine-copula. In short, a vine-copula is a structure of bivariate copulae which allows for greater flexibility in the modelling of higher-dimensional systems. Vine-copula fitting will be done in MATLAB, using a package called *MATVines*[18]. The best vine-copula will be selected out of all regular vines for 5-dimensional datasets. Using the vine-copula, it will be possible to randomly generate extreme wave characteristics that are representative to the wave climate of Genoa.

The generated offshore wave characteristics will be transformed by SWAN to get the onshore wave characteristics. The resulting data will be used for determining the loads that the structure will face during its lifetime. The design procedure will mostly follow Goda's method for vertical breakwaters, as described in his book *Random Seas and Design of Maritime Structures*[27]. In total, 10 of the most important failure modes will be considered. These may be divided into structural failure - involving the structural integrity of the breakwater itself - and functional failure - which refers to the occurrence of excessive surface water agitation inside the port.

The probabilistic design itself will be carried out using a Monte Carlo simulation. This is an iterative process that makes use of limit state functions. A limit state function is simply an equation which represents the balance between a resistance and a load. Every iteration the simulation generates random values for every parameter used in these equations. A positive result means success, while a negative results means the structure failed. These can be described for every relevant failure mode. At the end it will output a probability of failure. An allowable probability of failure for the design will be defined beforehand. Using this simulation process, several designs can be tested to see how well they perform. Every change could alter the probability of failure. A greater amount of design options tested will give a better idea of which ones are viable and which ones are not. This should help in achieving an optimal design.

The importance of dependence modelling will be analyzed by comparing it to an independent model, which is a far simpler method of modelling a wave climate. Univariate distributions will be fitted on every variable, completely neglecting correlations between wave and wind characteristics. The independent data will be used as input for the Monte-Carlo simulation, and the results compared to those produced by dependent data.

1.4. Structure

This thesis seeks to combine two different fields, statistics and engineering, in one project. The research questions posed divide this thesis into several parts. Each chapter will focus on a single sub-question, with the exception of Chapter 6 which will focus on both question 2.2 and 2.3.

The following outline provides the structure of this thesis;

- Chapter 2: Bias correction

- Chapter 3: Extreme value analysis
- Chapter 4: Multivariate modelling
- Chapter 5: Loads & failures
- Chapter 6: Probabilistic design
- Chapter 7: Effect of independence modelling
- Chapter 8: Discussion
- Chapter 9: Conclusion & recommendations

Chapter 2 will analyze the bias of WavewatchIII by comparing it to buoy records. The bias will be corrected through quantile mapping. It seeks to answer sub-question 1.1.

Chapter 3 will provide a description of the extreme wave and wind characteristics by applying the Peak over Threshold method on the offshore wave data. It seeks to answer sub-question 1.2.

In Chapter 4 a vine-copula model will be developed in order to model the dependencies between wave and wind characteristics. It seeks to answer sub-question 1.3.

Chapter 5 will provide descriptions of the relevant loads and failure modes for design of a vertical breakwater. It seeks to answer sub-question 2.1.

Chapter 6 will describe the methodology used for probabilistic design as well as propose a design based on results from the Monte-Carlo simulation. It seeks to answer sub-question 2.2 and 2.3.

Chapter 7 will compare the vine-copula model to an independent model and analyze the differences. It seeks to answer sub-question 1.4.

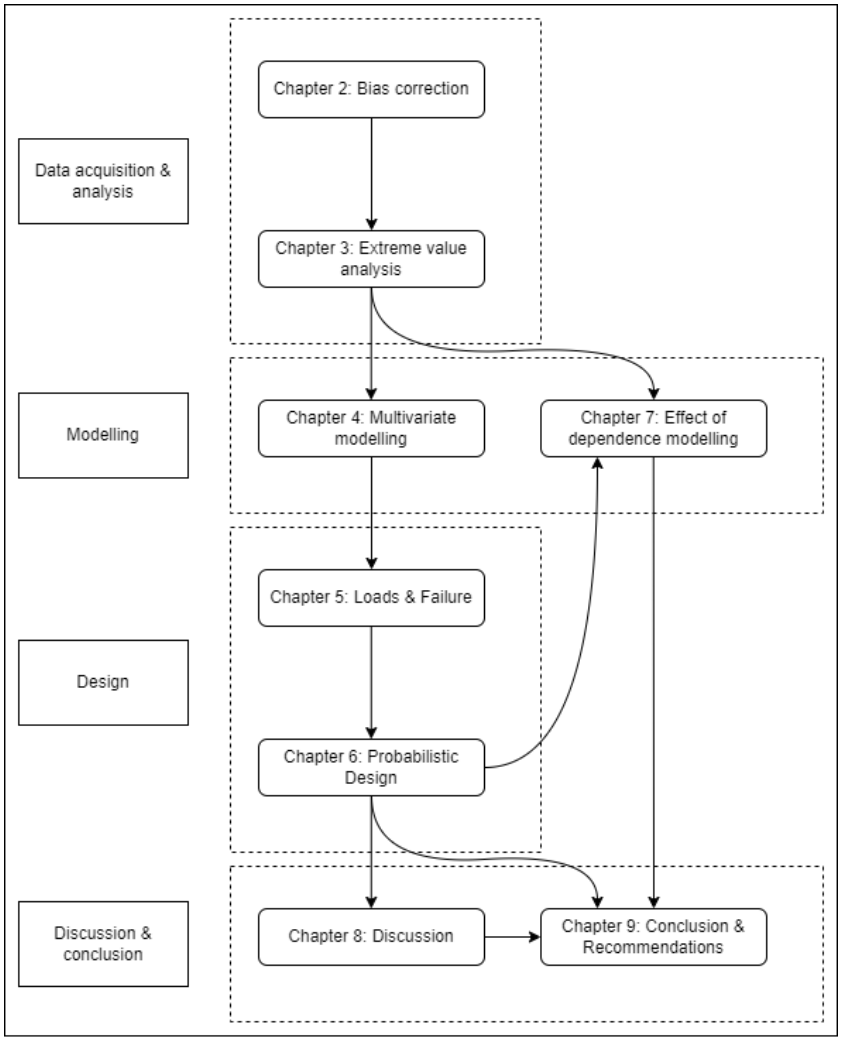

Figure 1.2: Reader's Guide.

2

Bias correction

This chapter seeks to answer research question 1.1: How can the bias of the hindcast model be corrected? It discusses the method used to correct the hindcast model WavewatchIII using recorded buoy data. Two buoys, one at La Spezia and the other at Capo Mele, provided several years worth of recorded waves.

2.1. Preliminary wave climate analysis

This section features a preliminary wave climate analysis of the buoy records placed at La Spezia and Capo Mele (see figure 2.1). This section is only a summary with some concluding remarks; the full analysis may be found in Appendix A. Three wave variables: the significant wave height, the peak wave period and the mean wave direction, and two wind variables: the wind speed and the wind direction, are of interest. It should be noted that measurement data was only available for waves, not wind. Wind data was supplied by WavewatchIII only. So, in this chapter the correction will only be applied to the waves.

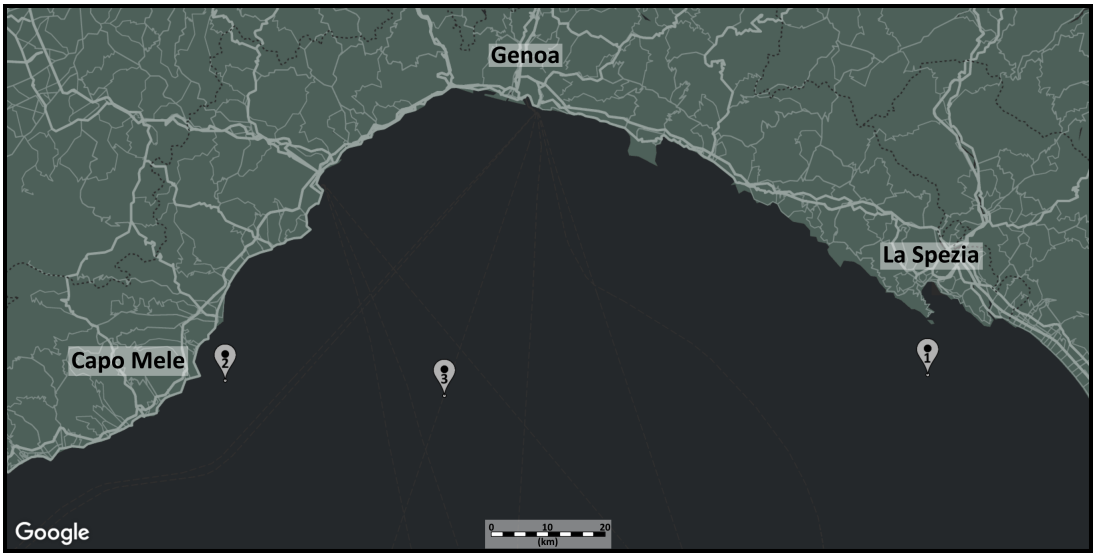

Figure 2.1: Locations of the three datapoints[29].

There were buoys at two locations within the Gulf of Genoa, one at La Spezia, and one at Capo Mele. A third point is located at the center of the Gulf of Genoa, which will henceforth be referred to as simply 'Offshore Genoa'. The latter point did not have any buoy data. All three points do have hindcast data, provided by WavewatchIII. See 2.1 for the exact location of all three points. Since the focus for now is primarily on describing the actual wave climate near Genoa, it was chosen to only discuss the buoy data. Plots of the data used can be found in Appendix A.

The findings of the wave climate analysis seen in Appendix A can be summarized as follows:

- The majority of waves are below 1.5 meters in height. Waves above 3 meters are rare, occurring only between 4 to 7 times a year in either dataset. Higher waves were more common in the La Spezia buoy records. The highest recorded wave in either dataset was measured at La Spezia, and was 6.8 meters tall.
- The distribution of the peak wave period seems to indicate that the region receives relatively few swell waves. The majority of waves were formed locally, or in neighbouring seas (particularly the Balearic and Tyrrhenian Seas). Waves generated further away cannot directly enter into the Gulf of Genoa due to blockage of the surrounding coastline or islands. Thus, it is likely that any waves inside the Gulf of Genoa are still being driven by the same wind forces that generated them in the first place.
- Most waves are coming from the South-West, from a region called the Balearic Sea. A smaller amount of waves came from the South-East (the direction of the Tyrrhenian Sea) and from within the Gulf of Genoa itself. There were also a few waves coming from landward directions, likely driven by land winds. The highest waves tended to come from the South-West as well.

Finally, a few things to keep in mind:

- Buoy measurements are, in general, subject to errors. The origin of these errors could be many, and it is impossible to explain exactly how without more information about these bouys. Especially the Capo Mele dataset was found to contain many unrealistic outliers.
- The Capo Mele buoy record is rather short at less than 7 years. It is sufficient to give an idea of the average wave climate, but it may give some wrong estimations for extreme events or correction factors.

2.2. QUANT method

The method used for correction will be quantile mapping (QM), specifically the QUANT method, which uses a non-parametric transformation function. QUANT estimates values of the exceedance distribution functions (EDFs) of observed and modeled time series for regularly spaced quantiles. Accordingly, QUANT uses interpolations to adjust a datum with unavailable quantile values[22]. It is a fairly straightforward yet robust way of correcting model data, and has been applied numerous times in various fields. QUANT was chosen because it is a non-parametric method; it doesn't require a selection of a theoretical distribution for the EDF or the correction.

2.2.1. How QUANT works

Figure 2.2 shows a visual explanation of the QUANT method. The QUANT method works as follows: First, the EDFs of the buoy record and the hindcast model are evaluated at predetermined probability intervals. The deviation between the model and buoy data is defined as the error. A positive error indicates that the hindcast model underestimates the corresponding buoy data, while a negative error indicates an overestimation. From figure 2.2 it can be seen that WavewatchIII tends to underestimate the wave heights, particularly the highest (those with the lowest probability of exceedance). Step two involes fitting a monotonic cubic spline through the error values, this will serve as the correction. In the third and last step, the spline is added back to the original model data, creating a new corrected dataset. As a result, the hindcast model will follow the EDF of the buoy record much more closely.

The quantiles or intervals along which the EDFs are evaluated determine the 'tightness' of the correction. Smaller intervals means a more precise correction. In *Osuch et all* [47] a regularly spaced interval of 0.01 was used. This works fine for the majority of the dataset, however it falls short for the extremes, as these have a probability of exceedance often far smaller than 0.01. This problem was especially apparent for the significant wave height and the peak wave period, which contained values with a very small probability of exceedance. This problem was solved by instead using a logarithmic space for evaluating the EDF error. A logarithmic space from 10^{-6} to 10^{0} was used, with 100 points spaced in total. This range was chosen because it includes even the variables with the smallest probability of exceedance, which is the inverse of the length of the dataset. The logarithmic space was only used for H_s and T_m. It was not necessary to use for the direction, as no direction had a particularly small probability (significantly smaller than 0.01). The resulting correction proved far more accurate for the extreme values, while maintaining a decent result for the lower values.

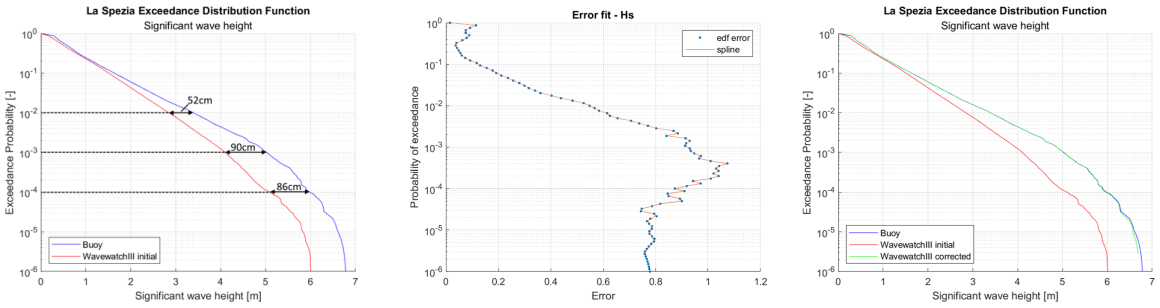

(a) Error evaluation. **(b)** Spline fitting. **(c)** Correcting the data.

Figure 2.2: Visual explanation of the QUANT method.

2.2.2. Results of applying QUANT

The QUANT method was applied to three variables: wave height, wave period and wave direction. This was done for the hindcast data at both Capo Mele and La Spezia. For every value in the hindcast model datasets, the value of the correction spline was interpolated. The result was added to the initial dataset, creating a new corrected dataset. Figure c of 2.2 shows the EDF plots of the buoy record (blue), the initial hindcast model (red) and the corrected hindcast model (green). As can be seen, the green line follows the blue line much more tightly, indicating a smaller error between the two buoy and hindcast model data. More figures can be found in Appendix B.

In figure 2.3 the wave heights for La Spezia are plotted against each other. A 45 degree reference line was added. The better the model, the more closely it follows the reference line. As can be seen in the graphs, the corrected hindcast data (green) follows the reference line much better than the initial hindcast data (red). There are still some deviations though, especially with the higher values of the wave height and wave period. This is because these values are relatively rare within the data (very low probability of exceedance). This is somewhat alleviated by the usage of a logarithmic space instead of a linear space for the correction. The QUANT method works better with a greater amount of data. This also explains why the correction method works better with the larger La Spezia dataset than with the smaller Capo Mele dataset.

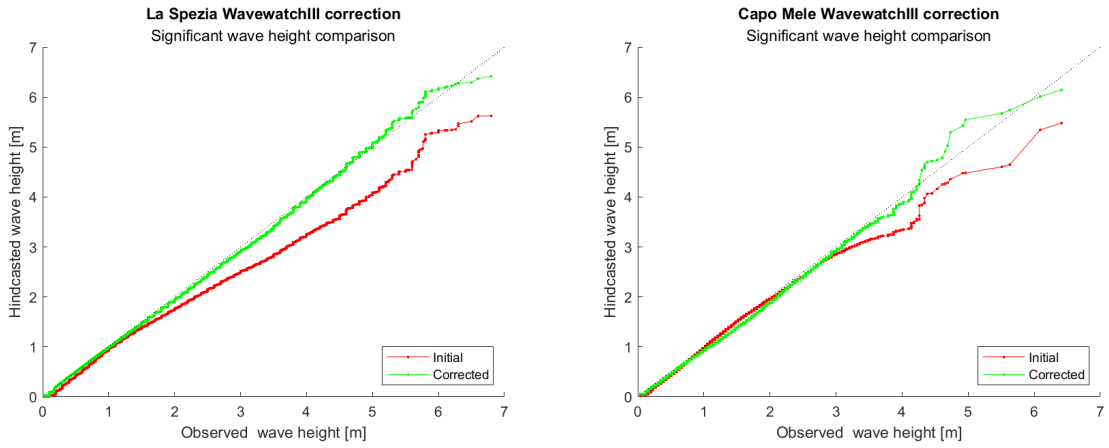

Figure 2.3: A direct comparison of the wave height at La Spezia and Capo Mele.

One simple way to quantify the difference between the datasets is with the Root-Mean-Square-Error. It is defined as follows:

$$RMSE = \sqrt{\overline{e^2}} = \sqrt{\overline{(X_{buoy} - X_{model})^2}} \tag{2.1}$$

Where X represents the parameter in question and e is the error between the hindcast model and the buoy record. The RMSE before and after correcting can be seen in table 2.1. The correction caused a decrease in the RMSE in every case. In many cases the decrease is about an order of magnitude.

Parameter	La Spezia initial	La Spezia corrected	Capo Mele initial	Capo Mele corrected
H_s	0.1488	0.0368	0.0664	0.0217
T_p	0.5647	0.0761	0.4483	0.0938
Dir	18.177	2.0713	34.0702	5.3073

Table 2.1: The RMSE values of WavewatchIII data compared to the respective buoy records, both before and after applying the correction.

2.2.3. QUANT inaccuracies

The QUANT method is not a perfect way of correcting model data. The method relies upon the EDF of both datasets. In many cases, it is possible that the range of values used for checking the EDF error is not by itself present in the known data. For example, when checking for a probability of exceedance of 0.10, it is possible only the wave heights corresponding to an exceedance probability of 0.12 and 0.08 are known. For these cases an interpolation between the known values is necessary. Interpolation works fine when used over a small interval, but may bring some inaccuracies when the data is sparse. For that reason the QUANT method works better for larger datasets, which also explains why the results were better for the La Spezia dataset than the Capo Mele dataset. It also explains why the QUANT method doesn't work as well for the values with a very low probability of exceedance. The lower the probability of exceedance, the less values in the dataset are available. This problem is quite visible in figure 2.3 for the higher values of the wave height.

The QUANT method also requires that the observed and the modelled datasets are of roughly the same length and measured with roughly the same frequency. This is because the probability of exceedance depends on the size of the total data. For example, if the hindcasted data is 100.000 values long and the observed data is 1.000.000 values long, then the highest values in the datasets have a probability of exceedance an order of magnitude apart (10^{-5} compared to 10^{-6}). As a result, it is impossible to find a correction of the hindcast model for any values with a probability of exceedance lower than 10^{-5}, as these values are simply not present in the data.

2.2.4. Corrected Offshore Genoa data

At Offshore Genoa (point 3, see figure 2.1), only hindcast data was known. Since it isn't possible to compare this data to a buoy record, it is necessary to look at the data of La Spezia and Capo Mele instead. Point 3 is located in-between these two buoys. Capo Mele and La Spezia are reasonably close together, so it is assumed the bias at a point between these two locations can be approximated by a weighted average of the bias at either point. This is based on the assumption that the hindcast model has a similar bias on a regional level. In both instances it was found that the hindcast model underestimates the highest waves, while overestimating the lowest waves. This finding was also confirmed by research on the accuracy of WavewatchIII in the Mediterranean Sea[15]. The corrected hindcast data while henceforth be the main dataset used for design.

To get a better estimation of the bias, more corrections will need to be obtained. Comparing WavewatchIII to buoys at other locations may prove informative, however it is possible buoy records far away from the point of interest are no longer relevant. Ideally, QUANT ought to be applied to a buoy record directly or very close-by to the point of interest.

3

Extreme value analysis

This chapters seeks to answer research question 1.2: How can the extreme wave characteristics be defined? Extreme values are of special interest for design, as these are the occurrences that put the greatest load on a structure. The extreme wave characteristics will be obtained via an Extreme Value Analysis (EVA) of the corrected Offshore Genoa data.

3.1. Peak over threshold method

Before the analysis can be carried out, it needs to be clear what exactly qualifies as an extreme. This is not so straightforward. The decision of what is extreme and what isn't can greatly influence the results. For selecting the extremes, the Peak over Threshold method is preferred, which involves selecting values that exceed a certain predefined threshold. The PoT method relies on two properties of extremes: they should occur randomly and independently in time according to an approximate Poisson process, and the exceedances themselves should have an approximate Generalized Pareto Distribution distribution and be approximately independent[58].

This method requires two parameters: the threshold and the timelag. Any values above the threshold value are counted as an extreme. The threshold shouldn't be too high, as this wouldn't yield enough data to make accurate predictions, but also not too low, as this would include non-extreme values. The timelag is needed to decluster the extremes. A single extreme event (a storm) can cause multiple extreme waves, which means that they tend to occur in groups. Declustering ensures that each extreme is an independent event. The timelag represents the period of time between independent events, and is usually the size of a couple of hours or days. If other extremes are found within the span of the timelag, only the highest of these will be used for analysis. The timelag should represent the average length of a storm in the area. Extremes that occur outside this time frame are unlikely to have been formed by the same storm, and could therefore be considered independent.

The threshold utilized by the PoT method is a univariate parameter. There is no general consensus to the definition of a multivariate threshold[46]. The following approach is taken to obtain a multivariate dataset of the extremes: The PoT method is applied to only the dominant variable in the dataset, and corresponding concomitant values (occurring at the same instance of time) are selected for the remaining variables. This approach respects the inter-dependencies between variables. Sampling the PoT method to each of the variables separately would, instead, likely yield combinations of extreme values that did not occur in the initial dataset. The significant wave height is selected as the dominant variable in this case, as it has the greatest influence on the wave-induced loads. Concomitant variables are the wave period, wave direction, wind speed and wind direction.

Seven different thresholds are considered in total. Each is defined by either a quantile or a combination of the mean and standard deviation of the dataset. Their definition and value for the buoy records are listed in table 3.1.

An extreme value analysis was performed for three datasets in total: La Spezia buoy records, Capo Mele buoy record, and the corrected WavewatchIII data for Offshore Genoa (Point 3). Only the latter is shown in this chapter. The corresponding graphs and a brief analysis for La Spezia and Capo Mele can be seen in Appendix C. The selected timelag for the corrected Offshore Genoa dataset was 24 hours

Name	Definition	Value [m]	Source
th1	μ + 1.4 σ	1.75	[57]
th2	μ + 1.9 σ	2.08	[57]
th3	$p_{97.5}$	2.65	[5]
th4	μ + 3 σ	2.81	[7]
th5	p_{99}	3.31	[5]
th6	$p_{99.5}$	3.84	[51]
th7	$p_{99.7}$	4.23	[38]

Table 3.1: The seven different thresholds considered for the Peak over Threshold method.

and the chosen threshold was the 99^{th} quantile th5, with a height of 3.31m. In the figures throughout this chapter, the selected threshold is indicated with a thick green line.

Only waves moving towards the breakwater are of interest for design. SWAN, the program used for wave propagation in section 5.2, cannot accurately process waves with an angle of incidence greater than 70 degrees[54]. The coastline is at roughly 105 degrees clockwise from North, which means the perpendicular is at 195 degrees. This puts limits between 125 and 265 degrees, see figure 3.1. All wave data not moving towards this direction was discarded and not used for the EVA.

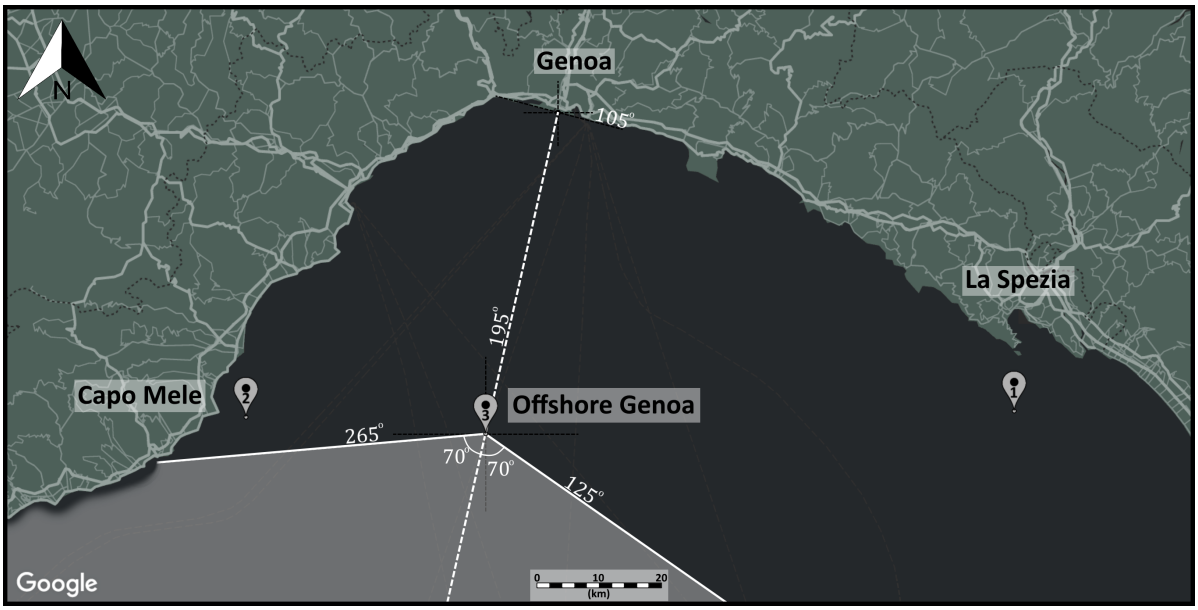

Figure 3.1: The directions relevant for design.

3.1.1. Timelag selection

As previously stated, randomly occurring independent events follow a Poisson distribution[58]. Whether this holds true for a specific dataset can be verified through a number of ways. Firstly with the extremal index. The extremal index is defined as the inverse of the mean cluster size or, equivalently, the mean time spent above the threshold[44]. The larger the timelag, the more independent the exceedances, resulting in an extremal index that tends towards 1. Generally, a higher threshold also means more independent exceedances, though this is not necessarily the case.

Exceedances were found by applying each of the seven thresholds for a varying timelag. The extremal index was then calculated for each set of exceedances. The result was the extremal index plot found in figure 3.2. A line was drawn at 0.7, as a minimum required extremal index. Extremal indexes below 0.7 do not follow the Poisson distribution[5], and can therefore not be seen as independent.

With an average depth on the open sea of about 2-3 kilometers, a wave would cross the Mediterranean in only a few hours. Storms in the Mediterranean typically last less than 72 hours[53], with the peak at about 24 hours[4]. The timelag should be as low as possible, because this would yield the

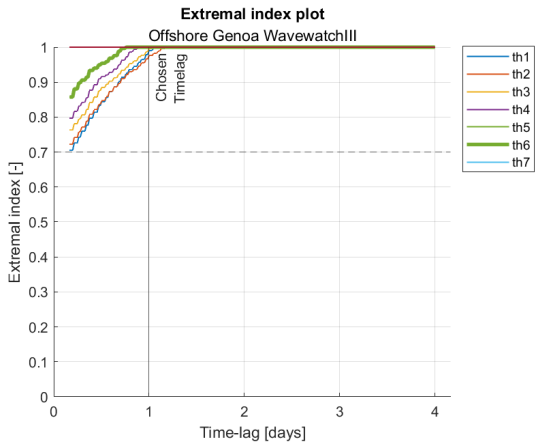

Figure 3.2: The Extremal Index for the considered thresholds over a varying timelag.

most extreme values. Based upon figure 3.2, the timelag was selected at 24 hours.

3.1.2. Threshold selection

When a variable X follows a GPD, then the mean exceedance over a threshold level u follows a linear function[58]:

$$E(X - u|X > u) = \frac{\sigma - ku}{1 + k} \tag{3.1}$$

Where k is the shape parameter of the Generalized Pareto Distribution. The mean residual life (MRL) plot shows the mean excess of the data over a certain threshold. If this plot shows a linear relation, then it indicates that the threshold level u is sufficient enough for the exceedances to follow a generalized Pareto distribution. The MRL plot is shown in figure 3.3. It is a graphical method for selecting a threshold for a given timelag.

The parameter stability plot is another graphical method based on the idea that, for a high enough threshold, the GPD parameters stabilize[10]. This means that there is no longer a significant change in the shape and scale parameters. A GPD was fitted for every threshold, resulting in figure **??**.

The dispersion index (DI) is the standard deviation of the excess divided by the mean of the excess[10]. For a Poisson distributed variable, the DI tends towards 1. So, a threshold giving a DI near 1 would suggest that the exceedances are independent. The DI is shown in figure 3.4.

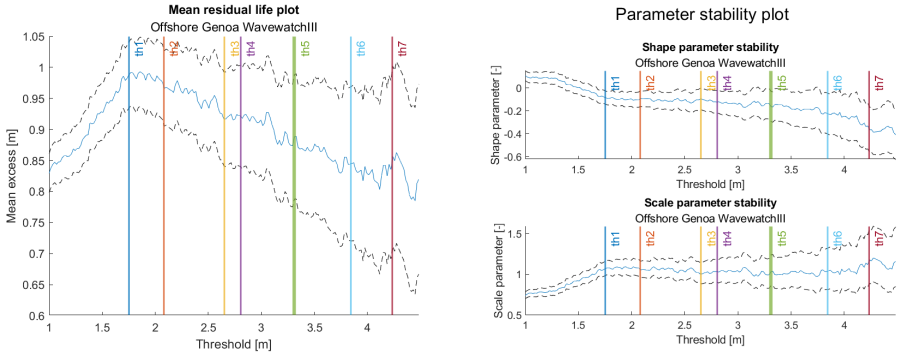

Figure 3.3: The mean residual life plot and the GPD shape- and scale parameter stability plot.

It should be noted that the assumptions for the Poisson distribution only hold if enough data remains. The higher the threshold, the less values are picked. At some point, there are simply not enough data points left to give a meaningful answer. It is therefore acceptable that some of the higher thresholds do not fulfill all the requirements in the plots above. These graphical methods serve only as an indication for what threshold would give a good result.

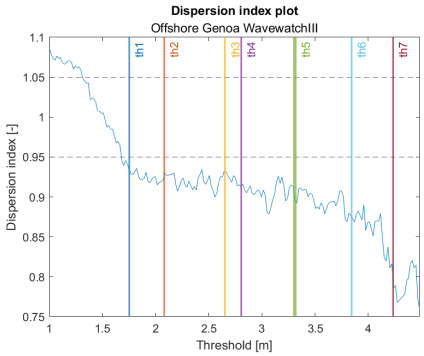

Figure 3.4: The dispersion index plot.

Threshold th5 was selected, which was defined as the 99th quantile of the wave heights. It fulfills the extremal index requirement for a fairly low timelag. The MRL plot gives a downwards linear trend. The shape and scale parameters remain stable. The DI is outside of the desired range, but is still close at roughly 0.90. The threshold th5, defined as the 99th quantile and with a height of 3.31m, was deemed a suitable threshold. This resulted in a total of 243 extreme events identified, or about 6 extreme events per year.

3.1.3. Generalized Pareto distribution fit

With the timelag and threshold selected, it is now possible to fit a GPD curve through the extremes, using the inverse GPD formula[11]:

$$H_{ss} = \gamma + \beta \left(\frac{P_{ex}^{-\alpha} - 1}{\alpha} \right) \tag{3.2}$$

Where P_{ex} is the exceedance probability per storm event, defined as:

$$P_{ex} = \frac{1}{RN_s} \tag{3.3}$$

With R as the return period in years, and N_s as the number of extreme events per year.

The results can be seen in figure 3.5, which gives a prediction of the wave height with a 1000 year return period. The fitting parameters can be found in table 3.2.

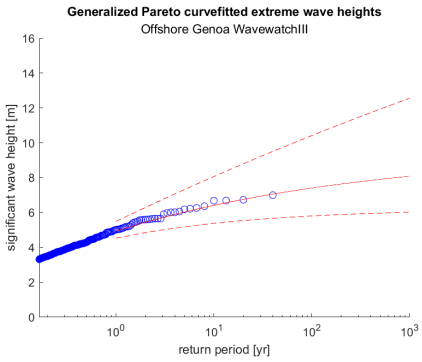

Figure 3.5: The GPD curve fitted through the extreme values found using the PoT method.

3.2. Characteristics of extreme waves

The PoT method is a univariate method for obtaining extreme values. However, in total, there are five variables of interest: wave height, wave period, wave direction, wind speed and wind direction. Wave height is the dominant variable for wave-induced loading. Wave period is related to the wave length and steepness, which is a wave characteristic employed in many design formulas. The wave direction

Curve	Shape parameter α	Scale parameter β	Location parameter γ
GPD fit	-0.1728	1.0512	th5 = 3.3123
GPD fit lower bound	-0.3036	0.8779	th5 = 3.3123
GPD fit upper bound	-0.0420	1.2587	th5 = 3.3123

Table 3.2: Fitting parameters for the Generalized Pareto Distribution function.

Return period [yr]	Predicted H_s L.B [m]	Predicted H_s [m]	Predicted H_s U.B [m]
10	5.35	6.35	7.95
25	5.57	6.82	8.97
50	5.69	7.12	9.69
100	5.79	7.38	10.38
250	5.89	7.68	11.25
500	5.95	7.87	11.88
1000	6.00	8.05	12.50

Table 3.3: The predicted wave heights per return period based on a GPD fit through the extreme wave heights.

determines the angle of incidence of the wave. Wind characteristics are of interest due to their influence on wave transformation from offshore to onshore. In section 5.2 the program SWAN will be used to simulate the transformation of the waves as they propagate towards the shoreline, requiring both wind speed and wind direction as input variables.

Multivariate data was obtained by taking the values of other variables which were concomitant to the extreme wave heights (occurring at the same instance of time). Figure **??** shows a plotmatrix of the extreme wave data. The extreme waves have a larger wave period on average. This is because wave period is related to wave length. The higher a wave, the greater its wave length, and thus the larger its wave period. A large number of the extreme waves came from the South-West. Previously it was found that this was the most frequent wave direction, coming from the Balearic Sea. Wave and wind direction were generally aligned, with few exceptions.

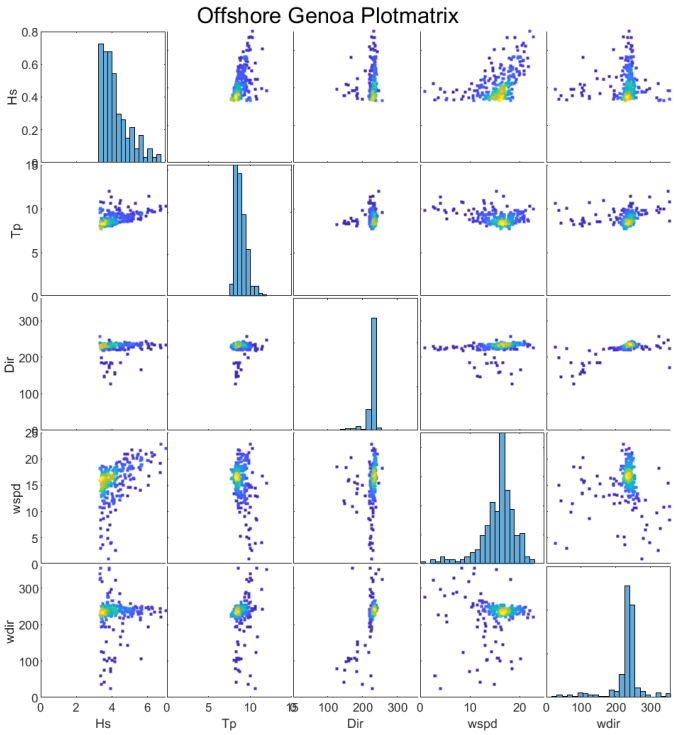

Figure 3.6: Plotmatrix of the extremes.

4

Multivariate modelling

This chapters seeks to answer research question 1.3: How can the dependence between extreme wave climate characteristics be modelled? The goal of the dependence modelling is to be able to realistically simulate the correlations between extreme values. A vine-based approach will be taken to achieve this goal.

4.1. Copulas & Vine-copulas

A copula is a function that describes the joint distribution between two or more variables. They can be used to model the dependence between variables. Most common copula models are only bivariate in nature, though there also exist copulas such as the Gaussian and Student's t-copula which can model higher dimensional systems. The problem with using copulas for higher dimensions is that they can become inflexible and they also do not allow for different dependency structures between pairs of variables[36].

A solution for the modelling of higher-dimensional systems is through usage of vine-copulas. Instead of using an N-dimensional copula directly, it decomposes the probability density into conditional probabilities, and further decomposes conditional probabilities into bivariate copulas[49]. As such, the vine-copula is in essence a structure of bivariate copulas, which together can form a system capable of simulating the dependency of any number of variables, including their conditional dependencies. This bypasses the limits of ordinary bivariate copulas. Because of the added flexibility of vine-copulas, these preferred for modelling higher-dimensional systems.

Simply put, a vine-copula model consists of three elements[36]:

$$Model = Vine + Copula\ families + Copula\ parameters \tag{4.1}$$

4.1.1. Vines

A vine is a nested set of trees that represents the probability distributions of higher-dimensional structures[37]. It defines how the joint distributions and conditional distributions are to be modelled[8]. Every vine-copula consists of one or multiple trees, depending on the amount of nodes it has. Each node represents a variable, while the edges connecting them represent the joint- or conditional-distributions between the variables. A regular vine on n elements is one in which two edges in tree j are joined by an edge in tree j + 1 only if these edges share a common node[37]. Regular vines are most interesting in uncertainty analysis[45], so henceforth all vines mentioned in this report will be of the regular kind. Figures 4.1 shows a graphical visualization of a vine with 5-nodes, specifically a D-vine (Drawable vine). The trees of the vine are separated in figure 4.2 to make the visualization more clear. The trees are denoted as T_1 to T_4. Tree T_1 contains the joint-dependencies of the nodes in the vine, while each subsequent tree contains conditional-dependencies of the nodes. Each tree contains one node less than the one before it.

The vine shown in figures 4.1 and 4.2 is an example of a D-vine, which is the most straightforward way of constructing a vine. In a D-vine, all nodes are set in a straight line with no side-branches. The degree of a node is defined as the amount of edges connected to it. In the D-vine for example: the two

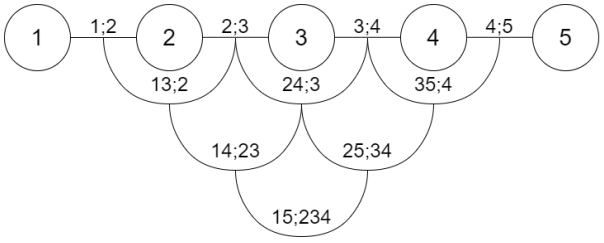

Figure 4.1: An example of a graphical representation of all trees inside a vine of 5 nodes, specifically a D-vine.

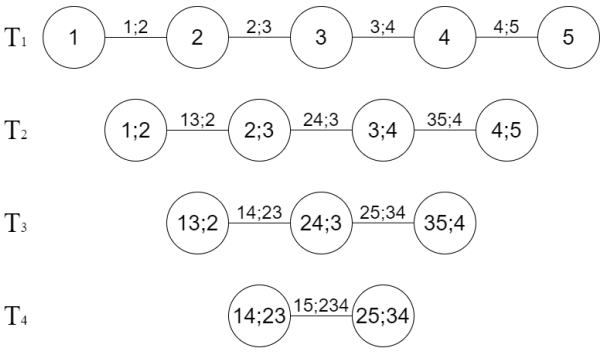

Figure 4.2: The 4 trees that compose the D-vine seen in figure 4.1.

ends have a degree of 1, while the other nodes have a degree of 2. For systems with up to 3 variables, D-vines are the only possible shape of a vine. The shape of a vine refers to the way the nodes are connected, regardless of their order. This is also known as an unlabeled tree[45], as opposed to a labeled tree where the order of the nodes is important. So, the tree 1-2-3-4-5 belongs to the same *unlabeled* tree as the tree 3-5-2-1-4, yet they are different *labeled* trees. The way in which the nodes may be ordered in an unlabeled tree may also be referred to as labelling[45]. Vines themselves may be classified according to the unlabeled trees used at each level in the vine: if two vines contain the same unlabeled trees, then these are called tree-equivalent[45]. Another way to classify them is through equivalence classes. Vines in the same equivalence classes can be matched after a permutation of indices[37].

Another common example of a vine is the C-vine, which becomes possible for systems of 4 variables or more. In a C-vine, all nodes are connected to one central node, as shown in 4.3. The central node has a degree of n-1, where n is the amount of nodes in the vine. Every other node in a C-vine has a degree of only 1, as these only share an edge with the central node.

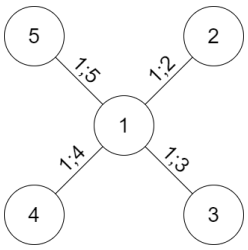

Figure 4.3: Example of a C-vine (Canonical vine) with 5 nodes.

For multivariate modelling, it may be desirable to fit all regular vines on the data to see which one performs best. The amount of unique regular vines follows the following formula[49][37]:

$$C = n(n-1)(n-2)!2^{(n-2)(n-3)/2}/2 \tag{4.2}$$

Where n is the number of nodes and C is the amount of unique vines possible. This amount increases incredibly fast, see table 4.1.

Amount of variables	Amount of unique regular vines
3	3
4	24
5	480
6	23.040
7	2.580.480
8	660.602.880
9	380.507.258.880
10	487.049.291.366.400

Table 4.1: The amount of possible vines increases rapidly when more variables are introduced.

Vine-copulas are a relatively new method for modelling dependency, as only recently computers have become fast enough to be capable of simulating them. However, calculation times may still increase to unreasonable amounts for systems with many variables, even if a high-performance computer is used. It isn't always necessary to fit every possible vine on a dataset. In practice, often only a handful vines are tested based on intrinsic beliefs on the data[49].

4.1.2. Goodness-of-fit indicators

Goodness-of-fit indicators are a measure of determining how well a model fit performs. The Bayesian Information Criterion (BIC) and the Akaike Information Criterion (AIC) are relative goodness-of-fit indicators based on the log-likelihood value. One of the problems with modelling in general is overfitting. Overfitting is when a large amount of parameters are added to the model in order to decrease the difference between the modelled and observed values. The problem with overfitting is that the model becomes very dependent on the data used for training. The essence of overfitting is to have unknowingly extracted some of the residual variation (i.e., the noise) as if that variation represented underlying model structure[13]. It is unlikely to predict unseen values very well and may even give gross over- or underestimations, resulting in a higher error. The AIC and BIC attempt to account for this by introducing a penalty for the number of parameters in the model. The difference between the two criteria is the way the penalty is defined, see the equations below[33][3]:

$$BIC = -2 \ln \hat{\mathcal{L}} + \ln N_{obs} N_{par} \tag{4.3}$$

$$AIC = -2 \ln \hat{\mathcal{L}} + 2 N_{par} \tag{4.4}$$

Where N_{par} is the amount of parameters in the model, and N_{obs} is the amount of observed datapoints. $\hat{\mathcal{L}}$ is the maximum value of the log-likelihood function $\mathcal{L}$ of the model, which is defined as the logarithm of the likelihood function. The likelihood function gives the probability that a set of values could be generated from a model. Generally, the higher this probability, the better fit a model is to the observations. The likelihood function is defined as:

$$\mathcal{L}(\theta \mid x) = p_\theta(x) = P_\theta(X = x), \tag{4.5}$$

There exists a lot of discussion over whether the AIC or the BIC is better. The answer isn't so straightforward, as each are best at different things. Previous research indicates that BIC is better at selecting the true model if it is in a list of candidate models[32]. Opponents of BIC claim that the difference is negligible, because the "true model" is often not included in the list of candidate models, as one can argue that the "true model" doesn't even exist in the first place[2]. Vrieze (2012) showed in a comparison between the two criteria that, for a finite amount of models, there is a non-negligible risk that BIC selects a worse model than AIC. AIC, in practice, selects the *best approximating model*. Since a good approximation is often the best thing possible, the resulting choice from AIC is appropriate [32]. Other research showed that, under the assumption that the "true model" is not in the candidate set, AIC converges faster to an optimum than BIC, and AIC often selected a model with a lower MSE than BIC [62]. Since it is unlikely the 'true' model is within set of models tested, AIC is preferred for finding the best approximating model.

The lowest AIC indicates the best fitting model out of all models considered, however this does not necessarily mean that the model is a good fit in general. The AIC (and also BIC) provide only a *relative* measure of the goodness-of-fit, compared to all other models considered. A more absolute indication for the goodness-of-fit is the RMSE or the sum of the differences in correlation parameters.

4.2. Vine-copula modelling in MATVines

Fitting of the vine-copula was done in MATLAB, through a custom toolbox called MATVines [18]. In total, five variables are of interest for modelling; wave height, wave period, wave direction, wind speed and wind direction. Dependence modelling was only performed on the extreme wave and wind characteristics obtained in Chapter 3.

Vine-copula fitting with MATVines is done through the *ssp()* function. This function requires pseudo-observations of the input data to work. Because of that, the extreme wave data had to be transformed to the standard uniform margins between 0 and 1, also known as the copula scale. This was done through the function *ksdensity(x,x,'function','cdf')*, which is a kernel estimator of the empirical cumulative distribution function. Values generated by a vine-copula in *MATVines* are also on the copula scale. These values were transformed back to the original scale using *ksdensity(x,x,'function','icdf')*.

The *ssp()*-function automatically determines the best copula family and copula parameters for a given vine based on a specified criterion. AIC was the preferred criterion due to the reasons stated in section 4.1. MATVines is capable of fitting 13 different copula families:

Gaussian	Frank	Survival Clayton
Student's t	Ali-Mikhail-Haq	Survival Gumbel
Clayton	Plackett	Survival Joe
Gumbel	Joe	
Farlie-Gumbel-Morgenstern	Tawn	

Table 4.2: The 13 copula families available in MATVines.

The remaining element, the vine itself, needs to be defined prior to fitting. The amount of possible vines for five variables is 480[45] (see also table 4.1). In order to find the best model, it is necessary to fit every regular vine. A vine may be represented with an n-by-n upper-triangular matrix[37][45], which is the input format that MATVines requires[18]. For example, the D-vine found in figures 4.1 and 4.2 may be written down as:

$$\mathbf{A} = \begin{pmatrix} 1 & 1 & 2 & 3 & 4 \\ & 2 & 1 & 2 & 3 \\ & & 3 & 1 & 2 \\ & & & 4 & 1 \\ & & & & 5 \end{pmatrix} \tag{4.6}$$

The way this matrix can be assembled can be seen in 4.4. Start with an n-by-n matrix with the values 1 to n on its diagonal, where n is the number of nodes. Each tree inside the vine is represented by a row inside the matrix. The colors indicate how the values ought to be placed inside the matrix.

Assembling 480 different matrices is arduous and time-consuming, but also not necessary. In fact, only a single matrix per equivalence class needs to be assembled, as every 5-node regular vine is a permutation of one of these[37]. For five nodes, there exist only six equivalence classes[37], which each contain the following 10 copulas:

$$\begin{aligned}
C &: C_{12}, C_{13}, C_{14}, C_{15}, C_{23|1}, C_{24|1}, C_{25|1}, C_{34|12}, C_{35|12}, C_{45|123} \\
B0 &: C_{12}, C_{13}, C_{14}, C_{15}, C_{23|1}, C_{24|1}, C_{35|1}, C_{34|12}, C_{25|13}, C_{45|123} \\
B1 &: C_{12}, C_{13}, C_{14}, C_{25}, C_{23|1}, C_{24|1}, C_{15|2}, C_{34|12}, C_{35|12}, C_{45|123} \\
B2 &: C_{12}, C_{15}, C_{14}, C_{23}, C_{25|1}, C_{24|1}, C_{13|2}, C_{34|12}, C_{35|12}, C_{45|123} \\
B3 &: C_{12}, C_{13}, C_{14}, C_{25}, C_{23|1}, C_{34|1}, C_{15|2}, C_{24|13}, C_{35|12}, C_{45|123} \\
D &: C_{15}, C_{12}, C_{23}, C_{34}, C_{25|1}, C_{13|2}, C_{24|3}, C_{35|12}, C_{14|23}, C_{45|123}
\end{aligned}$$

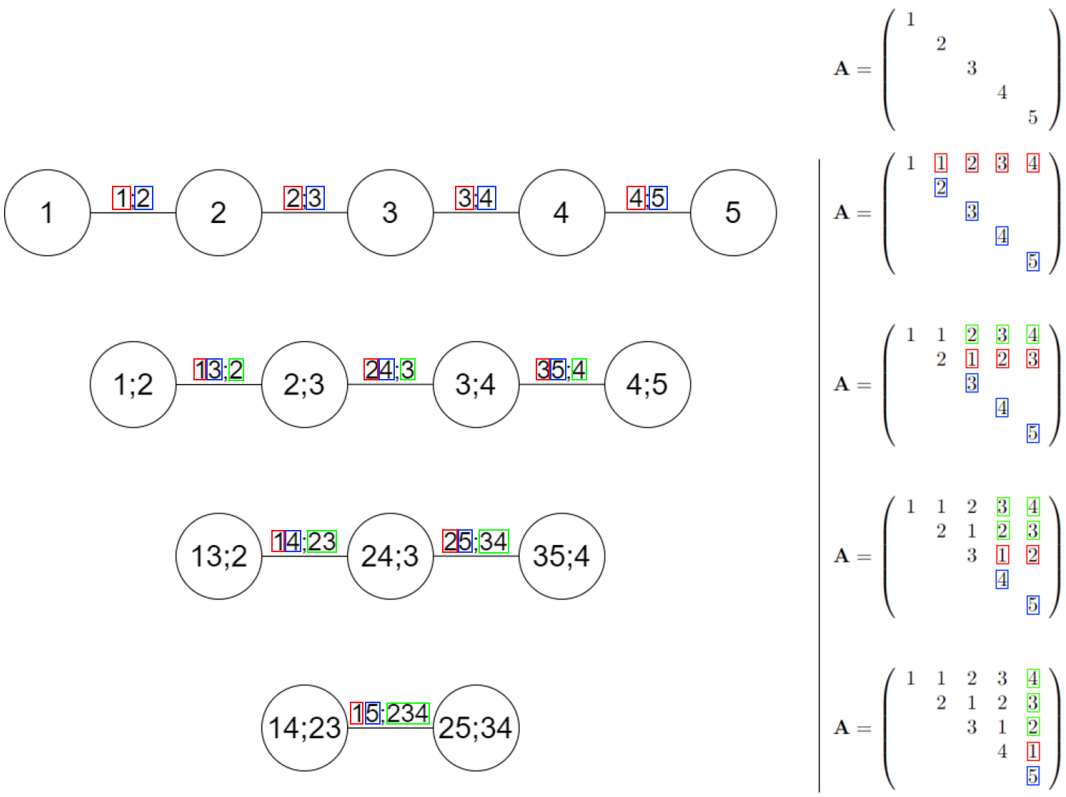

Figure 4.4: How the matrix representing a D-vine can be assembled.

MATVines already contains a function called *cdvinearray()* for creating the matrices of the C- and D-vine. The other four matrices had to be assembled by hand, using the method visualized in figure 4.4. The following six matrices were assembled:

$$\mathbf{A_C} = \begin{pmatrix} 1 & 1 & 1 & 1 & 1 \\ & 2 & 2 & 2 & 2 \\ & & 3 & 3 & 3 \\ & & & 4 & 4 \\ & & & & 5 \end{pmatrix}, \mathbf{A_{B0}} = \begin{pmatrix} 1 & 1 & 1 & 1 & 1 \\ & 2 & 2 & 2 & 3 \\ & & 3 & 3 & 2 \\ & & & 4 & 4 \\ & & & & 5 \end{pmatrix}, \mathbf{A_{B1}} = \begin{pmatrix} 1 & 1 & 1 & 1 & 2 \\ & 2 & 2 & 2 & 1 \\ & & 3 & 3 & 3 \\ & & & 4 & 4 \\ & & & & 5 \end{pmatrix} \tag{4.7}$$

$$\mathbf{A_{B2}} = \begin{pmatrix} 1 & 1 & 2 & 1 & 1 \\ & 2 & 1 & 2 & 2 \\ & & 3 & 3 & 3 \\ & & & 4 & 4 \\ & & & & 5 \end{pmatrix}, \mathbf{A_{B3}} = \begin{pmatrix} 1 & 1 & 1 & 1 & 2 \\ & 2 & 2 & 3 & 1 \\ & & 3 & 2 & 3 \\ & & & 4 & 4 \\ & & & & 5 \end{pmatrix}, \mathbf{A_D} = \begin{pmatrix} 1 & 1 & 2 & 3 & 1 \\ & 2 & 1 & 2 & 2 \\ & & 3 & 1 & 3 \\ & & & 4 & 4 \\ & & & & 5 \end{pmatrix} \tag{4.8}$$

The tree-equivalent vines for 5 nodes are shown in figure 4.5. It should be noted that, while there are six equivalence classes, there are only five tree-equivalent vines. The reason for this is that tree-equivalent vine $V8$ can be derived in two ways because of the symmetry of the two first order nodes connected to the third order node. For 5 nodes, this is the only tree-equivalent vine corresponding to multiple equivalence classes.

The only difference is in the way the nodes are labelled within the vine, which is why the vines in figure 4.5 are left unlabelled. The standard MATLAB function *perms()* is used to determine all possible permutations of the array *[1 2 3 4 5]*, of which there are 120 in total. Every permutation was looped through the six equivalence class matrices, allowing all 480 vines to be fitted on the data. See the following MATLAB code:

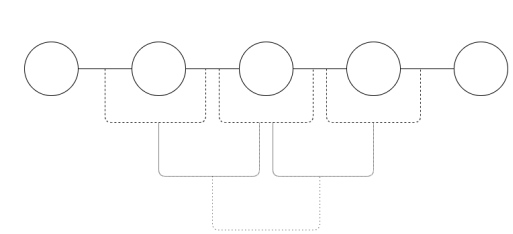

(a) Vine V6, a D-vine. Each node has degree at most 2. Corresponds to matrix A_D.

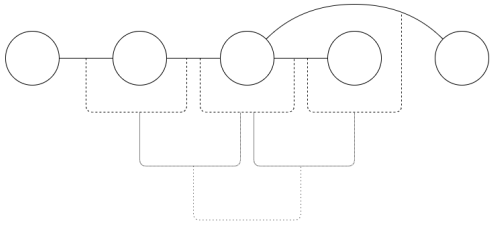

(b) Vine V7, a regular vine where one node in T_1 has degree 3 and each node in $T_j (j > 1)$ has degree at most 2. Corresponds to matrix A_{B1}.

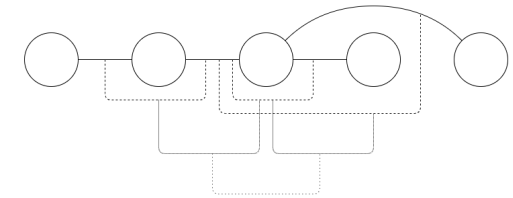

(c) Vine V8, a regular vine where one node in T_1 has degree 3, one node in tree T_2 has degree 3 and each node in $T_j (j > 2)$ has degree at most 2. Corresponds to matrices A_{B2} and A_{B3}.

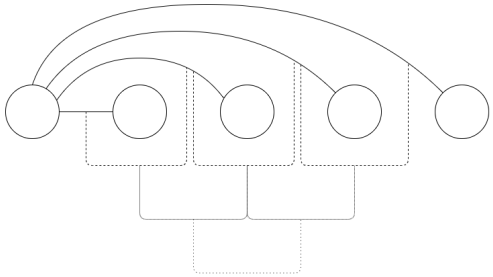

(d) Vine V9, a regular vine where one node in T_1 has degree 4 and each node in $T_j (j > 1)$ has degree at most 2. Corresponds to matrix A_{B0}.

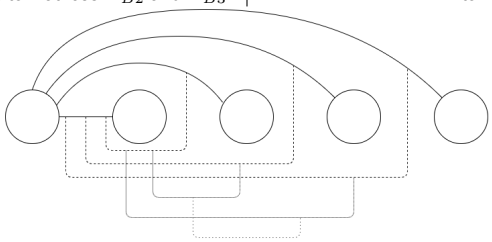

(e) Vine V10, a C-Vine. Each tree has a unique node of degree $n - i$. Corresponds to matrix A_C.

Figure 4.5: The five tree-equivalent regular vines for 5 nodes[45]. All 5-node regular vines are equivalent to one of these.

```
EqC = cat(3,D,B1,B2,B3,C,B0);                % 3D array of all equivalence classes
n_EqC = size(EqC,3);                         % number of equivalence classes
datafit = [Hs Tp Dir w_spd w_dir];           % data to be fitted
permutation = perms(1:1:size(datafit,2));    % all possible permutations of 5 nodes

% fit all possible vines
parfor ii = 1:length(permutation) % loop for every permutation
    % vary the permutation of the data each iteration
    data_perm(:,:,ii) = [datafit(:,permutation(ii,1)) datafit(:,permutation(ii,2))
↪   datafit(:,permutation(ii,3)) datafit(:,permutation(ii,4))
↪   datafit(:,permutation(ii,5))];

    for jj = 1:n_EqC % loop for every equivalence class
        [theta,~,sll] = ssp(data_perm(:,:,ii),EqC(:,:,jj),{'AIC'});          % fit
↪   vine
        AIC(jj,ii) = aicbic(sll,length(nonzeros(cell2mat(theta(1:16)))));    %
↪   calculate AIC
    end
end
```

The above code could also be expanded for higher-dimensional cases. *EqC* stands for Equivalence Classes, and it is a 3D matrix of every equivalence class matrix. *datafit* is the input data, and *permutation* is a list of all possible permutations of the data. The first loop ii runs for all permutations, while the second loop jj runs for all tree-equivalent vines. The best vine can then be selected by checking the index of the lowest AIC value.

Looping all permutations is not a very efficient way to handle this, as some permutations end up giving the same vines. See figure 4.6 for an example of two D-vines which are functionally the same due to a mirroring effect. In total, 720 vine-copulas are fitted, of which 480 are unique. This means 240 fittings are unnecessary. While it is possible to filter out these 240 vines before fitting, it was deemed not necessary as the process was sufficiently fast already. The entire code required less than 5 minutes of computation time. For higher-dimensional systems, this may become a bigger drawback however.

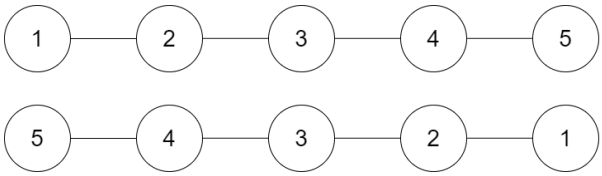

Figure 4.6: Two D-vines created by permutation of the labelling of the trees. While these two vines are different permutations, they are functionally the same vine as they mirror each other perfectly, and thus will produce the same vine-copula model.

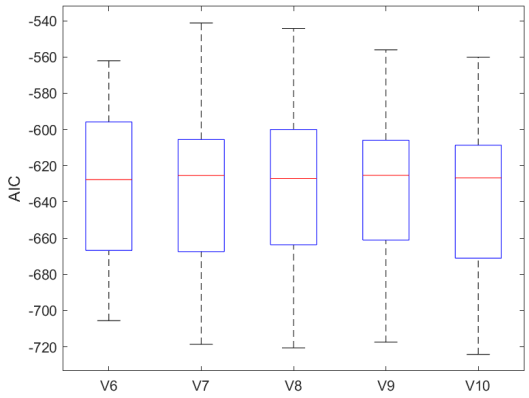

Figure 4.7: Boxplot of the AIC values per tree-equivalent vine.

Figure 4.7 shows a boxplot of the AIC-values per tree-equivalent vine. Non-unique AIC values were discarded, so the plot contains only unique regular vines. There were no outliers in the AIC values. There is very little variation in the median of the AIC values between the tree-equivalent vines. There is also very little difference in the AIC values of the best fits of each tree-equivalent vine, with the exception of vine V6 (which was the D-vine). This indicates that, in this case, most tree-equivalent vines are capable of producing a model that performs reasonably well. It should still be stressed that AIC is only a relative indicator of the goodness-of-fit, so from these values it cannot yet be concluded whether the best-fitting vines are actually good models of the data (for model validation, see section 4.3).

After fitting was completed, the best vine-copula was selected based on the lowest AIC, which was -724.16. The winning vine is illustrated in figure 4.8. It is a C-vine with the wave height placed at its center node. This indicates that the wave height is the dominant variable which influences the other variables. This may be related to the way the extreme wave data was selected: by applying the PoT method on only the wave height and taking the concomitant values of the other variables.

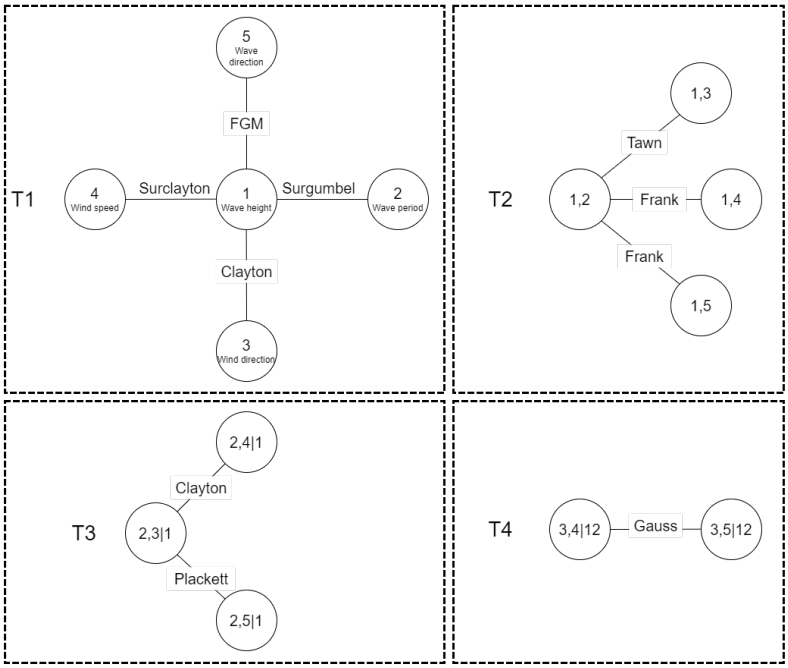

Figure 4.8: The vine-copula with the lowest AIC, which was chosen as the best fitting model. It is vine V10, a C-vine corresponding to a permutation of matrix A_C.

4.3. Vine-copula model validation

In this section the performance of this model will be validated by comparing it to the original dataset it models. A convenient way of visualizing the two datasets is through a plotmatrix. These are shown in figure 4.9. The plotmatrices show the bivariate clusterplots of all variables. An equal amount of data (243 datapoints) was generated for the purpose of comparison. As can be seen, both plots look alike, which is a good sign.

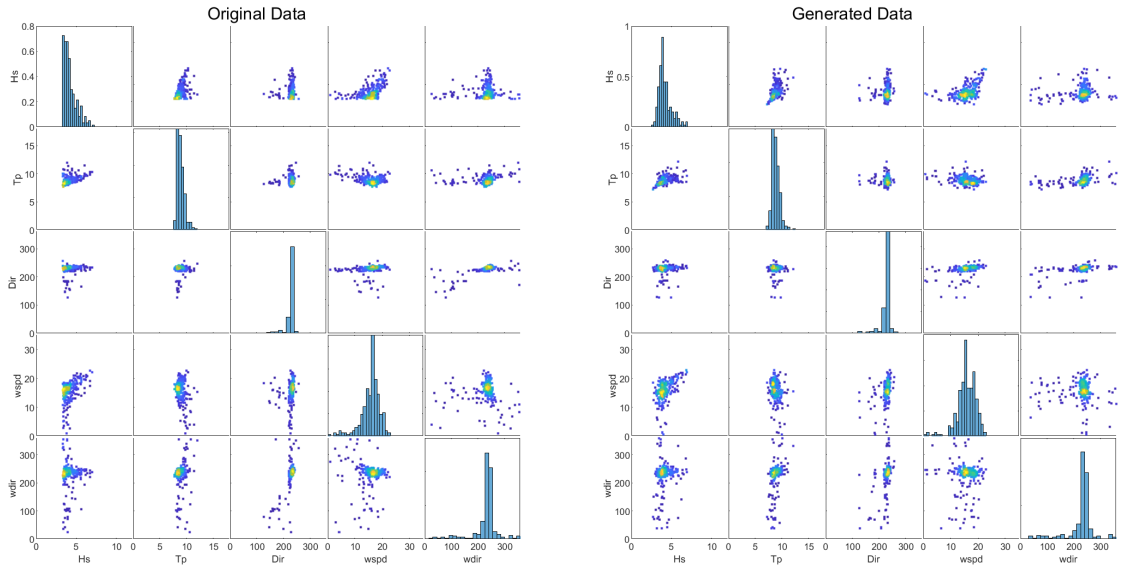

Figure 4.9: Plot-matrices comparing the extreme values to data generated with the vine-copula model.

A simple numerical way of validating the model is through the Normalized Root-Mean-Square-Error

(NRMSE). The RMSE is normalized by dividing it by the range of the data. The order in which the values appear in the datasets is not important, so both datasets are sorted from high to low prior to evaluating the RMSE. Since generating values with a vine-copula is a stochastic process, results are slightly different each time new values are generated. This deviation is removed by generating values a 1000 times, and taking the average of the NRMSE's. The average NRMSE's are summed up in table 4.3, expressed as a percentage. All NRMSE's are of roughly the same order of magnitude and rather small, indicating that the differences between the original dataset and the generated dataset are minimal. The largest deviation was with the wave height, which on average deviated about 1% from the original dataset.

Variable	**NRMSE**
Wave height	1.12%
Wave period	0.91%
Wave direction	0.66%
Wind speed	0.90%
Wind direction	0.97%

Table 4.3: The average NRMSE between the corrected WavewatchIII hindcast data and the data generated using a fitted vine-copula.

The vine-copula model should also simulate the correlations between the variables in a similar way as they are in the original dataset, i.e. if two variables in the original dataset show a strong correlation, then a similar correlation should be expected in the generated dataset. The correlation coefficient between two variables is a measure of their linear dependence. A common way to quantify this is the Pearson correlation coefficient, which is defined as:

$$cor(X_i, Y_j) = \frac{cov(X, Y)}{\sigma_X \sigma_Y} \tag{4.9}$$

Calculating the correlations of the entire dataset can be done with the *corrcoef()* function in MATLAB. This gives a correlation matrix, which contains every bivariate correlation coefficient. The correlation matrices of the original dataset and the generated dataset are shown in tables 4.4 and 4.5 respectively. Though there were some small differences, overall the two matrices have similar values. The sum of the absolute differences of all correlation coefficients equaled 0.40.

Wave height	1.00	0.46	0.12	0.49	-0.11
Wave period	0.46	1.00	0.11	-0.32	0.18
Wave direction	0.16	0.11	1.00	0.18	-0.72
Wind speed	0.51	-0.32	0.18	1.00	-0.27
Wind direction	-0.11	0.18	-0.72	-0.27	1.00
	Wave height	Wave period	Wave direction	Wind speed	Wind direction

Table 4.4: Correlation matrix of the original dataset.

Wave height	1.00	0.51	0.16	0.51	-0.10
Wave period	0.51	1.00	0.11	-0.27	0.21
Wave direction	0.16	0.11	1.00	0.22	-0.72
Wind speed	0.51	-0.27	0.22	1.00	-0.27
Wind direction	-0.10	0.21	-0.72	-0.27	1.00
	Wave height	Wave period	Wave direction	Wind speed	Wind direction

Table 4.5: Correlation matrix of the generated dataset.

5

Loads & failure

This chapter seeks to answer research question 2.1: How can the relevant loads and failure modes be identified and defined? Goda's method will be used for determining the wave-induced loading. 10 failure modes will be outlined in total.

5.1. Vertical breakwaters

A breakwater is, as the name suggests, a hydraulic structure meant to stop incoming waves. It is an important part of defending a coastline or port from the influence of waves. Humans have built these types of structures for thousands of years. Designs and materials are varied, but broadly speaking there's only two types of breakwater; mound breakwaters and vertical breakwaters. Mound breakwaters are sloped structures, typically constructed out of rubble. These types of breakwaters dissipate the energy of incident waves by forcing them to break on a slope[27]. One downside is the large amount of material and space these types of structures need, especially in areas of considerable depth. A vertical breakwater, sometimes called an upright breakwater, refers to a breakwater with at least one vertical section. Vertical breakwaters reflect the incident waves without dissipating much wave energy[27].

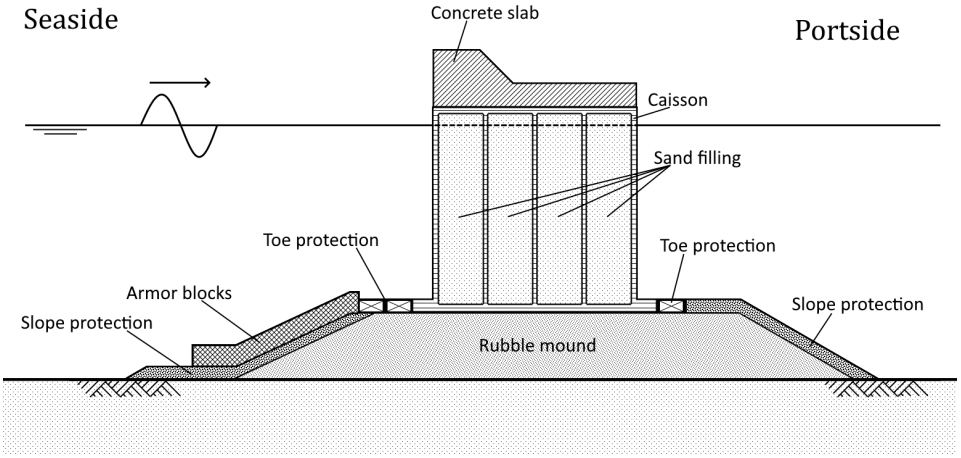

Figure 5.1: Example cross-section of a vertical breakwater. Figure is based upon the Onahama Port Offshore Breakwater, Japan[27].

Vertical breakwaters experience a lot more pressure from wave attack than a rubble mound breakwater, as they reflect almost all wave-energy. This can be alleviated a bit with the addition of a wide berm in front of the structure, which dissipates a part of the wave-energy before it comes into contact with the caisson. The weight of vertical breakwaters induces large pressures on the soil it sits on. A rubble mound is often placed to serve as a foundation to spread the pressure over a larger area. One

major upside of a vertical breakwater is that it requires less material than a rubble mound breakwater. This makes it a very common choice for locations with a water depth greater than 15 meters[11].

Apart of blocking waves from entering the port, a vertical breakwater may also be given other functions such as walkways, quaywalls or a wave-energy converter. The addition of these extra functions may make the functional requirements of the structure stricter, as for example less overtopping discharge is allowed if a walkway is present on or behind the caisson. In this thesis, however, it is assumed the breakwater will be used for preventing excessive port agitation, and no other functions are taken into account.

Prof. Goda has done extensive research on the design of vertical breakwaters and has summarized part of his work in his book *Random Seas And Design Of Maritime Structures*[27]. He has devised the modern-day method for determining the wave-induced force exerted against a vertical wall, which was proven to be quite accurate for design[61]. His method will function as the main guideline for determining the relevant loads, failure modes and design criteria in this chapter and the next.

5.2. Onshore waves

As a wave propagates towards the shore and enters shallower water, it transforms due to influence of the seabed and the wind. Several processes influence the height of the wave, such as shoaling, refraction and breaking. The process of wave shoaling results in higher, steeper waves. Wave refraction causes the direction of the waves to bend perpendicular towards the shoreline. Lastly, waves that become too steep begin to break, limiting their height.

The onshore wave transformation is calculated through SWAN (Simulating WAves Nearshore). SWAN is a numerical wave model developed at the Delft University of Technology, capable of transforming offshore wave conditions to nearshore. A simpler version of the program, called SwanOne, utilizes the 1D-mode of SWAN, which assumes that the bottom profile consists of parallel bottom contours[54]. The program still uses fully 2D calculations, so SwanOne includes refraction, directional spectra and directional spreading[54]. Utilizing a 1-dimensional bathymetry makes the calculation faster, at the cost of accuracy. In front of the Port of Genoa is a large complexly-shaped underwater canyon, which is massively simplified due to the 1-dimensional bathymetry. Bathymetry data was obtained from Navionics[1]. Figure 5.2 shows the bathymetry of the Gulf of Genoa as well as the bottom profile used as input for SWAN.

Normally SWAN needs manual input to perform a calculation. This makes performing a calculation arduous and repeating the process many times unpractical. A. Antonini provided a MATLAB procedure for looping the SWAN process. This procedure was altered to be more flexible, user-friendly and efficient. The code itself can be found in Appendix D. This section will explain how it works, so that later users may apply it to their own project. A basic understanding of SWAN and MATLAB is still advised.

In order for the procedure to work, it should be placed in the same folder as the files of SwanOne. In addition, two types of input files are necessary in order for the MATLAB procedure to work. First is the wave climate data (named *Offshore Data.txt*), with data for the significant wave height, peak wave period, wave direction, wind speed and wind direction at the offshore location. Directions should be in degrees and clockwise from North. The second is the bathymetry data (named *Bathymetry.txt*), with a column for distance in meters (measured from the offshore location and towards the shoreline), and a column for the bottom depth (measured relative to sea level, so it should be negative). The user should prepare these two files before attempting a calculation. In addition, a couple of parameters are to be specified before starting the procedure. These are:

- *coast_angle*: The coast angle clockwise from North. 105 degrees in this case.
- *ng*: The amount of grid points desired. 100 points were selected.
- *savepath*: The savepath for the output data.

Once started, the procedure generates two files necessary for the SWAN calculation: the project file (named *project_001.SWN*) and the bottom profile data (named *project_001_bot.DAT*). These files can be opened with a simple text editor such as notepad. They contain the input data in the format that SWAN uses. The bottom profile data will be generated once, before the loop starts. The project file will be generated once every iteration, continuously replacing the file from the previous iteration. Each generated project file has the same text, with only the wave and wind parameters changed. MATLAB will continuously perform a SWAN calculation for the length of the input data. If at any iteration an error

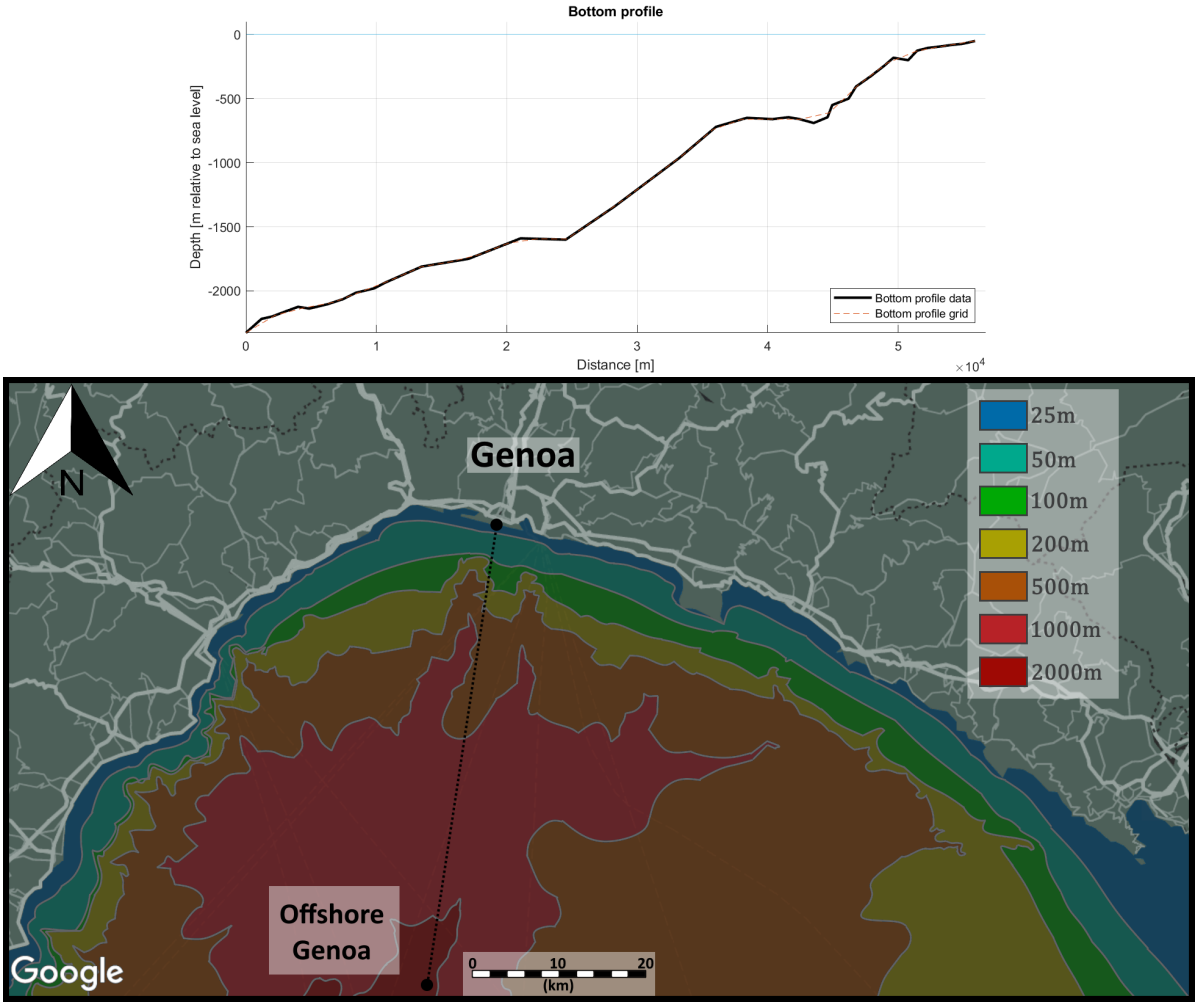

Figure 5.2: Above: 1-dimensional bottom profile used as input for SWAN. Below: Bathymetry of the Gulf of Genoa[1].

occurs, then the procedure will display an error message and continue with the next iteration. Once the loop is done the code will assemble the resulting onshore wave data in a table and write it to a new .txt file. By default the procedure only returns the significant wave height, peak wave period and wave direction, but it is also possible to return *RTpeak*, *Tm01*, *Tm_10*, *Dspr* and wave setup.

It should be noted that SWAN cannot handle waves with an angle of incidence greater than 70 degrees. When using SWAN manually it actually isn't possible to input waves outside of this range. If the input files contain any waves outside of this range, then the loop-procedure will produce a warning but still continue with the calculation. The accuracy of these results should be heavily disputed and are not advised to be used.

The SWAN loop-procedure was applied to the offshore wave data generated with the vine-copula (see Chapter 4). Figure 5.3 shows the offshore and the onshore data. The mean of the wave height increased from 4.2m to 4.35m between offshore and onshore respectively. The onshore data also contained more outliers, with the highest onshore wave measuring 9.01m compared to the highest offshore wave which was 7.67m. Changes in wave period were minimal. Wave refraction caused the direction of the waves to bend slightly towards the perpendicular of the coastline (towards 195°).

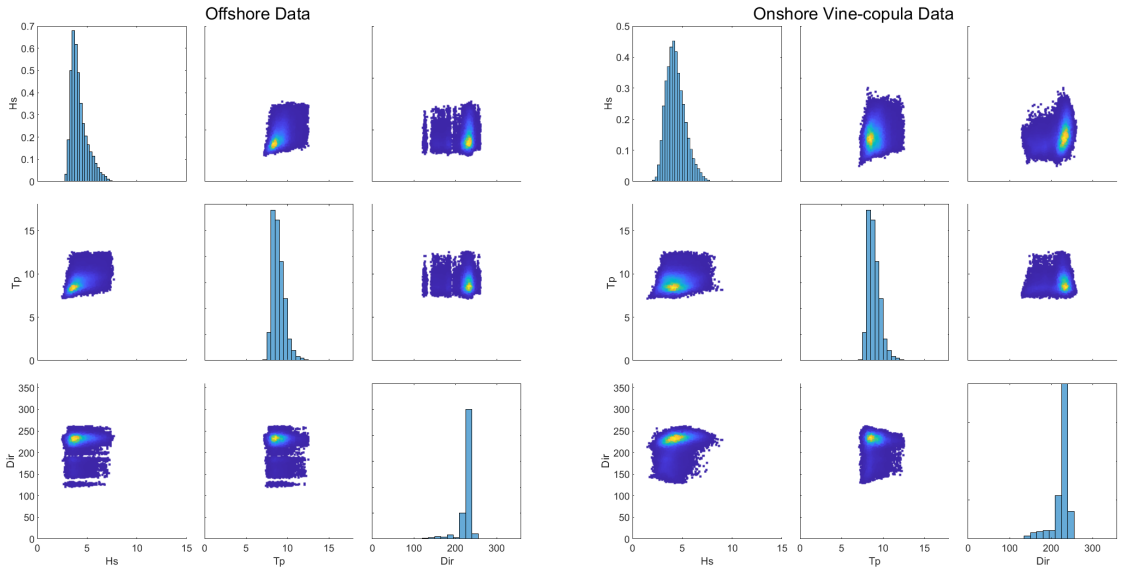

Figure 5.3: Plot-matrices of the ofshore and onshore wave characteristics.

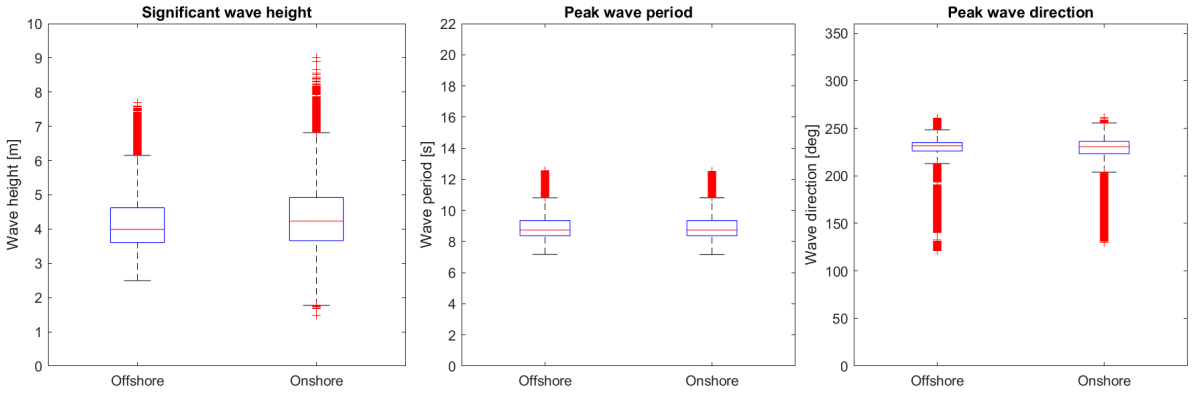

Figure 5.4: Boxplots comparing the wave characteristics between offshore and onshore.

5.3. Wave-induced pressure

A wave is a dynamic phenomenon, and as such the loading caused by the attack of waves is not constant. The onshore-directed forcing is highest when the wave crest is directly in front of the vertical structure. The pressure can partly attributed to the difference in water level between the two sides of the breakwater. This difference causes a force pushing towards the shoreline. Goda has provided a set of equations to calculate the presssure under a wave crest. If waves become too steep due to influence of the sea bed and the berm in front of the caisson, then wave breaking may become a risk. Wave breaking is a phenomenon that should generally be avoided directly in front of the structure. This is because the plunging crest of the wave induces a large impulsive load on the structure, up to several times the hydrostatic pressure force though lasting only for a very short span of time[28]. Wave breaking cannot always be avoided. Takahashi et al has provided an alternative of the Goda method for the case of breaking waves. A different forcing occurs when the wave trough is directly in front of the vertical structure. At this moment, the water level inside the port is higher than the water level on the other side of the breakwater. This difference causes a force pointing away from the shoreline. While no set of equations exist to calculate this force, Goda has provided a graphical method for determining its magnitude. Figure 5.5 illustrates the dynamic water level difference a vertical breakwater faces during wave attack, as well as the impulsive load of a wave breaking directly in front of it. In this section both

instances will be quantified in order to make the definition of the failure criteria possible.

Figure 5.6 shows a simplified cross-section of a vertical breakwater.

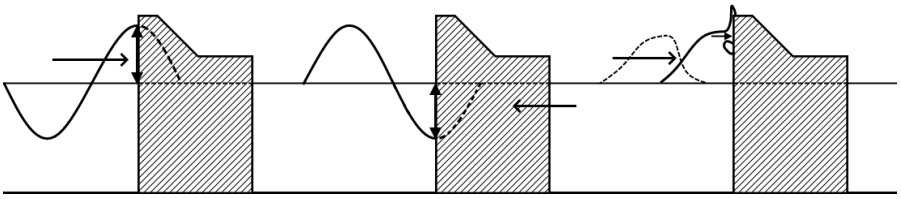

(a) Wave crest directly in front of the structure. **(b)** Wave trough directly in front of the structure. **(c)** Wave breaking directly in front of the structure.

Figure 5.5: Illustration of the breakwater during different phases of wave attack.

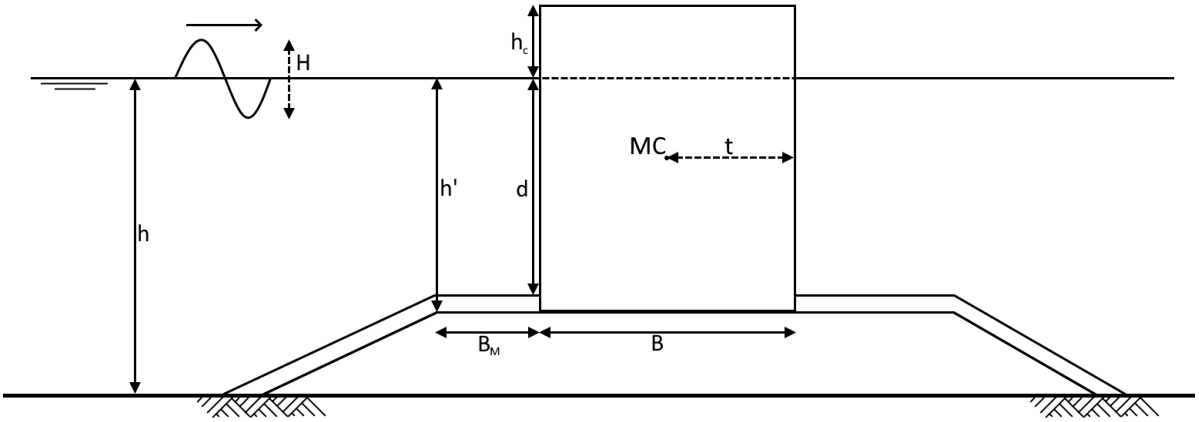

Figure 5.6: Simplified cross-section of a vertical breakwater.

5.3.1. Design wave height

For determination of the wave-induced loading, Goda suggested the use of H_{max}, defined as $H_{1/250}$. It is based on the principle that a breakwater should be designed to be safe against the single wave with the largest pressure among storm waves[27]. In deep water, H_{max} can be derived from the Rayleigh distribution as 1.8 H_s. However, in shallow water, wave breaking limits the height of the waves. This depends on a number of factors, such as the wave steepness, the water depth and the slope of the seabed. Goda proposed the following equation for the calculation of the maximum wave height inside the surfzone:

$$H_{\text{max}} \equiv H_{1/250} = \begin{cases} 1.8H_{1/3} \\ \min\left\{\left(\beta_0^* H_0' + \beta_1^* h\right), \beta_{\text{max}}^* H_0', 1.8H_{1/3}'\right\} & : h/L_0 < 0.2. \end{cases} \tag{5.1}$$

With the coefficients:

$$\begin{aligned} \beta_0^* &= 0.052\left(H_0'/L_0\right)^{-0.38} \exp\left[20\tan^{1.5}\theta\right] \\ \beta_1^* &= 0.63\exp[3.8\tan\theta] \\ \beta_{\text{max}}^* &= \max\left\{1.65, 0.53\left(H_0'/L_0\right)^{-0.29} \times \exp[2.4\tan\theta]\right\} \end{aligned} \tag{5.2}$$

5.3.2. Pressure under a wave crest

Goda proposed a set of formulas for the pressure distribution under a wave crest. See figure 5.7 for Goda's pressure distribution.

Waves form a horizontal trapezoid distribution against the vertical wall. According to Goda, wave crests give the largest pressure at the still water level, denoted as p_1. Pressure varies linearly, both

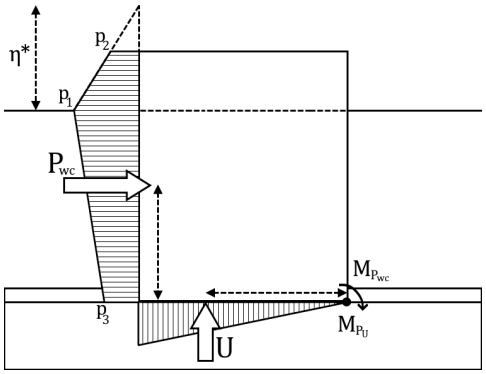

Figure 5.7: The wave pressure distribution against a vertical breakwater, as proposed by Goda[27].

upwards and downwards. Waves also cause an upwards pressure, denoted as p_u, at the underside of the caisson. Goda gave the following equations for the calculation of the wave-induced pressures:

$$p_1 = \frac{1}{2}(1 + \cos\beta)\left(\alpha_1 + \alpha_2 \cos^2\beta\right)\rho g H_{max} \tag{5.3}$$

$$p_2 = \alpha_3 p_1 \tag{5.4}$$

$$p_3 = \begin{cases} p_1\left(1 - h_c/\eta^*\right) & : \eta^* > h_c \\ 0 & : \eta^* \leq h_c \end{cases} \tag{5.5}$$

The uplift pressure is considered to be unaffected by wave overtopping[28].

$$p_u = \frac{1}{2}(1 + \cos\beta)\alpha_1\alpha_3\rho g H_{max} \tag{5.6}$$

In which:

$$\begin{aligned} \alpha_1 &= 0.6 + \tfrac{1}{2}\left[\tfrac{4\pi h/L}{\sinh(4\pi h/L)}\right]^2 \\ \alpha_2 &= \min\left\{\tfrac{h_b - d}{3h_b}\left(\tfrac{H_{max}}{d}\right)^2, \tfrac{2d}{H_{max}}\right\} \\ \alpha_3 &= 1 - \tfrac{h'}{h}\left[1 - \tfrac{1}{\cosh(2\pi h/L)}\right] \end{aligned} \tag{5.7}$$

Where h_b represents the water depth at a distance of 5 H_s from the breakwater. The height η^* is the elevation to which the wave pressure is exerted. This is not the same as the height of the incoming wave, though it is strongly related. This elevation is greatest for waves normal to the structure, and becomes smaller for any angle of incidence larger than 0 degrees:

$$\eta^* = 0.75(1 + \cos\beta)H_{max} \tag{5.8}$$

Where β represents the angle of incidence to the breakwater. However, wave direction is often a very uncertain parameter. In random sea waves there is always some wave spreading present, meaning that any attempt to quantify the wave direction with a single number is inherently inaccurate. Previously the mean wave direction was used, however this value is insufficient for design conditions. For design it is necessary to take into account the most critical case of loading. Goda suggests a margin of safety of 15 degrees. As such, the angle of incidence will actually be defined as:

$$\beta = max(Dir - 15°, 0) \tag{5.9}$$

Goda's equations for the wave-induced pressure were found to be insufficient if the risk of wave breaking is present. Breaking waves directly in front of the may induce a large impulsive pressure on the structure due to the impact of the plunging wave crest. As can be seen in figure 5.5.c. This force

can be up to 10 times the load caused by the hydrostatic pressure difference, however it lasts only for a brief instance of time[27]. The moment the crest of the wave makes contact with the structure, a pocket of air becomes trapped between the wave and the wall. It was found during model tests that this pocket of air actually dampens the impact pressure and prevents it from becoming exceedingly large. This limits the impulsive pressure of a breaking wave to 'only' two to three times the hydrostatic pressure. Takahashi et al proposed a modification of the coefficient α_2 to take into account the effect of the impulsive pressure, based on model tests by Tanimoto et al. The coefficient α_2 ought to be replaced by α^*, defined as the maximum between the original α_2 and a newly introduced α_I. The coefficient α_I may be calculated with the following set of equations:

$$
\begin{aligned}
\alpha_I &= \alpha_{IH_{max}} * \alpha_{IB} \\
\alpha_{IH} &= \min\{H_{max}/d, 2.0\} \\
\alpha_{IB} &= \begin{cases} \cos\delta_2 / \cosh\delta_1 \\ 1/\left(\cosh\delta_1 \cosh^{1/2}\delta_2\right) : \delta_2 > 0 \end{cases} \\
\delta_1 &= \begin{cases} 20\delta_{11} : \delta_{11} \leq 0 \\ 15\delta_{11} : \delta_{11} > 0 \end{cases} \\
\delta_2 &= \begin{cases} 4.9\delta_{22} : \delta_{22} \leq 0, \\ 3.0\delta_{22} : \delta_{22} > 0, \end{cases} \\
\delta_{11} &= 0.93\left(\frac{B_M}{L} - 0.12\right) + 0.36\left(0.4 - \frac{d}{h}\right) \\
\delta_{22} &= -0.36\left(\frac{B_M}{L} - 0.12\right) + 0.93\left(0.4 - \frac{d}{h}\right)
\end{aligned}
\tag{5.10}
$$

When α_I is smaller than α_2, the risk of wave breaking is negligible and the original coefficient α_2 is to be used instead. Wave breaking should generally be avoided, as the addition of the impulsive wave pressure greatly increases the loading the structure experiences.

It was found that the angle of incidence of the wave greatly affects the magnitude of impulsive wave breaking. Tanimoto has stated that, with angles of incidence greater than 20 degrees, the risk of impulsive wave breaking becomes negligible. As such, the breakwater can be orientated in such a way that waves do not attack it perpendicularly. Yet this also increases the risk of scour under the toe and berm protection or at the bed in front of the structure. Another important aspect is the rubble mound foundation the caisson is placed on top. Tall and wide rubble mounds greatly increase the risk of compulsive wave breaking. The size of the rubble mound foundation should be kept as small as possible, while still retaining sufficient bearing capacity and stability.

The wave force acted on the structure is the area of the pressure distribution. The total horizontal force P and the uplift force U are defined as:

$$P_{wc} = \frac{1}{2}\left(p_1 + p_2\right)h' + \frac{1}{2}\left(p_1 + p_3\right)h_c^* \tag{5.11}$$

$$U = \frac{1}{2}p_u B \tag{5.12}$$

The moments caused by these forces are largest at the toe on the rear-side of the vertical section. They can be evaluated as:

$$M_{P_{wc}} = \frac{1}{6}\left(2p_1 + p_2\right)h'^2 + \frac{1}{2}\left(p_1 + p_3\right)h'h_c^* + \frac{1}{6}\left(p_1 + 2p_3\right)h_c^{*2} \tag{5.13}$$

$$M_U = \frac{2}{3}UB \tag{5.14}$$

5.3.3. Pressure under a wave trough

When the wave trough is directly in front of the structure, the water level inside the port is higher than the water level at the seaward side. The hydrostatic pressure difference between the two sides causes a net seaward pressure, pushing the structure away from the coastline. The effect of breaking waves on this situation has not been examined in detail. However, Goda has provided graphs for determining

the pressure distribution under a wave trough for standing waves. It depends on the steepness of the wave and the ratio between the water depth and wave length. In comparison to the onshore-directed pressure under a wave crest, the pressure under a trough is seen to become larger than that under a crest if the ratio of the water depth to wavelength exceeds about 0.25[27]. The resulting force and its level arm will be determined using a digitized version of the figures in Goda's book. As this force is aimed towards the sea, the risk of overturning happens in seaward direction too. As such, the moment ought to be evaluated at the toe of the seaside of the breakwater, see figure 5.8. The moment can be calculated simply as:

$$M_{P_{wt}} = P_{wt} * s_{wt} \tag{5.15}$$

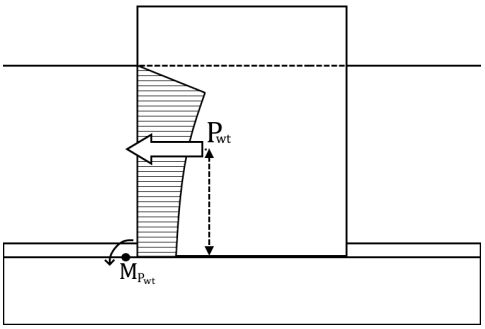

Figure 5.8: Illustration of the wave-induced pressure under the wave trough according to Goda's theory[27].

5.4. Water level

The still water level (SWL) is the water level at a given location averaged over time. There are temporal variations in the water level, such as tides and wind set-up or set-down, which depend on the time of day or the atmospheric conditions. While wave-induced set-up can be calculated with SWAN, it was found during the process that these were of the order 10^{-4} m at most. For simplicity's sake, wave-induced set-up is neglected.

5.4.1. Tides

While the Mediterranean Sea does have tides, the tidal range is of a much smaller scale than that of the Atlantic Ocean. This is because it is almost completely surrounded by land. Tidal surges can only enter the Mediterranean Sea through the thin strait of Gibraltar. The M2, S2 and K1 tidal constituents for Genoa are 8.5cm, 3.3cm and 3.5cm respectively[48][14]. Other tidal constituents were of the order of magnitude of a single centimeter or less, and are neglected. Tidal levels are calculated by the addition of the M2, S2 and K1 tidal constituents in the below equation:

$$h_{tide} = M2 \cos\left(\frac{2t\pi}{44700}\right) + S2 \cos\left(\frac{2t\pi}{43200}\right) + K1 \cos\left(\frac{2t\pi}{86160}\right) \tag{5.16}$$

Where t is the time in seconds. The denominators of the fractions inside the cosine functions are the periods of the tidal constituents in seconds.

5.4.2. Wind set-up and set-down

Wind set-up and set-down is the balance between the mass of the water and the wind shear stress. When a strong wind blows over a shallow body of water, the surface water tilts. This causes one side to lower and the other to rise, depending on the direction of the wind. See figure 5.9a for an illustration. At the coast of the Ligurian Sea, this can mean a water level difference of a few decimeters[6].

Wind set-up and set-down may be calculated with the following equation[43]:

$$\frac{dS}{dx} = C_2 \frac{u^2}{gd} \tag{5.17}$$

In which:

- S is the total wind set-up/down in m.
- x is the fetch in m.
- C_2 is the drag coefficient for wind set-up or set-down. Typical values range between 3.5*10^{-6} and 4.0*10^{-6}[43].
- d is the water depth in m.
- u is the wind velocity in m/s.

Offshore wind speed and direction were generated with the vine-copula model explained in chapter 4. It is assumed offshore wind conditions vary very little from onshore conditions, as there is less than 60 kilometers of distance between the two points. The fetch is the distance over which the wind stimulates the surface water. It depends on the wind direction, location of the coastlines and the depth of the sea. There is a ravine inside the Ligurian Sea quite close to the coastline, which reaches about 1-2 kilometers deep. The deeper the water, the less of an effect wind set-up and set-down has. In the deep ocean, the water set into motion in the upper layers can easily spread out. Vertical exchange of water makes this possible. On the continental shelf there is no escape due to the limited water depth and the surface water is driven ashore[12]. Because of that, the fetch for wind set-up and set-down is limited to shallow waters up to about 200 meters deep. The fetch was approximated by dividing the directions into quadrants and measuring the average fetch per quadrant. A choice was made for 24 quadrants of 15 degrees each. A map of the fetch for wind set-up and set-down can be seen in **??**. Wind set-up and set-down was calculated for all wind data, see figure 5.9b.

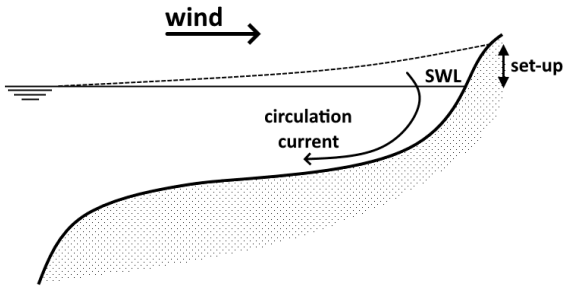

(a) Illustration of wind set-up.

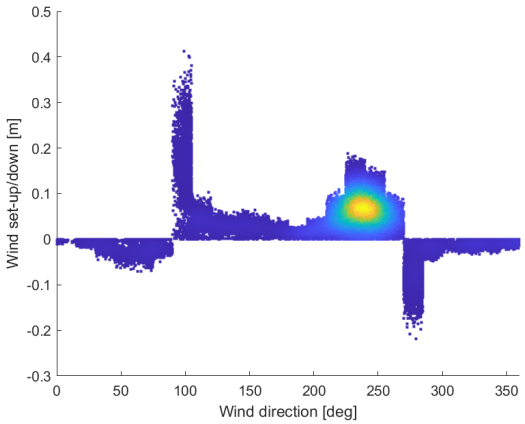

(b) The calculated wind set-up and wind set-down.

5.5. Overview of the failure modes

A failure mode is a process through which failure may occur. The definition of failure is broad, but generally it refers to the occurrence of damage and/or the inability of the structure to fulfill its functions. This section serves to illustrate all relevant failure modes for design of the vertical breakwater. Section 6.2 will explain how these failure modes function in a probabilistic setting.

5.5.1. Fault tree

Figure 5.10 shows the fault tree for the vertical breakwater. In total, 10 failure modes are to be considered for the design of the breakwater. These are illustrated in figure 5.11. A distinction between two types of failure is made: structural failure and functional failure. Structural failure is further divided into either failure of the vertical section (caisson failure) or failure of the foundation. Caisson failure is a result of excessive wave-induced pressure. This happens when an imbalance of forces causes the

vertical structure to move. Foundational failure may also occur as a result of wave-induced forcing or the weight of the vertical section exceeding the bearing capacity of the rubble mound. Events such as seismic occurrences, tsunami's or the collision of a ship are out of scope and not considered in design. The breakwater has only one function: to prevent excessive port agitation. There are several ways port agitation could occur, though only wave overtopping and transmission are considered. Processes such as wave reflection, resonance within the port and penetration of waves and currents through the port entrances, are out of scope as the design focusses on a single cross-section only.

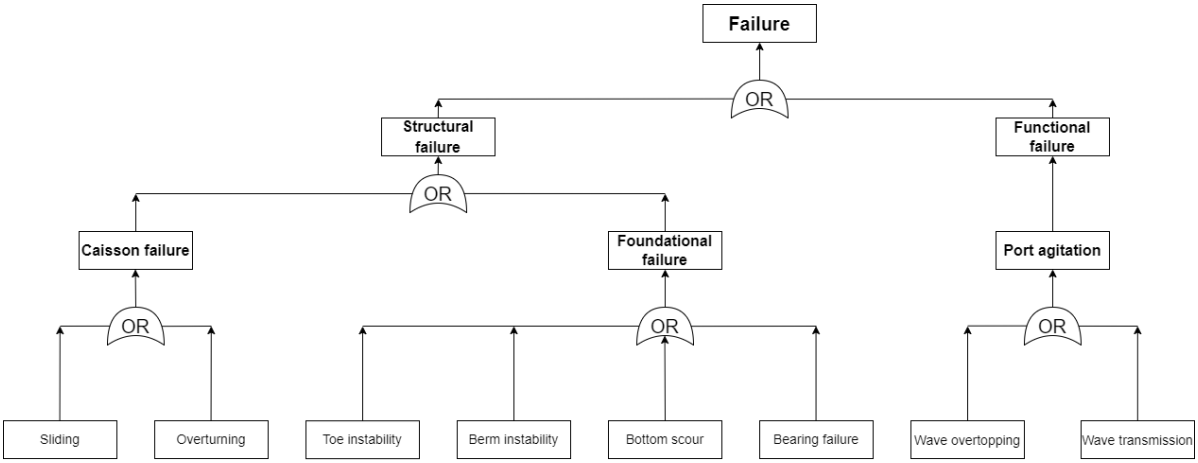

Figure 5.10: The fault tree of the new breakwater at the port of Genoa.

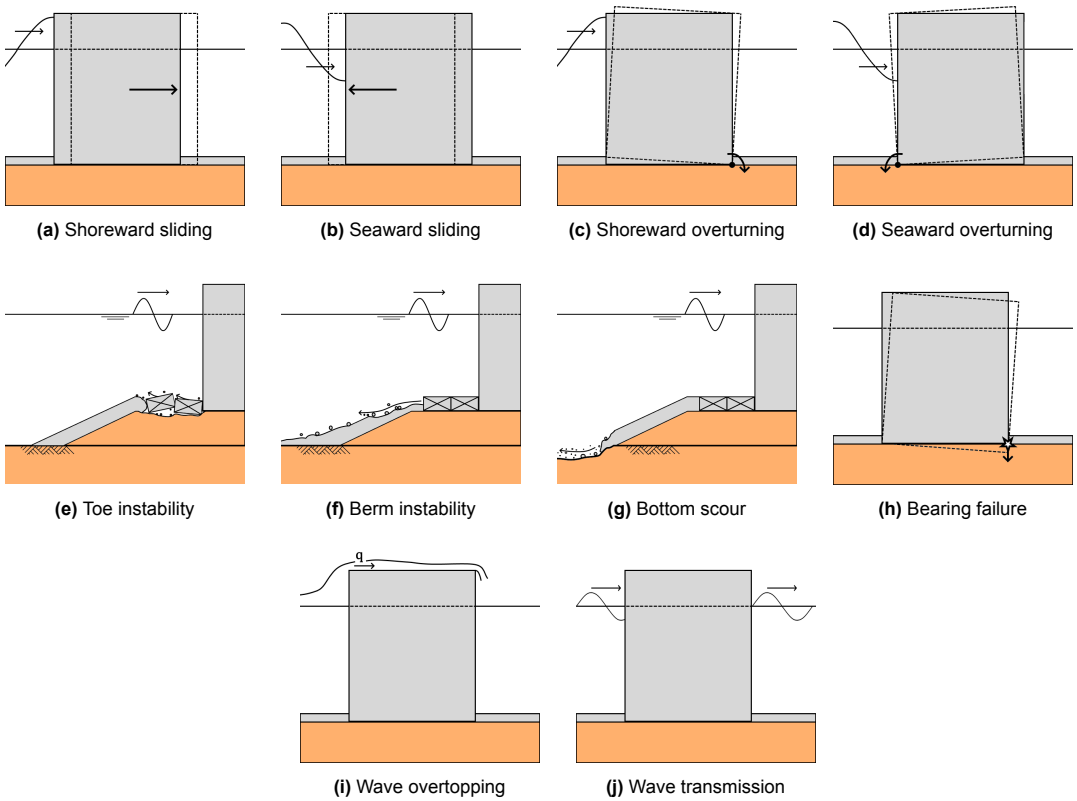

(a) Shoreward sliding **(b)** Seaward sliding **(c)** Shoreward overturning **(d)** Seaward overturning

(e) Toe instability **(f)** Berm instability **(g)** Bottom scour **(h)** Bearing failure

(i) Wave overtopping **(j)** Wave transmission

Figure 5.11: Illustrations of all failure modes considered in design.

5.5.2. Caisson failure

Sliding refers to a horizontal movement of the caisson. It is the result of an unbalance of horizontal forces. Due to the attack of waves, there is a dynamic difference in water level between the two sides of the breakwater. This difference results in a horizontal pressure force, which may induce sliding. Sliding can occur in two directions: seaward and shoreward. Shoreward sliding is most likely when the crest of the wave is directly in front of the breakwater, while seaward sliding is most likely when the wave trough is directly in front of it.

Goda defined the safety factor (SF) for sliding as follows[28]:

$$SF_{sliding} = \frac{\mu(W - U)}{P} \tag{5.18}$$

The force P could be either P_{wc} or P_{wt}, for the wave crest and wave trough respectively. This actually means there are two safety factors for sliding: one for shoreward motion and one for seaward motion. The parameter μ is the coefficient of friction between the upright section and the rubble mound, W is the weight of the caisson and U is the uplifted weight. For the friction factor, Goda suggests a value of 0.6[28].

Overturning, sometimes called tilting, refers to a rotational movement of the caisson towards the shoreline. It is a result of an unbalance of moments. Similar to sliding, overturning may also occur in either a shoreward or seaward direction.

Goda defined the safety factor (SF) for overturning as follows[28]:

$$SF_{overturning} = \frac{Wt - M_U}{M_P} \tag{5.19}$$

Similar to the safety factor(s) for sliding, the moment M_P may be either the moment caused by the pressure of the wave crest or by the wave trough. Just like sliding, this means there are also two safety factors for overturning for shoreward and seaward motion. The parameter t is the horizontal distance between the center of gravity and the toe of the upright section, see figure 5.6. This is typically half of the width of the caisson, but it can be extended with the addition of a wider bottom slab.

5.5.3. Foundational failure

Bearing failure occurs when the bearing pressure of the caisson exceeds the bearing capacity of the rubble mound foundation, and the foundation collapses as a result. For calculation of the bearing pressure, Goda recommends a simplified technique[27]. The bearing pressure can be evaluated as the the weight of the structure minus the wave-induced uplift force, see the figures in 5.12.

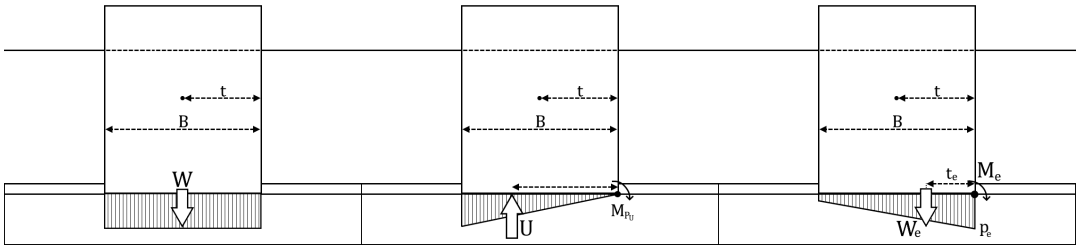

(a) Weight of the upright section. **(b)** Uplifting pressure. **(c)** Bearing pressure.

Figure 5.12: Bearing pressure distribution and its two constituents: the weight and the uplifting pressure.

The largest bearing pressure, p_e, can be calculated as:

$$p_e = \begin{cases} \frac{2W_e}{3t_e} & : t_e \leq \frac{1}{3}B \\ \frac{2W_e}{B}\left(2 - 3\frac{t_e}{B}\right) & : t_e > \frac{1}{3}B \end{cases} \tag{5.20}$$

With:

$$t_e = \frac{M_e}{W_e}, \quad M_e = Mgt - M_U - M_p, \quad W_e = Mg - U \tag{5.21}$$

The upright section is partially submerged in water. Therefore, the weight of the displaced water should be subtracted from the total weight of the structure. A uniform weight distribution is assumed. The force W_e is the force resulting after the uplifting force has been subtracted from the weight. This force employs a moment M_e at the rear-side toe of the structure over the arm length t_e.

Toe instability refers to the stability of the units at the toe of the structure. Wave-induced scour for vertical breakwaters is most severe right at the toe of the structure[28][27], which is why they recommended the placement of toe protection at both sides of the breakwater. In Japan, toe protection typically consists of a few rows of heavy concrete blocks. An example of such a block and the dimensions necessary for design of the toe protection can be found in figure 5.13. The example block in the figure contains two rectangular holes to allow water to flow through and reduce the wave-induced pressure at the toe.

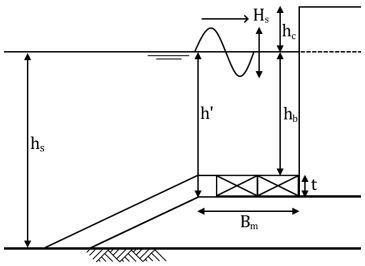

(a) Location and dimensions of the toe protection.

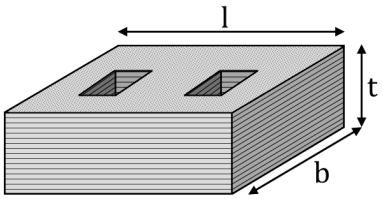

(b) Example of a toe protection block.

Figure 5.13: Toe protection for a vertical breakwater.

Takahashi[35] has done extensive research on the design of toe protection blocks. He provided the graph and table in figure 5.14[23] for the design of the dimensions of the blocks. The deeper the water is right in front of the breakwater, the less severe the scour will be under the toe protection. The graph contains two lines, one for the trunk and one for the head of the structure. At the head of the structure water is able to flow around the breakwater more freely, resulting in stronger currents and a higher probability of toe instability. For this reason the required thickness of the toe protection is higher around the head of the structure. A digitized version of this graph will be utilized to select the necessary toe thickness.

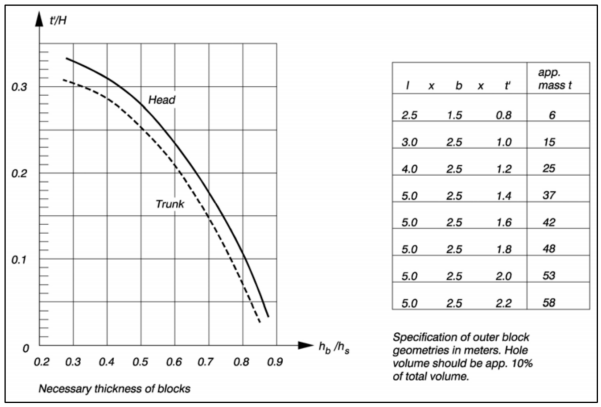

Figure 5.14: Design of the toe protection blocks. Graph and table are from the Coastal Engineering Manual, VI-5-53[23].

Berm instability refers to stability of the armor layer on the berm and slope of the rubble mound. Wave-induced currents may cause movements of these rocks if wave action is sufficiently severe. Motion of the armor layer could induce scour of the rubble mound foundation, risking structural failure of the breakwater. Berm or slope protection usually consists of large natural rocks, though in some cases prefabricated concrete armor blocks are used.

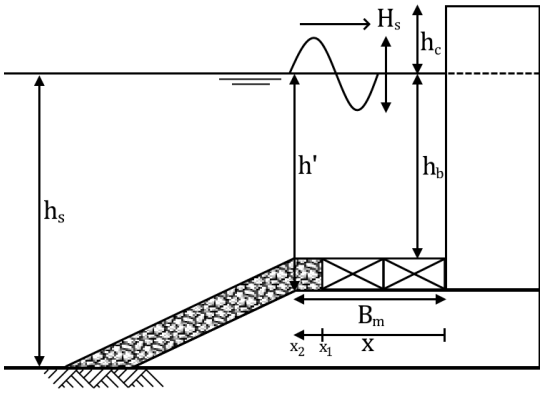

Figure 5.15: Illustration of the berm protection.

A Hudson-type equation by Tanimoto et al[34] may be used for determining the stability of a two-layer quarry stone rubble mound armor:

$$W = \frac{\rho_r}{N_s^3 \left(S_r - 1\right)^3} H_{s^3} \tag{5.22}$$

Where W is the rock weight, ρ_r the density of the element, S_r is the ratio of ρ_r to the specific weight of seawater, H_s the significant wave height and N_s the stability number. The value of the stability number depends on the wave conditions, the dimensions of the rubble mound and on the rock shape. It is a value found through model tests. Tanimoto et al[34][23] suggested the following set of equations for the stability number of berm armor:

$$\begin{aligned} N_s &= \mathsf{max}\{1.8, 1.3\alpha \div 1.8\,\mathsf{exp}[-1.5\alpha(1-\kappa)]\} \\ \alpha &= \left\{(1-\kappa)/\kappa^{1/3}\right\}\left(h'/H_{1/3}\right) \\ \kappa &= \kappa_1\kappa_2 \\ \kappa_1 &= \left(4\pi h'/L'\right)/\,\mathsf{sinh}\left(4\pi h'/L'\right) \\ \kappa_2 &= \mathsf{sin}^2\left(2\pi B_M/L'\right) \end{aligned} \tag{5.23}$$

However, this set of equations works only for normally incident waves. For obliquely incident waves, an adjustment needs to be made. Tanimoto et al[35][23] has suggested the following modification to the calculation of the coefficient κ to take into account the angle of incidence of the waves β:

$$\begin{aligned} \kappa =& \frac{4\pi h'/L'}{\mathsf{sinh}\left(4\pi h'/L'\right)}\kappa_2 \\ \kappa_2 =& \mathsf{max}\left\{\alpha_S\,\mathsf{sin}^2\,\beta\,\mathsf{cos}^2\left(\frac{2\pi x}{L'}\,\mathsf{cos}\,\beta\right)\right. \\ & \left.\mathsf{cos}^2\,\beta\,\mathsf{sin}^2\left(\frac{2\pi x}{L'}\,\mathsf{cos}\,\beta\right)\right\} : 0 \le x \le B_M \end{aligned} \tag{5.24}$$

Where x is a distance measured from the foot of the structure up to the end of the even section of the berm, see figure 5.15. The value of x should be varied to give the maximum value of κ_2. Because of the presence of the toe protection blocks, it won't be necessary to vary x over the entire length of

the berm, but only over the unprotected stretch (indicated by x_1 and x_2 in figure 5.15). Another factor, α_S, has been introduced by Kimura[34][27] et al to take into account the effect of the slope. A value of 0.45 is given based on model tests.

An important aspect to take into account is the need for a filter under the berm armor to ensure the stability of the rubble mound core. This becomes necessary if the differences in size between two layers is too large. The core of the rubble mound will be constructed out of quarry-run rock, while the berm protection will likely need to consist of large armor stones weighing several tons. In a geometrically closed filter, the size of the pores is much smaller than the grains themselves, which means it is not possible for the grains to erode away between the pores. The following three filter criteria need to be fulfilled for a geometrically closed filter[26]:

$$Stability: \frac{d_{15F}}{d_{85B}} < 5, \qquad Int.Stab: \frac{d_{60}}{d_{10}} < 10, \qquad Permeability: \frac{d_{15F}}{d_{15B}} > 5 \tag{5.25}$$

Where F stands for the filter layer (the top layer), and B stands for the base layer (the lower layer). If the two layers do not fulfill all criteria, then the filter is not considered stable. A solution is to place one or more layers between them, each of which fulfill the criteria with their neighbouring filter layers. Chapter 3 of *The Rock Manual*[16] lists several standard gradings to be used in construction.

Bottom scour occurs when wave-induced currents at the seabed near the structure flush away the particles of the seabed. Vertical breakwaters reflect most of the wave energy, meaning that the wave-induced currents are stronger in front of it than would be with a rubble mound breakwater[27]. Figure 5.16 shows the orbital motions created by the presence of waves.

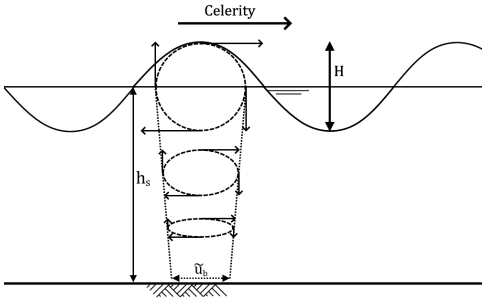

Figure 5.16: Orbital motions induced by propagating waves.

A simple preliminary check of the stability of the sea bed grains can done by applying the Shields equation for grain stability. The waves induce a shear velocity u_{*b}^2 at the bed. Grain movement will occur at the critical velocity u_{*c}, according to Shields[26]. If the shear velocity exceeds the critical velocity, then there is a risk of motion of the bed grains.

The critical shear velocity is defined according to the Shields equation[26]:

$$d_{n50} = \frac{u_{*c}^2}{\Psi_c \Delta C^2} \tag{5.26}$$

Where:

- Ψ_c is the Shields stability parameter. Figure 5.17 shows the Shields parameter as a function of grain size.
- Δ is the relative density between the grains and water, typically with a value of 1.65.
- d_{n50} is the median nominal grain diameter.
- C is the Chézy number, which may be evaluated with:

$$C = 18 \log(12 * h/k_r) \tag{5.27}$$

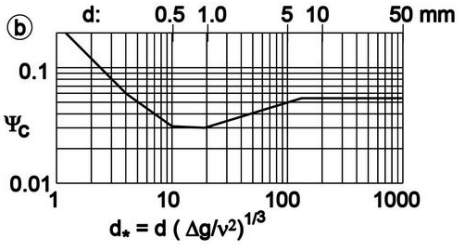

Figure 5.17: Simplified diagram of Shields parameter. Graph by Van Rijn[50].

According to Bijker, 1967[9], the maximum wave-induced shear velocity can be calculated with:

$$u_{*b,max} = \sqrt{\frac{c_f}{2}}, \tag{5.28}$$

With:

$$\tilde{u}_b = \frac{\omega * H/2}{\sinh(kh)} \tag{5.29}$$

$$c_f = \max(0.237(\frac{a_b}{k_r})^{-0.52} \tag{5.30}$$

Where $\hat{u}_b$ is the maximum wave-induced orbital velocity at the bottom[26], and c_f is the friction coefficient. The parameter k_r appears in the formulas for C and c_f, and is known as the bed roughness. It is usually defined as a factor of the diameter of the grains. Ψ_c = 0.03 and $k_r = 2d_{n50}$ is a reasonable combination and a practical choice in case a statically stable protection needs to be designed[26].

5.5.4. Port agitation

Wave overtopping refers to a quantity of water from the wave that spills over to the other side of the breakwater. This usually doesn't result in major damages, however it does cause port agitation.

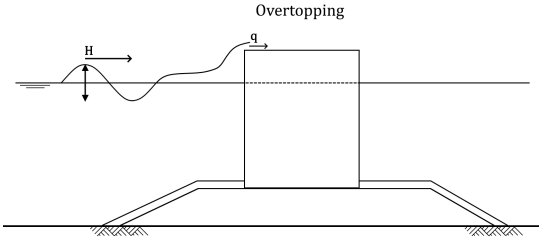

Figure 5.18: Illustration of the occurrence of wave overtopping.

For determining the overtopping discharge, the EuroTop Manual[40] is used as a reference. It depends on a number of conditions. Figure 7.2 of the EuroTop Manual contains a useful flowchart which illustrates all conditions.

If the foreshore has no influence on the waves (deep water conditions), then Equation 7.1 of the EuroTop Manual may be applied for the mean overtopping.

$$\frac{q}{\sqrt{g \cdot H_{m0}^3}} = 0.047 \cdot \exp\left[-\left(2.35\frac{R_C}{H_{m0}}\right)^{1.3}\right] \tag{5.31}$$

With a reliability of σ(0.047) = 0.007 and σ(2.35) = 0.23.

When the foreshore does have an influence, the EuroTop Manual makes a distinction between vertical and composite types. This difference is determined by the ratio between the submerged caisson height and the total water depth, d/h (see figure 5.7).

$$\begin{aligned} d/h > 0.6 \rightarrow vertical \\ d/h < 0.6 \rightarrow composite \end{aligned} \tag{5.32}$$

The overtopping process changes when wave breaking occurs. This happens when:

$$\begin{aligned} vertical : h^2/(H_{m0}L_{m-1,0}) < 0.23 \\ composite : h * d/(H_{m0}L_{m-1,0}) < 0.65 \end{aligned} \tag{5.33}$$

When wave breaking doesn't occur, 7.5 of the EuroTop Manual is used:

$$\frac{q}{\sqrt{gH_{m0}^3}} = 0.05 \exp\left(-2.78\frac{R_c}{H_{m0}}\right) \tag{5.34}$$

With a reliability of σ(0.05) = 0.012 and σ(2.78) = 0.17.
For vertical breakwaters with wave breaking, EuroTop equations 7.7 and 7.8 are used.:

$$\begin{aligned} R_c/H_{m0} < 1.35 : \frac{q}{\sqrt{gH_{m0}^3}} = 0.011\left(\frac{H_{m0}}{hs_{m-1,0}}\right)^{0.5} \exp\left(-2.2\frac{R_c}{H_{m0}}\right) \\ R_c/H_{m0} > 1.35 : \frac{q}{\sqrt{gH_{m0}^3}} = 0.0014\left(\frac{H_{m0}}{hs_{m-1,0}}\right)^{0.5}\left(\frac{R_c}{H_{m0}}\right)^{-3} \end{aligned} \tag{5.35}$$

With a reliability of σ(0.011) = 0.0045 and σ(0.0014) = 0.0006.
For composite breakwater with wave breaking, EuroTop equations 7.14 and 7.15 are used:

$$\begin{aligned} R_c/H_{m0} < 1.35 : \frac{q}{\sqrt{gH_{m0}^3}} = 1.3\left(\frac{d}{h}\right)^{0.5} 0.0014\left(\frac{H_{m0}}{hs_{m-1,0}}\right)^{0.5}\left(\frac{R_c}{H_{m0}}\right)^{-3} \\ R_c/H_{m0} > 1.35 : \frac{q}{\sqrt{gH_{m0}^3}} = 1.3\left(\frac{d}{h}\right)^{0.5} 0.0110\left(\frac{H_{m0}}{hs_{m-1,0}}\right)^{0.5} \exp\left(-2.2\frac{R_c}{H_{m0}}\right) \end{aligned} \tag{5.36}$$

With a reliability of σ(0.011) = 0.0045 and σ(0.0014) = 0.0006.
In addition to the above equations, a wave height reduction factor, γ_β, is introduced for oblique wave attack. It depends on the angle of incidence of the wave:

$$H = \gamma_\beta * H_s = \max(1 - 0.0062\beta, 0.72) * H_s \tag{5.37}$$

Wave transmission is the final failure mode considered. Waves hitting the breakwater transfer part of their energy into the harbour, whether by energy through the breakwater, or by energy transfer over the breakwater if the run-up of the waves exceeds the top level of the breakwater[30].

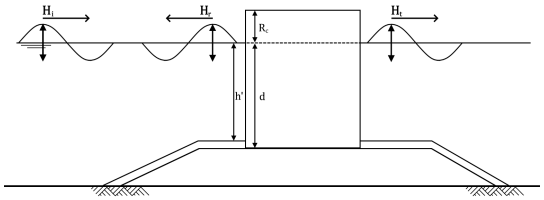

Figure 5.19: Illustration of the occurrence of wave transmission.

The transmitted wave is the incident wave times the transmission coeffcient. Heijn 1997[30], proposed a simple equation for calculation of the transmission coefficient, K_t:

$$K_t = \sqrt{\left[\alpha \cdot \exp\left(-\frac{1}{k}\frac{R_c}{H_s}\right)^n\right]^2 + \left[0.15 \cdot \left(1 - \frac{h'}{h_s}\right)\right]^2} \tag{5.38}$$

For conventional vertical breakwaters, α = 0.35 and n = 2 are suggested. The value of the parameter k depends on the ratio between the crest height of the breakwater and the water depth over the berm in front of the breakwater.

6

Probabilistic design

This chapter seeks to answer research question 2.2: How can the failure modes be verified in a fully probabilistic approach?, and research questions 2.3: What design measures result in a cross-sectional design with an acceptable probability of failure? This chapter features a fully probabilistic design of a cross-section of the breakwater. Probabilistic design will be carried out using a Monte-Carlo simulation.

6.1. Placement of the new breakwater

Figure 6.1 shows an overview of the Port of Genoa as well as the plans for the new breakwater.

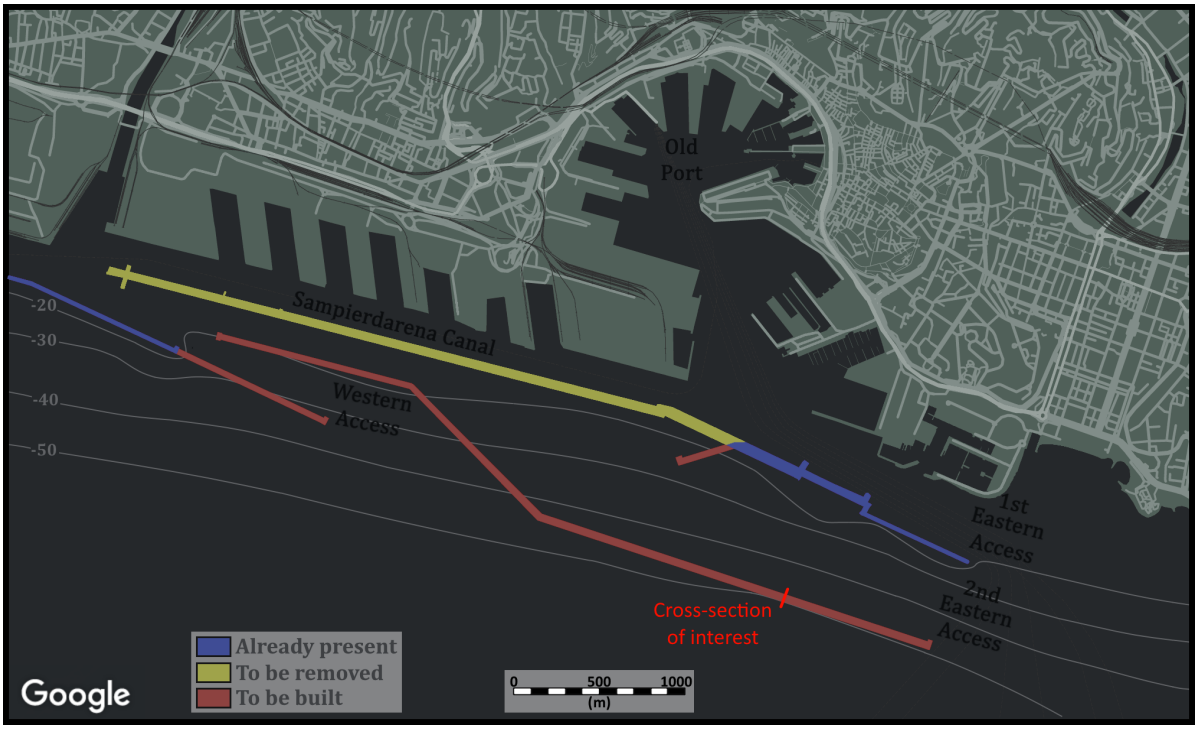

Figure 6.1: Overview of the plans for the new breakwater and the cross-section of interest.

The plan for the expansion of the Port of Genoa involves constructing a new breakwater further away from the coast, as well as demolishing part of the existing breakwater. The greater distance between the breakwater and the harbor allows larger ships to utilize the harbor. There were several proposals for the placement of the new breakwater. While finding the ideal placement is out of scope for this report, it does have major implications on the design. The design in this report will mainly be based on the premise of Solution 2 of the Ports of Genoa Project Dossier[60], as visualized in figure

6.1. This particular solution was preferred by both the Port Authorities and the nautical service, as as it offered better guarantees and greater safety margins in terms of ship maneuverability, in relation to the development of the access channel[60]. Incidentally, this solution is the most challenging (and interesting) from a design point of view, particularly due to the large water depth the breakwater reaches.

As can be seen in figure 6.1, the new breakwater stretches over a considerable difference in depth, from about 20m up to 50m. The new breakwater sections will be placed at various angles as well. Several kilometers of breakwater will be constructed in total. However, this chapter will only focus on a single cross-section, highlighted in figure 6.1 with a red line. This section is chosen as it is the longest part of the new breakwater. It sits at the deepest end, at 50 meters. It is also susceptible to wave attack from a wide range of angles.

6.2. Probabilistic design procedure

This section describes the method applied for the probabilistic design of the new breakwater. A fully probabilistic design will be carried out using a Monte-Carlo simulation of 10 different failure modes. For this purpose the relevant design criteria and target probabilities of failure need to be selected first.

6.2.1. Structure lifetime & probability of failure

This design working life, also referred to as the (design) lifetime, is the minimum amount of time that the structure is intended to maintain its function. Over the course of its life it is still possible the structure faces extreme loads that exceed those it was designed for, and thus failure may occur. While failure is not desirable, it is impossible to completely negate the possibility of failure transpiring. Therefore, design probabilities of failure will have to be chosen prior to design.

There exist standardized guidelines for determination of the design lifetime and the allowable probabilities of failure, several of which are summarized in the PIANC[19]. Italian guidelines[55] may be found in tables 6.1 and 6.2. The safety classes inside table 6.1 are defined as[19][55]:

- **Safety class 1:** Installations of local interest, minimum risk of loss of human life and environmental damages in case of collapse (coastal defences, minor or sea port works, sea wastepipes, coastal roads, etc.)
- **Safety class 2:** Installations of general interest, moderate risk of loss of human life or environmental damages in case of structural collapse (large port works, sea discharge exits of big cities, etc.)
- **Safety class 3:** Installations for flood protection, works of supernational interest, high risk of loss of human life and environmental damages in case of structural failure (protection of urban or industrial centres, etc.)

	Safety classes		
	Class 1	*Class 2*	*Class 3*
Type of work	**Minimum design working life [yr]**		
Infrastructure of general use	25	50	100
Infrastructure of specific use	15	25	50

Table 6.1: Italian Guidelines[55] for safety classes and design working life, as stated in the PIANC[19].

The new breakwater at the port of Genoa will be of large economic importance to the city. It will be placed significantly further away from the coast than the current breakwater, allowing larger ships to utilize the port. As a large port work and infrastructure of general use, it falls under safety class 2 with a minimum design working life of 50 years, according to table 6.1. 50 years is a typical lifetime for a breakwater structure[56][19].

A limit-state is a condition beyond which the breakwater no longer fulfills its function. It is a way of defining the fundamental requirements for the design situation[52]. Multiple limit-states may be defined. The probability of occurrence per limit-state depends on the consequences of the failure associated with it. A distinction is made between three limit-states:

- **Serviceability Limit-State (SLS)**: the structure no longer fulfills its function or performs significantly worse.

Incipient Damage	**Risk to Human Life**	
Economic Repercussion	Limited	High
Low	0.50	0.30
Medium	0.30	0.20
High	0.25	0.15
Total Destruction	**Risk to Human Life**	
Economic Repercussion	Limited	High
Low	0.20	0.15
Medium	0.15	0.10
High	0.10	0.05

Table 6.2: Italian Guidelines[55] for maximum probability of admissible damage Pf in the period of working life, as stated in the PIANC[19].

- **Repairable Limit-State (RLS)**: minor damage to the structure that could hinder the fulfilment of its function and/or integrity if ignored.
- **Ultimate Limit-State (ULS)**: major damage to the structure that destroys it partially or completely, rendering the fulfilment of its function null.

During SLS conditions, excessive port agitation endangers the operation and mooring of ships inside the port. A port should function as a safe haven for ships during a storm. Sailing during storm conditions is very dangerous, so it will be assumed that most navigation into- and out of the port will be halted for the duration of the storm, regardless of the agitation inside the port itself. If port agitation is severe enough, this may limit the manoeuvrability of emergency vessels and even put ships moored inside the port in danger. Economic repercussions for this event are relatively low. Damages and the risk to human lives are also kept to a minimum. Based on table 6.2, an appropriate probability of failure for SLS of 0.50 is chosen.

During RLS conditions, the breakwater suffers (slight) damages. These damages do not immediately put the integrity of the entire structure in danger. However, if neglected for a longer period of time, damages will increment and increase the risk of partial or total destruction. To alleviate this, checks on the structure should be enacted periodically, and damages found should be repaired. Risk to human life is still very limited, while economic repercussions are moderate. Based on table 6.2, an appropriate probability of failure for RLS of 0.30 is chosen.

Finally, during ULS conditions, the breakwater suffers large amounts of damages, possibly even (partial) destruction. This happens under extreme storm conditions. If severe enough, repair of the damages may result in closure of (part of) the port for months or even years. It is also possible that part of the harbor itself, or any ships moored during the event, suffer some damages. Based on table 6.2, a probability of failure for ULS of 0.15 is chosen.

The probabilities of failure described above are for the entire lifetime of the structure. Since the extreme values follow a Poisson distribution, the yearly probability of failure may be calculated with:

$$P_{f,L} = 1 - (1 - P_{f,yr})^L \tag{6.1}$$

Where $P_{f,L}$ is the lifetime probability of failure, $P_{f,yr}$ is the yearly probability of failure, and L is the design lifetime. The return period R may be calculated with:

$$P_{f,L} = 1 - e^{-L/R} \tag{6.2}$$

The exceedance probability gives the probability that a certain value will be exceeded. It means the probability that a single storm event causes a wave that exceeds the design wave. It may be calculated with:

$$P_{ex} = \frac{1}{N_s R} \tag{6.3}$$

Where N_s is the expected number of occurrences per year. During the extreme value analysis in Chapter 3, it was found there were on average 6.05 storms per year. Values for SLS, RLS and ULS are summed up in table 6.3.

Limit-state	$P_{f,L}$	$P_{f,yr}$	R	P_{ex}
SLS	50%	1.38%	72.1	0.229%
RLS	30%	0.71%	140.2	0.117%
ULS	15%	0.32%	307.7	0.054%

Table 6.3: Probabilities and return periods for various limit-states.

6.2.2. Monte-Carlo simulation

A Monte-Carlo simulation is a simple way to approximate the reliability of a complex system. In essence, a Monte-Carlo simulation is a brute force method which involves generating random variables and evaluating the structure's performance a large amount of times. The structure's performance will be evaluated through one or multiple limit-state functions, which are generally of the form:

$$Z = R - S \tag{6.4}$$

Where R resembles the structure's Resistance, and S resembles the load (or Solicitation) acting on the structure[52]. The parameter Z is known as the limit-state, which indicates whether the structure has failed or not depending on its sign. Both S and R are stochastic in nature, or consist of a combination of stochastic variables. Because of the stochastic nature, the result varies each time variables are generated. When S is larger than R, Z becomes negative, and this would signify a failure. This can be seen in figure 6.2. In the right figure, the diagonal reference line is where R = S. Any realizations above this line (colored red) are counted as failures. A limit-state function has to be defined for each failure mode considered in the design.

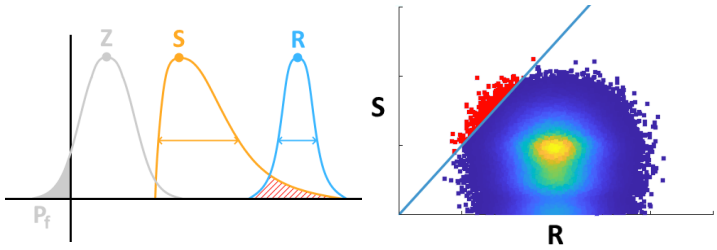

Figure 6.2: Left: Example distributions of an resistance R, load S and resulting limit-state Z. Right: Example of many realizations of R and S.

The resulting probability of failure per Monte-Carlo run can then be approximated with:

$$P_f \approx \frac{\sum Z(Z<0)}{\sum Z} \tag{6.5}$$

Where the numerator is the amount of failures, and denominator is the total amount of simulations. The more simulations realized, the more reliable the result gets. In theory, an infinite amount of simulations is required to get an exact answer for the probability of failure, which is obviously not possible in practice. A finite number of Monte-Carlo runs only give an approximation of the probability of failure. However, for a large amount of Monte-Carlo runs the probability will converge and eventually stabilize.

6.2.3. Design criteria

Design criteria are the precise goals that a project must achieve in order to be successful. In terms of design, that means the failure modes that the structure ought to resist. In section 5.5, 10 failure modes were highlighted for design. The corresponding limit-state functions are summed up as follows:

$$
\begin{aligned}
&Shoreward\ sliding: && Z_1 = \mu(W-U) - \gamma_{Goda} P_{wc} \\
&Seaward\ sliding: && Z_2 = \mu(W-U) - \gamma_{Goda} P_{wt} \\
&Shoreward\ overturning: && Z_3 = (Wt - M_U) - \gamma_{Goda} M_{P_{wc}} \\
&Seaward\ overturning: && Z_4 = (Wt - M_U) - \gamma_{Goda} M_{P_{wt}} \\
&Bearing\ failure: && Z_5 = p_{bc} - p_e \\
&Toe\ instability: && Z_6 = t - t_{cr} \\
&Berm\ instability: && Z_7 = W - W_{cr} \\
&Bottom\ scour: && Z_8 = u_{*cr} - u_{*b} \\
&Wave\ overtopping: && Z_9 = q_{cr} - q \\
&Wave\ transmission: && Z_{10} = H_{t,cr} - H_t
\end{aligned}
$$

The origin of the loads that act upon the structure was already explained in section 5.5. The suffix *cr* stands for critical. This is the critical value that denotes the threshold between failure and non-failure.

Caisson failure
Motion of the caisson, whether by sliding or overturning, puts the functionality of the entire structure at risk. In light cases, it significantly lowers the integrity of the structure and it is already difficult to repair. In more severe cases, entire rows of caissons could be displaced, effectively rendering the breakwater useless and a hazard for ships navigating nearby. Sliding and overturning, in either direction, correspond to the ULS condition.

Bearing failure
Bearing failure occurs when the bearing pressure exceeds the bearing capacity. If this happens then the rubble mound foundation collapses, causing the caisson to tilt and fracture. This has massive consequences for the breakwater. The crest height is lowered, causing greater wave overtopping and transmission. Fractures are not limited to a single caisson unit and could span large sections of the breakwater. Risk of heavy sliding or overturning is also significantly increased. In severe cases, the structure could completely collapse. Repairing this kind of damage, even in an early stage, is very difficult and expensive. For that reason, bearing failure should be avoided altogether, and therefore corresponds with the ULS condition.

Armor stability & scour
Scour and armor instability are the processes of erosion of the rubble mound foundation. It is a process that takes time, often taking many heavy waves to show significant damage. It also does not immediately put the integrity of the structure in danger. However, when neglected, structural failure becomes much more likely. Scour and armor instability may be allowed to some degree, but it should be detected and repaired before it becomes problematic to the structure. Checks of the rubble mound foundation should be carried out once in a while to make sure the breakwater remains safe. Still, scour should be a rare occurrence, as reparation of scour damage is expensive and difficult, and also requires part of the port to be closed during repair. Scour will be designed for RLS conditions only. It is assumed the ULS is never reached if periodic controls and reparations are performed.

Port agitation
Port agitation involves the failure modes of (excessive) wave overtopping and wave transmission. These failure modes are unlikely to directly cause heavy damage to the breakwater, but they do interfere with its serviceability and therefore correspond to the SLS condition. Excessive port agitation puts the harbor operations in danger, making navigation and mooring significantly more difficult. It is assumed that, during a storm event, normal navigation routines are kept to a minimum. During a storm the waves outside of the port easily reach higher than 2.5 meters, which is the threshold to allow for safe navigation[60]. While travel inside the port will be restricted during a storm, it should still be safe to traverse in case of emergencies and for utility vessels. In addition, ships moored at the berth basins should not experience heavy swaying or damages.

Table 6.4[39] shows the maximum significant wave height at which various port operations are still safe. Anchoring and mooring should remain possible under storm conditions, as the port should provide refuge for the ships. As stated before, it will be assumed that normal port operations are halted until after the storm has passed. It is not necessary for ships to be able to load and unload during a storm. A limit is selected at 50 centimeters for wave transmission so that the quay for rest is still available.

Port facility	Maximum significant wave height
Anchoring and mooring in a port is possible	0.70 m
Water way is available	1.20 m
Loading and unloading is possible	0.40 m
Quay for rest is available	0.50 m

Table 6.4: The maximum wave height at which port facilities and operations remain safe[39].

The EuroTop Manual has guidelines for the maximum allowed overtopping discharge, q_{cr}, for the safety of vessels inside a port. These are summed up in table 6.5. For larger waves the damage by overtopping is worse than for smaller waves, even if the overtopping discharge is the same[40]. Large vessels will suffer significant damage or sinking at 10 l/s/m for waves higher than 5m, and at 20 l/s/m for waves smaller than 5m. At these quantities there is still some danger for large ships navigating the canal or small ships moored at the berthing basins. However, fragile vessels may be moored at the Old Port, which is better sheltered against hazards.

Hazard type and reason	Mean discharge q (l/s/m)
Significant damage or sinking of larger yachts; H_{m0} >5 m	>10
Significant damage or sinking of larger yachts; H_{m0} = 3-5 m	>20
Sinking small boats set 5-10 m from wall; H_{m0} = 3-5 m	>5
Damage to larger yachts	
Safe for larger yachts; H_{m0} >5 m	<5
Safe for smaller boats set 5-10 m from wall; H_{m0} = 3-5 m	<1
Building structure elements; H_{m0} = 1-3 m	<1
Damage to equipment set back 5-10 m	<1

Table 6.5: General limits for overtopping for property behind the defence in the EuroTop Manual[40].

6.2.4. Stochastic parameter distributions

Wave characteristics are generated through a vine-copula model, see Chapter 4. Apart from wave and wind characteristics there are several other parameters with a stochastic nature. These will be discussed in this section. For a quick summation, see table 6.7. In theory, every parameter has a distribution of some kind. However, in many cases a deterministic simplification already suffices if deviations are quite small. Every parameter not mentioned in this section will be modelled deterministically.

Goda's method for wave-induced forces

Wave-induced pressures were estimated using Goda's method, as can be seen in section 5.3. While overall Goda's method was found to be quite reliable for vertical breakwater design[61], especially with Takahashi's modification for impulsive wave breaking, there have still been cases where the method provided flawed results[27]. Goda has taken a survey to assess the reliability of his method. He did so by calculating the safety factor for sliding for a few dozen breakwaters, some of which had failed under sliding. His results can be seen in figure 6.3.

The factor of safety for sliding is simply the resistance to sliding divided by the wave-induced horizontal force. If it is below 1, then the structure is likely to fail and vice versa. Overall, most breakwaters that failed had an S.F. lower than 1, and most that didn't fail had an S.F. greater than 1. This would indicate that Goda's method is reliable for design of vertical breakwaters[27]. There were, however, a number of cases where the structure failed even though it had an S.F. larger than 1, and vice versa. In deterministic calculations, Goda advises a safety factor of 1.2[27].

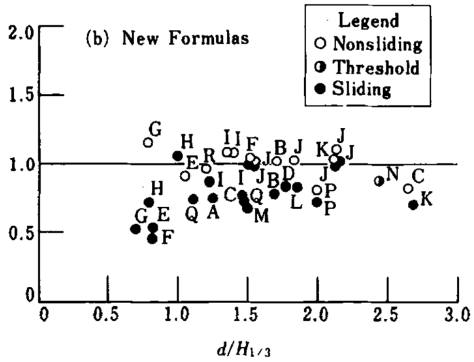

Figure 6.3: Goda's survey for a number of breakwaters[27].

The reliability of Goda's method has been analyzed through model tests on various vertical structures carried out at the Danish Hydraulic Institute and Delft Hydraulics[41]. The reliability could be expressed as the ratio between the measured and calculated forces and moments. It was found that, on average, Goda actually overestimates the wave-induced loading by about 10%. Based on the average of the highest 1/250-th values, van der Meer *et al.* (1994)[41] proposed the following reliability factors:

	Ratio measured/calculated	Mean	Standard deviation
Horizontal force	r_{Fh}	0.90	0.25
Horizontal moment	r_{Mh}	0.81	0.40
Vertical force	r_{Fb}	0.77	0.25
Vertical moment	r_{Mb}	0.72	0.37

Table 6.6: Comparison between the Goda method and measured values, from Van der Meer *et al.* (1994)[41].

The maximum wave-induced force is related to the number of waves that the breakwater faces during a storm, and not simply the 0.4% or 1/250-th wave only[41]. Van der Meer *et al.* (1994)[41] proposed an extra coefficient, r_N, for calculating the maximum wave-induced loading per storm:

$$r_N = \frac{F_{max}}{F_{0.4\%}} = \sqrt{\frac{ln(1/N)}{ln(0.004)}} \tag{6.6}$$

Where N is the number of waves per storm, typically ranging between 2000 and 3000 waves. To reflect this, N shall be modelled with a normal distribution of N(2500,500). The design equation for the maximum wave-induced force then becomes:

$$F_{max} = r_X \; r_N \; F_{Goda} \tag{6.7}$$

Where r_X represents the reliability factor corresponding to the force or moment in question, as listed in table 6.6.

Wave overtopping and transmission

The EuroTop Manual[40] stated the reliability of all empirical values used in the equations for overtopping. The standard deviations were already mentioned in section 5.5. All will be modelled with normal distributions. Heijn analysed the reliability of their wave transmission equation by comparing the calculated coefficient to the measured coefficient, and gave a reliability of $\sigma(K_t)$ = 0.015[30].

Material properties

The standard design density for quarry rock may be selected at 2650 kg/m^3. Density variation is a good indicator of quality variation, as it is correlated with stone porosity and degree of weathering. In general, the variability of mass density of one type of rock is limited, and the 90% exceedance value is not more than 100 kg/m^3[16]. A distribution of N(2650,50) is applied for rubble rock density. The weight of (dry) sand typically ranges between 1520 and 1680[16], so a distribution of N(1600,80) is applied.

For a plane concrete slab resting on quarried rubble stones, Takayama (1992) found as an average a static friction coefficient of μ = 0.636 and a coefficient of variation of 0.15[23]. A distribution of N(0.636,0.0954) is applied.

The Shields parameter is not a physical constant, but a value found by curvefitting[26]. The standard deviation of the Shields parameter is in the order of 15%[59]. For sand grains (with diameters of the order 0.1 - 1 mm), the mean value of the Shields stability parameter is 0.03[26]. A distribution of N(0.03,0.0045) is applied.

Water level and density

The seawater density in the Mediterranean Sea varies very little, only ±0.003 percent[42]. As such, it is modelled with a deterministic value of 1030 kg/m^3.

The still water level (SWL) will be modelled deterministically. It varied depending on the cross-section in question (see figure 6.1). Wind set-up and wind set-down depend on the fetch and the wind conditions section (see subsection 5.4). The drag coefficient for wind set-up and set-down will be modelled with a normal distribution N(3.75*10^{-6},0.25)[43]. Tide will be simulated by generating a random time. This will be done through a uniform distribution U(0,86160).

Parameter	Unit	Description	Distribution	Mean	STD	Source
H_s	m	Significant wave height	Vine-copula*	4.31	0.91	-
T_p	s	Peak wave period	Vine-copula*	8.90	0.74	-
Dir	°	Wave direction	Vine-copula*	229.2	17.4	-
w_{spd}	m/s	Wind speed	Vine-copula	15.6	3.7	-
w_{dir}	°	Wind direction	Vine-copula	-	-	-
H_0	m	Deepwater wave height	Vine-copula	4.21	0.83	-
T_0	s	Deepwater wave period	Vine-copula	8.90	0.73	-
r_{Fh}	-	Goda horizontal force reliability factor	Normal	0.90	0.25	[41]
r_{Mh}	-	Goda horizontal moment reliability factor	Normal	0.81	0.40	[41]
r_{Fb}	-	Goda vertical force reliability factor	Normal	0.77	0.25	[41]
r_{Mb}	-	Goda vertical moment reliability factor	Normal	0.72	0.37	[41]
N	-	Number of waves in storm	Normal	2500	500	[41]
μ	-	Friction factor (concrete and rubble)	Normal	0.636	0.095	[23]
ρ_w	kg/m^3	Seawater density	Deterministic	1030	-	[42]
ρ_r	kg/m^3	Rubble rock density	Normal	2650	50	[16]
ρ_s	kg/m^3	Sand density	Normal	1600	80	[16]
ρ_c	kg/m^3	Concrete density	Normal	2400	25	[16]
Ψ_c	-	Shields stability parameter	Normal	0.03	0.0045	[59]
0.047	-	EuroTop eq. 7.1	Normal	0.047	0.007	[40]
2.35	-	EuroTop eq. 7.1	Normal	2.35	0.23	[40]
0.05	-	EuroTop eq. 7.5	Normal	0.05	0.012	[40]
2.78	-	EuroTop eq. 7.5	Normal	2.78	0.17	[40]
0.011	-	EuroTop eq. 7.7 & 7.14	Normal	0.011	0.0045	[40]
0.0014	-	EuroTop eq. 7.8 & 7.15	Normal	0.0014	0.0006	[40]
K_t	-	Transmission coefficient	Normal	Varies	0.015	[30]
h	m	Still water level	Deterministic	50	-	[60]
t_{tide}	s	Tidal time	Uniform	43080	24872	[48][14]
C_2	-	Drag coefficient for wind set-up/down	Normal	3.75*10^{-6}	0.25*10^{-6}	[43]

Table 6.7: Distributions of every stochastic parameter for the Monte-Carlo simulation.

6.3. Design proposal

A Monte-Carlo simulation was developed in MATLAB using the design criteria and limit-state functions described in previous parts. The simulation ran for 150.000 iterations with 10 limit-state functions. The simulation was run several dozen times with slight adjustments to optimize the design. Optimized meaning here: fulfills the design criteria for the lowest material cost. For the MATLAB code, see Appendix E. This section only describes the choices made for the cross-sectional design. See Appendix F for a few of the preliminary Monte-Carlo simulations, which show the effect of some of the design decisions taken. Figure 6.4 shows the cross-section of the proposed design. Measurements are given in meters. Table 6.8 shows all materials used for the design as well as their volume and weight per meter width. It should be noted that the design proposal in this section serves only as a preliminary cross-sectional design. Only the 10 failure modes as described in Chapter 5 are taken into consideration.

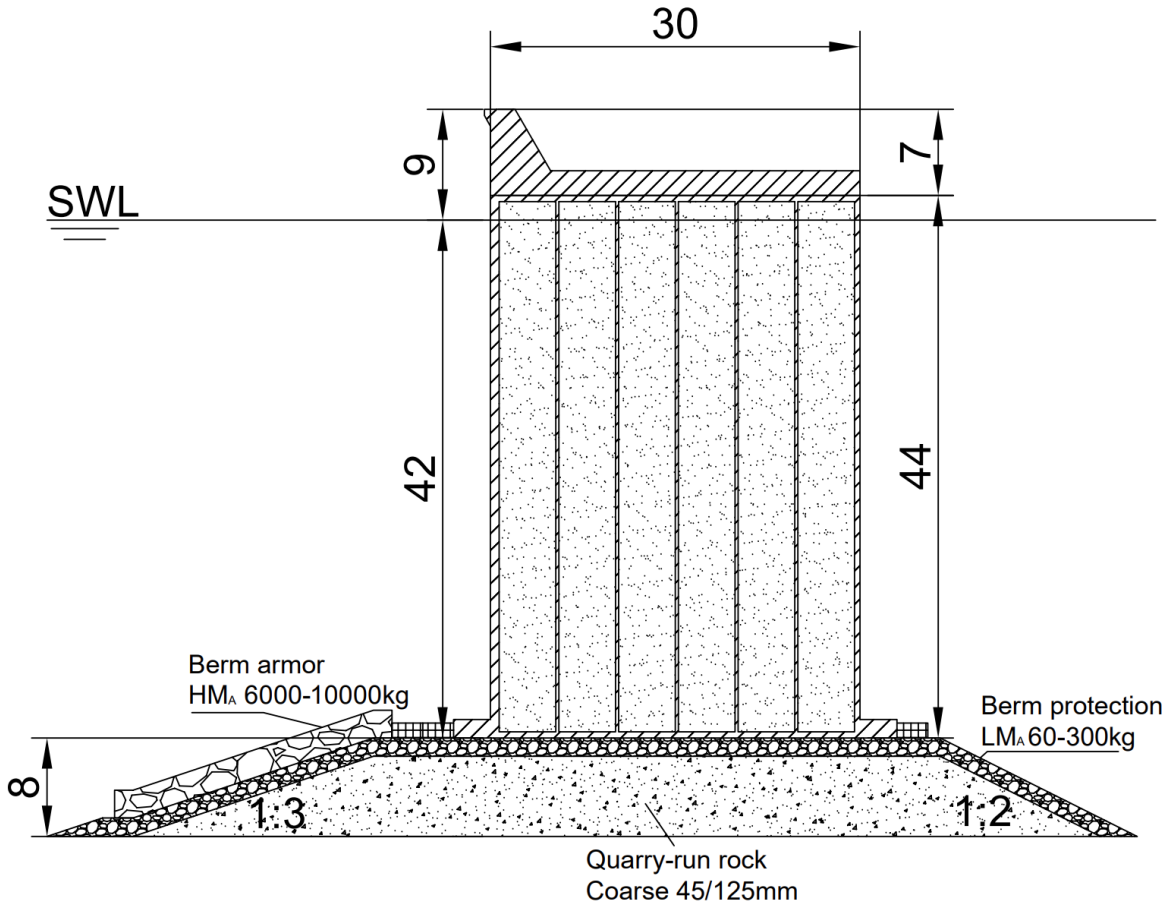

Figure 6.4: Overview of the proposed design.

Component	Material	Mean density [kg/m^3]	Volume [m^3/m]	Weight [ton/m]
Caisson walls	Concrete	2400	142	341
Caisson filling	Sand	1600	1187	1899
Crown	Concrete	2400	78	187
Toe protection	Concrete	2400	9	22
Berm armor	HM_A 10-15t	2650	50	133
Berm protection	LM_A 60-300kg	2650	127	337
Mound core	Coarse 45/125mm	2650	405	1073
Total	**-**	**-**	**1998**	**3992**

Table 6.8: Materials and weight per meter width of the design proposal.

6.3.1. Caisson design

It was found during the simulation that bearing failure was the most frequently occurring failure mode for the ULS, see table 6.9. This was best counteracted by increasing the width of the caisson, which spreads the bearing pressure exerted on the rubble mound over a larger area. This in turn also reduced the amount of cases of sliding. A downside of increasing the overall width of the caisson is that it requires a larger amount of material, increasing its weight. While the increased width spreads the bearing pressure over a larger area, it also increases the absolute bearing pressure force exerted because the caisson is heavier. It also creates larger arms for the moments, which increased the risk of overturning. A width of 30 meters was not enough to fulfill the design criteria for bearing failure. However, instead of further increasing the width, the addition of a wider bottom slab was applied. This is a large concrete slab connected to the caisson which increases the area of the caisson without making it significantly heavier. The bottom slab added another 3 meters of width on either side of the caisson. This brought the total bottom width of the caisson to 36 meters, without significantly increasing its weight. It should be noted that there is a risk that the concrete slab cracks due to wave-induced pressures. This is a new failure mechanism, which wasn't considered in the design.

While running the simulation, it was found quite a large freeboard was needed to properly counteract wave overtopping. A freeboard of 11 meters was needed to fulfill the design criterion for overtopping. One way to reduce the risk of excessive wave overtopping is by applying a bullnose to the crest of the structure. This is a ridge that sticks out at the front and directs overtopping discharge back to the sea. A bullnose is most useful for small overtopping quantities and when it is significantly above the still water level, because otherwise the bullnose will simply be submerged and have little to no effect[40]. The EuroTop manual contains detailed equations and guidelines for bullnoses. After applying the bullnose, it was found that the freeboard could be reduced to 9 meters. A choice was made for a bullnose of half a meter wide with an angle of 60 degrees, as this was a relatively small extension. Changes in the wave-induced pressure distribution and the risk of cracks occurring in the bullnose were not considered. To decrease the weight of the caisson, a concrete crown was applied to the top of the structure. The crown reduces the amount of material needed to reach the same crest height. It is a large prefabricated concrete slab with a wall on one end. The wall will function as the crest which faces wave attack. Cracks and collapse of the crown wall as a result of wave attack was not considered in design.

The caisson will be partitioned into compartments which will be filled with sand. This makes it easier to transport and place, as well as reduces the total weight of the structure. Goda advises outer walls of 50 centimeters thick, as these face the blunt force of the wave attack. The partition walls between the sand-filled compartments only need to be 25 centimeters thick. Goda also advises keeping the width of the sand-filled compartments below 5 meters. So, the entire width of the caisson will be divided into 6 compartments, each 4.6 meters wide.

6.3.2. Rubble mound design

The rubble mound functions as a foundation to spread the weight pressure of the caisson over the seabed. It is best to keep the rubble mound as low as possible to prevent the generation of large wave pressure due to wave breaking[27]. On the other hand, the deeper the top of the rubble mound is, the more difficult it is for divers to reach. Divers are necessary for level placement of the caisson or reparations. Due to a difference in pressure, gases in breathing air can become toxic and induce a drunkenness effect. Nitrogen narcosis becomes a hazard beyond 30 meters deep, which influences the diver's judgement, vision and hearing[21]. This could lead to dangerous situations during construction activities. To prevent this, special gear, training and even breathing gas are necessary for deep diving operations. A choice was made to set the rubble mound height at 8 meters, which sets the top of the rubble mound at approximately 42 meters deep relative to the still water level. At this depth it is still possible for a trained diver to breath normal air[21].

Goda advises the placement of two toe protection blocks at the front and one at the rear[27]. Based on the results of the Monte-Carlo runs, the thickness of the toe protection blocks was selected at 1.3m. The dimensions of the toe protection blocks were selected at (l x b x t): 5 x 2.5 x 1.3. It was found that armor stones with a weight of 8 tons were sufficient to ensure the criteria for berm armor stability. The grading HM_A 6-10t was taken, which is the second largest standard grading listed in Chapter 3 of *The Rock Manual*[16]. A secondary layer of berm protection is placed underneath the berm armor to serve as a filter as well as to protect the rubble mound from wave-induced currents on the portside of the structure. The grading of this layer was determined on the three filter criteria for geometrically

closed filters[26], as previously explained in section 5.5. A grading of LM_A 60-300kg sufficed the filter criteria. The core of the rubble mound will be constructed out of quarry-run rock, of the grading Coarse 45/125mm. Goda advises applying a slope of 1:3 at the seaside and a slope of 1:2 at the portside[27].

6.3.3. Results of the Monte-Carlo simulation

The design was made using the Monte-Carlo simulation, which had to be run several dozen times to find an optimized design. The resulting cross-sectional design sufficed for all design criteria. Results are summed up in table 6.9. The Monte-Carlo simulation was run for a total of 150.000 iterations. OR statements were used for counting the failures for the limit-states, so that a multiple failures within the same limit-state would only be counted once per iteration. For example, during one iteration it is possible the structure fails on both shoreward and seaward sliding. These two failure modes both belong to the Ultimate Limit-State, so only 1 ULS failure will be counted for this iteration. See the code below:

```
if Z1(ii)<0 || Z2(ii)<0 || Z3(ii)<0 || Z4(ii)<0 || Z5(ii)<0 % total destruction
    nfail_ULS(ii) = 1;
end
if Z6(ii)<0 || Z7(ii) <0 || Z8(ii)<0 % scour & armor instability
    nfail_RLS(ii) = 1;
end
if Z9(ii)<0 || Z10(ii) <0 % port agitation
    nfail_SLS(ii) = 1;
end
```

Where *nfail* is an array filled with zeroes and ones. The sum of *nfail* is the total number of failures for a limit-state. The proposed design fulfilled the limit-state criteria for ULS (15%), RLS (30%) and SLS (50%). It should be noted that, since the Monte-Carlo simulation gives only approximations of the probabilities of failure, results differ slightly if the simulation was run again with newly generated input variables. Generating wave and wind variables was very time-consuming due to the complexity of the vine-copula model and the onshore wave transformation in SWAN. So, only a single, previously-generated, set of 150.000 wave and wind variables was utilized for all Monte-Carlo simulations. Every other parameter, as listed in table 6.7, was newly generated with each run.

Failure mode	**Number of failures**	$\mathbf{P_{f,yr}}$	$\mathbf{P_{f,L}}$
Shoreward sliding	23	0.09%	4.5%
Seaward sliding	8	0.03%	1.59%
Shoreward overturning	26	0.1%	5.07%
Seaward overturning	0	0%	0%
Bearing failure	44	0.18%	8.43%
Toe instability	130	0.52%	22.95%
Berm instability	2	0.01%	0.4%
Bottom scour	0	0%	0%
Wave overtopping	307	1.23%	46.09%
Wave transmission	3	0.01%	0.6%
Limit-state			
ULS	77	0.31%	14.29%
RLS	132	0.53%	23.26%
SLS	310	1.24%	46.41%

Table 6.9: Results of 150.000 Monte-Carlo runs.

Figure 6.5 shows the scatterplots of all 10 failure modes. As can be seen, some failure modes never occurred at all, while others occurred relatively frequently. The dominant failure mode for the ULS was bearing failure, which occurred 44 times out of 77 ULS cases. It was found that this type of failure was very sensitive to adjustments to the width of the caisson, particularly the width of the bottom slab. The dominant failure for RLS was toe instability, as it occurred 130 times out of 132 RLS cases.

Bottom scour never occurred in any iteration, as the critical shear velocity was always several times larger than the wave-induced shear velocity. Finally, overtopping was the dominant failure mode for the SLS condition, occurring 307 times out of 310 SLS cases, the most often out of all failure modes analysed.

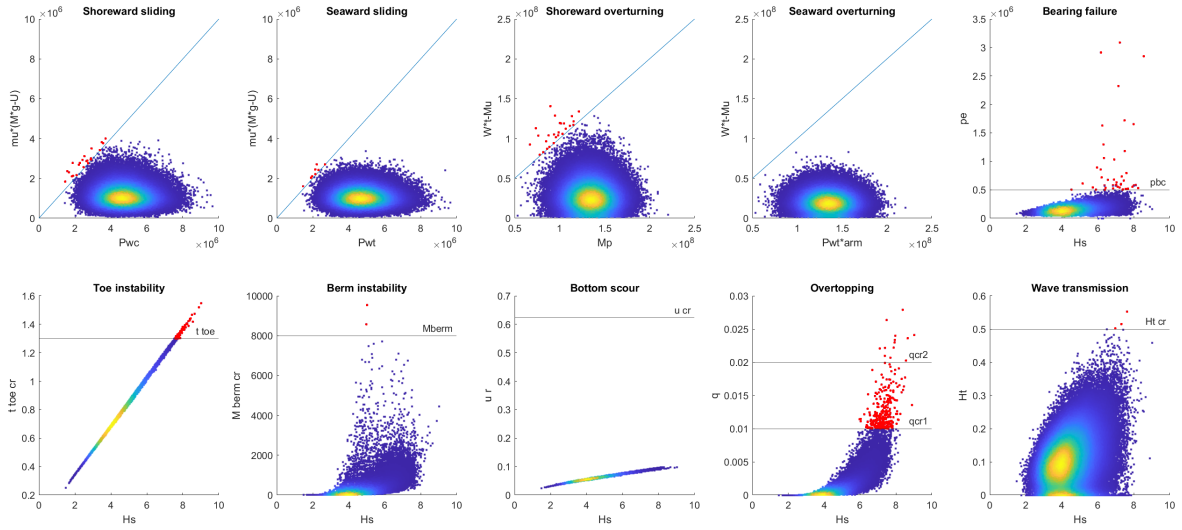

Figure 6.5: Scatterplots of all 10 failure modes.

Figure 6.6 shows the probabilities of failure for the three limit-states as a function of the amount of iterations used in the simulation. As can be seen, the longer the simulation, the less the probabilities tend to deviate. Running the simulation for the entire length of the dataset took about 8 minutes. As can be seen in figure 6.6, the probabilities already start to stabilize at around 50.000 iterations. The lack of variance in the calculated probabilities of failure indicates the reliability of the result of the Monte-Carlo simulation. Running the simulation again did not result in significant differences in the probability of failure.

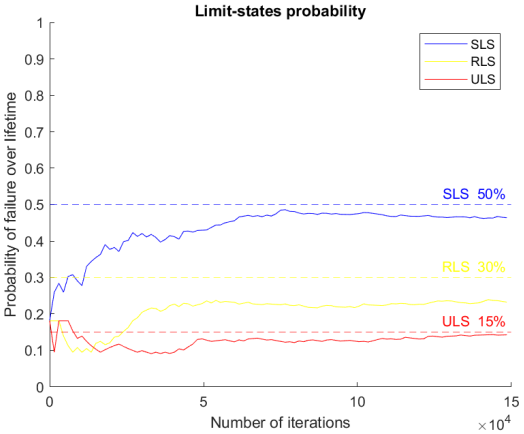

Figure 6.6: Stability of the probability of failure for the three limit-states.

7

Effect of dependence modelling

This chapter seeks to answer research question 1.4: What is the effect of accounting the dependencies between wave climate variables? In this chapter, the same design will be tested against values generated from an independent model. The purpose of this exercise is to examine the effect of taking correlations into account and see how differently an independent model performs in a Monte-Carlo simulation for the same breakwater design.

7.1. Independent model

In an independent model, all variables are generated separately with only univariate distributions. Correlations between the variables are not taken into account. This simplifies and speeds up the process of fitting a model and generating values. However, ignoring correlations between variables might lead to unrealistic combinations of variables which are very likely, if not impossible, to occur in nature. As a result, the generated dataset may not accurately represent the original data it was fitted on, which can give erroneous estimations when using them in design equations. This chapter seeks to find out the effect of using an independent model, as opposed to the vine-copula model developed in Chapter 4.

The independent model will be developed through a MATLAB script called *fitmethis*[24], which finds the best fitting distribution on a dataset out of all standard MATLAB probability distributions. By default, MATLAB contains 20 continuous and 5 discrete distributions. *Fitmethis* was applied to each of the five variables. Just like in Chapter 4, the AIC is chosen as the preferred criteria for picking the best fitting distribution. The five resulting distributions are listed in table 7.1.

150.000 values were generated with the independent model. Figure 7.1 shows two plotmatrices, comparing data generated by the vine-copula and the independent model. There are some clear differences in both the univariate and bivariate distributions. Firstly, the independent data contains heavier tails. This might be related to the input methodology used for fitting. The fitting data used for the vine-copula model was transformed to the copula scale using the *ksdensity(x,x,'function','cdf')* function, because copula functions are defined in the unit domain with uniform marginals (between 0 and 1). This function estimates the probability of values not observed in a different way than univariate probability distributions, resulting in more outliers. The highest wave in the original data measured 6.8 meters, while it was 7.7 in the vine copula and 12.3 in the independent model. Secondly, the independent data contains combinations of variables which didn't occur in the original data. For example, wind

Variable	**Distribution**	μ	σ	ν
Wave height	Generalized extreme value	0.116	0.574	3.80
Wave period	Generalized extreme value	0.016	0.564	8.57
Wave direction	t location-scale	231.9	4.36	1.47
Wind speed	Extreme value	17.29	2.92	-
Wind direction	t location-scale	237.7	9.35	1.08

Table 7.1: Distributions and parameters of the independent model. The fitting was done using *fitmethis*[24].

and wave direction are often somewhat aligned, resulting in a dense cluster of datapoints with few outliers, as can be seen in the vine-copula data. In the independent model the cluster is a lot less dense, and a cross-shape of outliers appears. There were several cases where the wind and wave directions opposed each other, which in reality only occurs with swell waves (which aren't present in this region). Another aspect is the relation between the wave height and the wave period, which is linked to the wave steepness. Waves can only obtain a certain amount of steepness before their height is limited by wave breaking. A short wave period means a shorter wave length, which results in a higher steepness. Higher waves are limited by their steepness, and thus require a high wave period to prevent breaking. This is why there is often a positive correlation between wave height and wave period. This correlation is absent in the independent data.

The independent model was validated the same way as the vine-copula was in Chapter 4. The Normalized Root-Mean-Square Errors (NRMSE) are shown in figure 7.2. Overall, the independent data scored worse than the vine-copula. The sum of the absolute differences of all correlation coefficients for the independent model equaled 5.91, as opposed to only 0.40 for the vine-copula.

Variable	NRMSE Vine-copula	NRMSE independent
Wave height	1.12%	1.19%
Wave period	0.91%	1.01%
Wave direction	0.66%	6.39%
Wind speed	0.90%	11.77%
Wind direction	0.97%	7.39%

Table 7.2: The NRMSEs between the extreme data and data generated using the independent model.

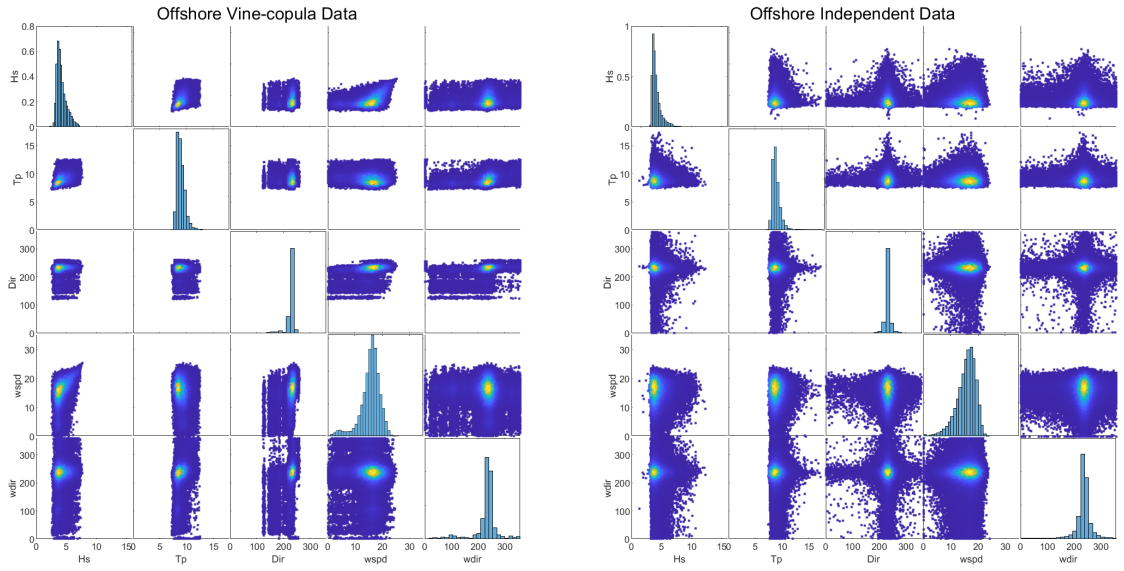

Figure 7.1: Plotmatrix comparison between offshore independent data and vine-copula data.

To get the onshore data, the data from the independent model had to be transformed in SWAN. For more information about this, see section 5.2. The onshore waves are at a location with a water depth of 50 meters. The result are shown in figures 7.2 and 7.3. Wind data was excluded from this figure since SWAN only transforms waves.

One stark difference between the two datasets is that the independent data contains significantly larger waves than the vine-copula data. This was found to already be the case in the offshore data. Shoaling has increased the size of the waves significantly. There is a heavy tail of high waves with relatively short wave periods. Waves with a low wave period also have a shorter wave length and are thus steeper. Shoaling starts influencing a wave once it enters transitional water, which starts at $h/L = 1/2$. Wave breaking may occur once the wave enters shallow water, at $h/L = 1/20$[31]. The

SWAN calculation stops at 50 meters deep, because that is the depth where the breakwater will be placed. This is not yet shallow enough for the wave heights to be limited by breaking, but plenty for shoaling to take effect. On average, waves of the independent model experienced slightly greater shoaling than those from the vine-copula. The onshore waves end up larger, because the independent offshore data already contained much higher waves than the vine-copula. The independent onshore data had some very steep waves due to the combination of low wave periods and high wave heights, with the highest steepness of 0.1.

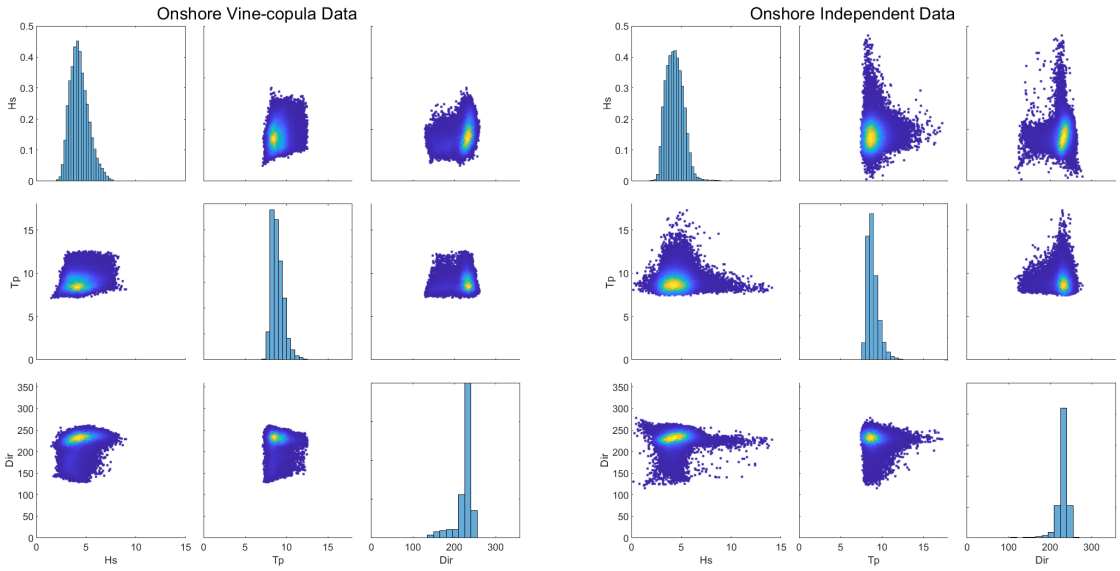

Figure 7.2: Comparison between independent data and vine-copula data after applying SWAN.

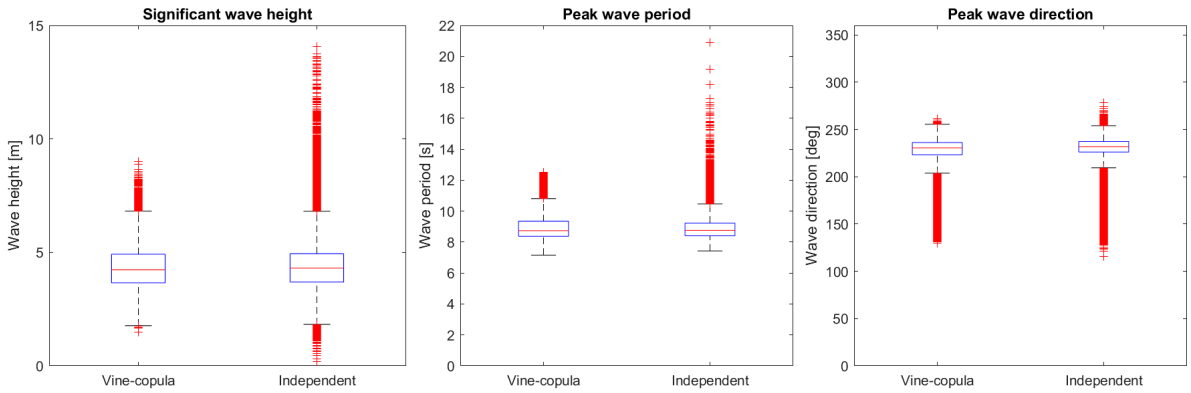

Figure 7.3: Boxplot comparing the onshore vine-copula model with the onshore independent model.

7.2. Performance evaluation

For the final step, the onshore independent data was used as input for the Monte-Carlo simulation. The same design and the same settings as described in Chapter 6 were used to allow for a fair comparison with the vine-copula model. Results of the Monte-Carlo simulation are shown in table 7.3.

Failures occurred more often in almost all cases. The amount of ULS cases roughly doubled, namely due to an increase in the amount of occurances of shoreward sliding, shoreward overturning and bearing failure. The amount of cases of RLS cases increased more than sevenfold due to more cases of toe and berm instability. Lastly, the amount of RLS cases tripled. As a result, the probabilities of failure became far larger than the acceptable threshold. The worst change was in RLS, which now has more

Failure mode	Number of failures	$P_{f,yr}$	$P_{f,L}$
Shoreward sliding	62	0.25%	11.68%
Seaward sliding	7	0.03%	1.39%
Shoreward overturning	43	0.17%	8.25%
Seaward overturning	0	0%	0%
Bearing failure	89	0.36%	16.33%
Toe instability	971	3.88%	86.2%
Berm instability	171	0.68%	29.05%
Bottom scour	0	0%	0%
Wave overtopping	1069	4.28%	88.75%
Wave transmission	89	0.36%	16.33%
Limit-state			
ULS	156	0.62%	26.87%
RLS	975	3.9%	86.32%
SLS	1070	4.28%	88.78%

Table 7.3: Results of 150.000 Monte-Carlo runs.

than a 85% probability of occurring in 50 years, while the design criterion was only 30%. In short, the same breakwater performed significantly worse with the independent data. Clusterplots of all failure modes can be found in figure 7.4. Not only did failures occur much more often, there were also significantly larger solicitations overall. This can be seen with every failure mode, but particularly with wave overtopping and berm stability. With the vine-copula data, the largest overtopping discharge was about than 30 l/s/m, while the simulation with independent data returned many discharges above 100 l/s/m. The highest required berm protection weight was about 8 tons for the simulation with vine-copula data, while for the independent data there are a few cases where more than 40 tons is required.

If the independent model was used for designing the breakwater then it would've required much larger dimensions. The crest height would need to be several meters higher, the caisson wider, and the berm and toe protection much heavier. This would drive up construction costs significantly in order to build a structure that can satisfy the design criteria. Judging from the above results, it stands to reason that correlations between wave and wind variables should not be neglected in a probabilistic design.

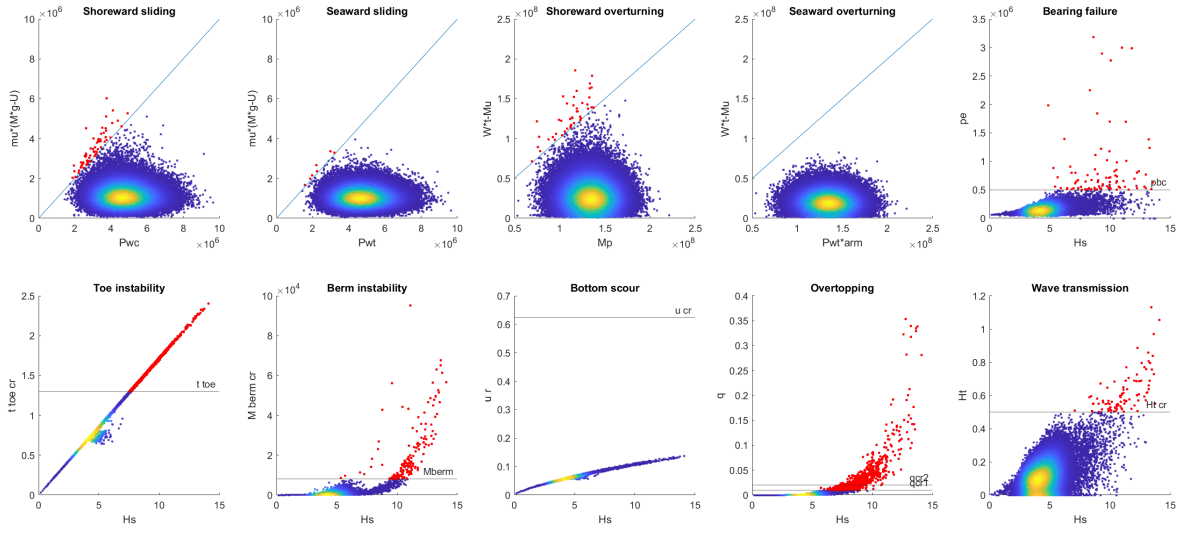

Figure 7.4: Scatterplots of all 10 failure modes.

8

Discussion

During the course of this report several assumptions were made which could skew the results and could possibly lead to wrong estimations. These assumptions were often made for the sake of simplicity and/or due to a lack of available data on the subject. This section discusses the main assumptions made in this thesis.

8.1. WavewatchIII for wave climate data

A large difficulty in this project was the lack of wave and wind data available. Only two buoy records were present in the Gulf of Genoa, neither of which were located near the area of interest. While La Spezia contained a record of 26 years long, the data from Capo Mele was only 7 years long. It was found out that 7 years was too short to give a meaningful result in an extreme value analysis (see Appendix C). In addition, both datasets contained numerous erroneous values or missing entries. The lack of data was resolved in Chapter 2, where data was obtained by correcting the biases found in WavewatchIII. This was done so by first correcting WavewatchIII against the buoy records of La Spezia and Capo Mele, which gave two different correction splines. The correction used for Offshore Genoa was simply the weighted average of the correction splines, based on the distance between the two buoys and the point of interest.

It was assumed that WavewatchIII shows a similar bias on a regional level, and that taking the weighted average of two biases would give an accurate approximation of the bias for a location in the middle. A performance evaluation of WavewatchIII in the Mediterranean basin[15] showed that, overall, WavewatchIII contains similar biases between various locations. For example, WavewatchIII tended to underestimate the highest waves in particular. Still, in this thesis only the biases on two locations could be analyzed in detail. To get a more accurate estimation, the QUANT method ought to be applied to more locations before an average is taken. It was also assumed that the buoy records were long enough to give an accurate estimation of the bias of WavewatchIII. While this may be the case with La Spezia, the buoy record of Capo Mele was rather short and could give a wrong impression of WavewatchIII's bias for extreme values.

For the wind, data from WavewatchIII was used, as this was the only data available. The bias of WavewatchIII with regards to wind data is unknown. Since the wind plays a large factor in the transformation to onshore waves done in SWAN, biases in the wind data could lead to an erroneous calculation of the onshore wave characteristics.

8.2. Multivariate modelling

A vine-copula model was developed to consider the correlation between extreme parameters. The best-fitting vine-copula was chosen based on AIC, out of all 480 possible regular vines as well as all 13 copula families available in MATVines.

There are two issues concerning the input used for model-fitting. The first is fairly straightforward. The vine-copula was fitted on 243 extreme events, which was then used to generate 150.000 values. It might be possible that the small amount of extreme values was not enough input for the model to be

representative of the extreme wave climate. Obviously, the accuracy of the model will increase if more input was available to be used. While more data was not available, the amount of extremes could be 'increased' by lowering the threshold for selecting extremes. While it is desirable to retain as much input data for the model as possible, one must also be strict with the choice of threshold. This brings up the second issue: the definition of what constitutes as extreme. In Chapter 3, extremes were selected using the Peak over Threshold method, which functions with a predefined threshold and timelag. While this method works fine in a univariate case, the way it needs to be applied becomes more ambiguous in the multivariate case. The threshold is a single value which can only be used to select the extremes of one variable. A way to select a multivariate threshold has not been formally defined yet. One way to resolve this is by selecting one of the variables as the dominant one and applying the PoT method to only this variable[46]. Values of other variables which were concomitant to the extremes found (occurring at the same instance of time) are picked to get the multi-variable extreme dataset. The problem with this solution is that it isn't always obvious which variable is dominant. In this case, the wave height was deemed as the biggest contributor to wave-induced loading on the structure and was thus selected as the dominant variable.

A third point arises with the methodology applied in the modelling itself. *MATVines* utilizes 13 different copulas for fitting. This isn't a small amount, in fact, MATLAB only contains 5 different copulas by default (Gaussian, Student's t, Clayton, Gumbel and Frank). However, there are many more ways to define a copula function. It is possible that the 'best' copulas are ones that aren't utilized by the package, and will therefore be missed in the fitting process. Furthermore, while a vine-based approach was taken in this thesis, this is hardly the only way to model multivariate data. Assuming independence, a single multivariate copula (such as the Gaussian or Student's t) or computation fluid dynamics may also be sufficient ways for developing a model of the wave climate. Chapter 7 gives a comparison between an independent model and the vine-copula. The vine-copula model was validated by comparing it to the initial dataset (extremes of Offshore Genoa). This was numerically expressed by calculating the normalized root-mean-square-errors and the sum of the absolute differences between the correlation coefficients. This returned relatively low values, which indicates a favorable result. The same was done for the independent model in Chapter 7, which performed worse in that regard.

The fourth and final point is in regards to the stability of the wave climate. In this thesis, it was assumed that the wave climate remains constant, i.e.: what is seen as an extreme occurrence today is no different to what is seen as extreme in the future. The problem with this is, of course, that the wave climate is not static. Changes in both global and local climates have been well-documented for decades. The breakwater is designed to last for a minimum of 50 years. It is possible that during this time period the wave climate becomes more extreme, therefore increasing the loads on the structure and increasing the probability of failure. Not to mention sea level rise. Current forecasts predict a rise in the Mediterranean Sea between 9.8 and 25.6 centimeters by 2050[25]. The vine-copula model was not built to predict changes in the wave climate in the future, and could underestimate the actual loads that the structure will face during its lifetime. The magnitude of the consequences of assuming a static wave climate has not been analyzed.

8.3. 1-Dimensional bathymetry in SWAN

Wave transformation between offshore and onshore waves is a complex process which depends heavily on the bathymetry. While SWAN is capable of processing a 2-dimensional bathymetry, only a 1-dimensional bathymetry was used as input. This was a practical choice, as during the process it was found out that SWAN was by far the largest bottleneck. While obviously much faster than the manual process, the SWAN loop was capable of processing about 10 cases per second. This meant that it took several hours to transform all 150.000 values. Applying a 2D bathymetry instead of 1D would've slowed the process down significantly more. Therefore it was determined that applying a 2D bathymetry simply wasn't possible within a reasonable timeframe, and a 1-dimensional abstraction was used instead. The consequences of this decision are difficult to estimate. There is a large underwater canyon inside of the Gulf of Genoa, which consists of many complexly-shaped higher and lower areas. The largest influence this would likely have is on wave refraction, which influences the direction of the waves. The presence of the canyon may also induce wave focusing resulting in higher waves onshore.

8.4. Failure modes considered

The interaction between a breakwater and its environment is a complex setting that required several simplifications to be able to be modelled in a Monte-Carlo simulation. Only 10 different failure modes were considered in the design, other failure modes were neglected. A choice was made to include only these 10 failure modes, as they were deemed most important for design. This was decided based on sources about the design of vertical breakwaters, particularly in accordance with Prof. Goda's book *Random Seas and Design of Maritime Structures*[27].

Some failure modes were intrinsically very hard to model in a probabilistic setting. These include accidents (ship collision), destructive natural events (earthquakes, tsunami's) or even deliberate destruction (acts of terrorism). The causes for all of these are complex and varied, and go beyond the scope of this thesis. Other failure modes were neglected for the sake of simplicity. These include any 2-dimensional fluid dynamics, as the focus for the design was for a single cross-section only. In the case of port agitation for example, phenomena such as wave reflection, diffraction, resonance and penetration inside the port were all neglected. These could not be analyzed in a 1-dimensional approach, and would require a model of the entire port. Other examples are material erosion, internal structural integrity, slope stability and settlement of the subsoil.

Finally, there are the unknown unknowns: failure modes which were not considered because little to nothing was known about them. These may be so unexpected that they were never even considered a possibility to begin with. This does not mean they are completely irrelevant. In fact, failure often occurs through a hazard which wasn't recognized prior[52]. This group becomes smaller over time as more research is gathered and experience is gained.

8.5. Reliability of the design equations

The failure modes that were considered in the Monte-Carlo simulation were analyzed with limit-state functions. These functions were based on empirical equations found in literature. However, empirical equations provide only an estimation. Some of the most important calculations used in this thesis were Goda's method for wave-induced loading, in combination with Takahashi's extension for compulsive wave breaking. This is a method used throughout the world[61]. It was used for five of the ten failure modes considered in this thesis. Research conducted by van der Meer *et al.* (1994)[41] showed that, on average, Goda tends to underestimate the wave-induced loads. However, there was a considerable scatter present in the ratio between measured and calculated loads. The reliability of Goda's method was modelled by applying reliability factors taken from this research. However, because of the large amount of scattering in the data, Van der Meer advises to always conduct model tests to reduce the standard deviation of design loads[41]. This wasn't a possibility in this project, and as a consequence there is a large uncertainty in the results.

For wave overtopping the EurOtop Manual was consulted. The design equations were very detailed and the standard deviation of each was also provided. Still it can be concluded that overtopping rates calculated by empirically derived equations, should only be regarded as being within, at best, a factor of 1 - 3 of the actual overtopping rate[40]. This means the actual overtopping quantity could be between three times smaller up to three times larger, which is almost an entire order of magnitude in difference. In addition, it is known that the size of overtopping quantities are very sensitive to the geometry of the structure. The general equations used in the EurOtop Manual only serve as very rough estimations. For greater accuracy, it is advised to construct either a computational fluid dynamics model or a physical model to verify the overtopping quantity.

9

Conclusion & Recommendations

9.1. Conclusion

The main goal of this thesis was to perform a fully probabilistic preliminary cross-sectional design of the new breakwater of Genoa by applying a vine-copula model in a Monte-Carlo simulation. This goal was managed by posing two main research questions:

1) How can a representative wave climate for Genoa be modelled?

2) What does a fully probabilistic cross-sectional design of the new breakwater in Genoa look like?

In regards to the first research question, a vine-based approach was taken for modelling the multivariate extreme wave climate. This is a relatively new method for modelling that has only recently been gaining popularity for utilization in probabilistic design. All possible 5-node regular vines were fitted on the dataset. The best vine out of these was selected based on the lowest AIC value. However, after the fitting process, it was found that there wasn't actually that much variation in the AIC values. Out of the 5 tree-equivalent vines V6 to V10, only the D-vine V6 performed notably worse. This indicates that, in this case, most tree-equivalent vines are capable of yielding a model that performs reasonably well. Whether the D-vine always performs worse cannot be concluded from just this result. It should still be stressed that AIC is only a relative indicator of the goodness-of-fit, so from these values it cannot yet be concluded whether the best-fitting vines are actually good models of the data. Validation of the vine-copula model was done through NRMSEs and the sum of the absolute differences in correlation coefficients. This provided favorable results, indicating the model was a good fit of the data.

The importance of dependence modelling was analyzed by comparing its performance to that of an independent model. The independent model was obtained by fitting univariate distributions on each of the variables based on AIC. It was found that the independence of the data resulted in more scattering as well as larger extreme values in general. The scattering meant that certain combinations of variables were present that aren't representative of the original data used for fitting. Using the independent data as input for the Monte-Carlo simulation returned significantly higher probabilities of failure for all failure modes. Ignoring correlations meant that a more expensive design is needed to fulfill the design criteria. However, the resulting structure would actually be over-designed, as the independent data contains (combinations of) loads that would not occur in reality. Therefore, it can be concluded that correlations between wave and wind characteristics shouldn't be neglected in probabilistic design.

Regarding the second research question, there are many design decisions that can be made for a structure such as this. Several dozen Monte-Carlo simulations were run in order to iteratively find an optimized design. Optimized meaning here: fulfills the design criteria for the lowest material cost. Aspects such as construction feasibility or the effect of additional failure modes (such as concrete cracking) were not considered in this design process. See Appendix F for a few of the preliminary Monte-Carlo simulations to see the effect of some of the design decisions taken.

Reducing the weight of the caisson is very important for design, as it 1) reduces the amount of material needed, and 2) is the best deterrent against bearing failure. Yet a minimized caisson weight also increases the risk of sliding and overturning in shoreward or seaward direction. A balance must be found between the failure modes and the necessary amount of construction material to find an optimized design. This involved several design dimensions such as: the width of the caisson, the width of the bottom slab, the height of the rubble mound and the concrete crown. The bottom slab was a necessary addition for increasing the width of the structure while keeping its weight at a minimum. This helped prevent sliding and bearing failure, which were one of the most critical failures for the ULS condition. The bottom slab added 3 meters of width to either side of the breakwater, bringing the total width to 36 meters. The greater width allows the weight of the caisson to be spread over a larger area, lowering the maximum bearing pressure. Decreasing the width of the bottom slab had a large effect on the amount of occurrences of bearing failure. However, the extended width of the bottom slab does allow the possibility for a new failure mode which wasn't considered in design: cracks in the concrete slab as a result of wave-induced loading. It is possible a part of the relatively thin bottom slab breaks, negating the additional width it is supposed to bring. The proposed design in Chapter 6 had a rubble mound height of 8 meters. The purpose of the rubble mound foundation is to spread the weight of the structure over the seabed. A higher rubble mound means the caisson itself can be shorter. This reduces the weight of the caisson at the cost of a heavier foundation, reducing the cases of bearing failure. Yet decrease of the weight of the caisson is a double-edged sword, as a lighter caisson also suffers more from cases of sliding and overturning. The same was found for the addition of the concrete crown, which reduced the amount of material needed to reach the same amount of freeboard.

Freeboard is very important for wave overtopping and transmission. During the simulations it was found that wave overtopping was normative out of these two. A 50 centimeter wide bullnose was added to the structure to keep the overtopping discharge at a minimum. With the addition of the bullnose, it was found that the crest height could be reduced by two meters. This brought the freeboard relative to the still water level from 11 meters to 9. However, the addition of the bullnose introduces a new failure mode to the structure which was not considered in the design: the emergence of cracking in the bullnose structure. It is possible the wave-induced pressure distribution changes as a result of the bullnose. Wave making contact with the bullnose may induce forces significant enough to damage the crest of the structure, resulting in failure. The severity of this effect has not been analyzed.

There are many design decisions that could be made. Although the proposed design is optimized through the Monte-Carlo process, this does not necessarily mean it is the best possible design. Additional failure modes have not been checked, so it is possible that features such as the bullnose or the bottom slab negatively affect the probability of failure. Nevertheless, the simulations illustrate that these additions can have a great effect on the failure modes considered. These should definitely be considered in a final design, but not before more research is done to assess how they affect the performance of the structure.

9.2. Recommendations

Based on the findings of this thesis, a number of subjects call for more elaborate research:

- The lack of wave and wind data in the Gulf of Genoa was a large issue for this project. While the (corrected) data of WavewatchIII may be an acceptable alternative, it is by no means a substitute of measurement data. Observed data should always be preferred over any numerical model. By taking long-term measurements at the place of interest, the reliability of the result should increase.
- While it was found that vine-copulas can provide an adequate model of the dependence between variables, it is not a concept that can be easily applied to any dataset. In this thesis, copulas were fitted over all 480 possible regular vines for 5 nodes using *MATVines*[18]. This was done by permuting the 5 tree-equivalent vines until every possible vine was fitted (including 240 excess ones). The problem with this approach is that the tree-equivalent vines had to be defined prior to fitting. While these have been documented for an ample amount of nodes[45], it can be arduous to make matrices for every single one, especially in higher-dimensional systems. A procedure to automatically generate matrices for all regular vines does exist[46], but this is not yet available in MATLAB. Development of this code as an extension to *MATVines* will allow vine-copula modelling to be readily available to anyone with basic knowledge of MATLAB.
- Methods for modelling multivariate data exist other than the ones utilized in this thesis. For example, it might be interesting to see how well a single multivariate copula performs in comparison to a vine-copula. Research should be conducted into alternative methods of multivariate modelling.
- Application of a 1-dimensional bathymetry instead of a 2-dimensional one undoubtedly introduced a great amount of uncertainty in the onshore wave data. 2-dimensional bathymetry couldn't be applied because of the slow processing speed of the SWAN loop. To make this possible, automation of onshore wave transformation should be made much faster. Perhaps parallel computing techniques could prove useful. A modified version of SWAN focused on speed could also alleviate this issue, but this may be at the cost of accuracy. It might be necessary to look for a faster alternative to SWAN, or to make one from scratch. Another alternative could be wave measurements at the port itself (referring back to the first point), which would bypass the need of a wave transformation program.
- The design equations utilized in this thesis may serve as a good first-guess of the loads and resistances of the structure. There is however always a large amount of uncertainty in utilizing empirical equations. For increased precision, physical model tests should be conducted. If not possible, then computational fluid dynamics may be a good substitute. The problem with this is that it may be very time-consuming to utilize in a Monte-Carlo simulation.
- As mentioned, some failure modes were neglected in the design process. Some of these, such as the influence the bullnose has on the wave-induced pressure distribution could be modelled through computational fluid dynamics. The preliminary design proposed in this thesis has highlighted that several design decisions could lead to a cheaper yet more reliable structure. The exact effect that these design decisions have on the performance of the structure should be analyzed with more detail before a definitive choice can be made.

References

[1] URL: https://www.navionics.com/fin/.

[2] Ken Aho, DeWayne Derryberry, and Teri Peterson. “Model selection for ecologists: the worldviews of AIC and BIC”. In: *Ecology* 95.3 (2014), pp. 631–636. DOI: https://doi.org/10.1890/13-1452.1. eprint: https://esajournals.onlinelibrary.wiley.com/doi/pdf/10.1890/13-1452.1. URL: https://esajournals.onlinelibrary.wiley.com/doi/abs/10.1890/13-1452.1.

[3] H. Akaike. “A new look at the statistical model identification”. In: *IEEE Transactions on Automatic Control* 19.6 (1974), pp. 716–723. DOI: 10.1109/TAC.1974.1100705.

[4] Miglietta et al. 2013, p. 2404.

[5] A. Antonini et al. “Survivability assessment of fastnet lighthouse”. In: (2019).

[6] Tania Del Giudice Antonio Iengo. “Analysis of the 29 October 2018 sea-storm in the Ligurian sea”. In: (2019).

[7] Arne Arns et al. “Estimating extreme water level probabilities: A comparison of the direct methods and recommendations for best practise”. In: *Coastal Engineering* 81 (Nov. 2013), pp. 51–66. DOI: 10.1016/j.coastaleng.2013.07.003.

[8] Tim Bedford and Roger Cooke. “Probability Density Decomposition for Conditionally Dependent Random Variables Modeled by Vines”. In: *Ann. Math. Artif. Intell.* 32 (Aug. 2001), pp. 245–268. DOI: 10.1023/A:1016725902970.

[9] Eco W. Bijker. “Some considerations about scales for coastal models with movable bed”. In: 1967.

[10] E. Bommier. “Peaks-Over-Threshold Modelling of Environmental Data”. In: (2014), pp. 3–11.

[11] J.P. van den Bos and H.J. Verhagen. *Breakwater design Lecture notes CIE5308*. 8th ed. Page 62 - 64. Delft, Netherlands: TU Delft, 2018.

[12] Judith Bosboom and Marcel J.F. Stive. “Coastal Dynamics”. In: (2021).

[13] Kenneth P. Burnham and David R. Anderson. “Model selection and multimodel inference : a practical information-theoretic approach”. In: *Journal of Wildlife Management* 67 (2003), p. 45.

[14] R. Vieira C. de Toro and M.J. Sevilla. “Ocean Tidal Models of M2 and S2 Constituents for the Western and Central Mediterranean Sea”. In: (1992).

[15] Lorenzo Mentaschi Giovanni Besio Federico Cassola and Andrea Mazzinoa. *Performance evaluation of Wavewatch III in the Mediterranean Sea*. 2015.

[16] CIRIA CETMEF. “The Rock Manual - The Use of Rock in Hydraulic Engineering - Chapter 3”. In: (2007).

[17] CIRIA CETMEF. “The Rock Manual - The Use of Rock in Hydraulic Engineering - Chapter 5”. In: (2007).

[18] Maximilian Coblenz. “MATVines: A vine copula package for MATLAB”. In: *SoftwareX* 14 (2021), p. 100700. ISSN: 2352-7110. DOI: https://doi.org/10.1016/j.softx.2021.100700. URL: https://www.sciencedirect.com/science/article/pii/S2352711021000455.

[19] *Criteria for the selection of breakwater types and their related optimum safety levels*. PIANC, 2016.

[20] Daniel Pereira. *Wind Rose*. 2021. URL: https://nl.mathworks.com/matlabcentral/fileexchange/47248-wind-rose (visited on 08/02/2021).

[21] U.S. Navy Supervisor of Diving. “U.S. Navy Diving Manual”. In: REVISION 7 (2008).

[22] Maedeh Enayati et al. “Bias correction capabilities of quantile mapping methods for rainfall and temperature variables”. In: (2021).

[23] United States. Army. Corps of Engineers. *CEM: Coastal Engineering Manual*. U.S. Army Corps of Engineers, 2002. URL: https://books.google.nl/books?id=QLO%5C_jwEACAAJ.

[24] Francisco de Castro. *fitmethis*. 2021. URL: https://www.mathworks.com/matlabcentral/fileexchange/40167-fitmethis (visited on 07/26/2021).

[25] Gaia Galassi and Giorgio Spada. "Sea-level rise in the Mediterranean Sea by 2050: Roles of terrestrial ice melt, steric effects and glacial isostatic adjustment". In: *Global and Planetary Change* 123 (2014), pp. 55–66. ISSN: 0921-8181. DOI: https://doi.org/10.1016/j.gloplacha.2014.10.007. URL: https://www.sciencedirect.com/science/article/pii/S0921818114002008.

[26] H.J. Verhagen Gerrit J. Schiereck. "Introduction to Bed, bank and shore protection: Engineering the interface of soil and water". In: (2019).

[27] Yoshimi Goda. *Random Seas and Design of Maritime Structures*. 3rd. WORLD SCIENTIFIC, 2010. DOI: 10.1142/7425. eprint: https://www.worldscientific.com/doi/pdf/10.1142/7425. URL: https://www.worldscientific.com/doi/abs/10.1142/7425.

[28] Yoshimi Goda. "THE DESIGN OF UPRIGHT BREAKWATERS". In: ().

[29] Google. *The Gulf of Genoa*. 2021. URL: https://www.google.nl/maps/@44.0638295,8.652181,9.75z (visited on 08/04/2021).

[30] K.M. Heijn. "Wave transmission at vertical breakwaters". In: (December 1997).

[31] Leo H. Holthuijsen. *Waves in Oceanic and Coastal Waters*. Figure 1.1, page 4. Adapted from Munk, 1950. New York, United States: Cambridge University Press, 2007.

[32] Vrieze S. I. "Model selection and psychological theory: a discussion of the differences between the Akaike information criterion (AIC) and the Bayesian information criterion (BIC)." In: *Psychological methods* 17 (2012), pp. 228–243. DOI: https://doi.org/10.1037/a0027127.

[33] Robert E. Kass and Larry Wasserman. "A Reference Bayesian Test for Nested Hypotheses and its Relationship to the Schwarz Criterion". In: *Journal of the American Statistical Association* 90.431 (1995), pp. 928–934. DOI: 10.1080/01621459.1995.10476592.

[34] Katsutoshi Kimura, Shigeo Takahashi, and Katsutoshi Tanimoto. "Stability of Rubble Mound Foundations of Composite Breakwaters under Oblique Wave Attack". In: Aug. 1995, pp. 1227–1240. DOI: 10.1061/9780784400890.090.

[35] Katsutoshi Kimura, Katsutoshi Tanimoto, and Shigeo Takahashi. "Stability of Armor Units for composite Breakwater Mound in Deep Seas". In: *PROCEEDINGS OF CIVIL ENGINEERING IN THE OCEAN* 10 (Jan. 1994), pp. 189–194. DOI: 10.2208/prooe.10.189.

[36] Nicole Krämer and Ulf Schepsmeier. "Introduction to vine copulas". In: *NIPS Workshop,Granada* (Dec. 2011).

[37] Dorota Kurowicka and Harry Joe. *Dependence Modeling: Vine Copula Handbook*. Dec. 2010, pp. 1–360. ISBN: 978-981-4299-87-9. DOI: 10.1142/7699.

[38] Alberto Luceño, Melisa Menendez, and Fernando Mendez. "The effect of temporal dependence on the estimation of the frequency of extreme ocean climate events". In: *Proceedings of The Royal Society A: Mathematical, Physical and Engineering Sciences* 462 (June 2006), pp. 1683–1697. DOI: 10.1098/rspa.2005.1652.

[39] Charles P. Fournier Michael W. Mulcahy K. Ander Chow Otavio J. Sayao M.ASCE. "WAVE AGITATION CRITERIA". In: ().

[40] J. W. van der Meer et al. *EurOtop: Manual on wave overtopping of sea defences and related sturctures : an overtopping manual largely based on European research, but for worlwide application*. eng. 2016, p. 264.

[41] J.W. van der Meer, K. d'Angremond, and J. Juhl. "PROBABILISTIC CALCULATIONS OF WAVE FORCES ON VERTICAL STRUCTURES". In: *Coastal Engineering Proceedings* 1.24 (1994).

[42] Frank J. Millero, Dana Means, and Carolyn Miller. "The densities of Mediterranean Sea waters". In: *Deep Sea Research* 25.6 (1978), pp. 563–569. ISSN: 0146-6291. DOI: https://doi.org/10.1016/0146-6291(78)90644-6. URL: https://www.sciencedirect.com/science/article/pii/0146629178906446.

[43] M.Z. Molenaar W.F. Voorendt. “Manual Hydraulic Structures”. In: (2016).

[44] N. R. Moloney, D. Faranda, and Y. Sato. “An overview of the extremal index”. In: *Chaos 29* (2019). URL: https://doi.org/10.1063/1.5079656.

[45] Cooke R.M. Morales-Napoles O. and Kurowicka D. *About The Number of Vines and Regular Vines on n Nodes*. Delft Institute of Applied Mathematics.

[46] S. Sellés Valls MSc. “A vine-based approach for defining critical infrastructure loads”. In: (2019).

[47] Marzena Osuch et al. “Projected changes in flood indices in selected catchments in Poland in the 21st century”. In: (2016).

[48] Stefano Vignudelli Paola Picco and Luca Repetti. “A Comparison between Coastal Altimetry Data and Tidal Gauge Measurements in the Gulf of Genoa (NW Mediterranean Sea)”. In: (2020).

[49] Hansen Pei. “Copula for Statistical Arbitrage: A Practical Intro to Vine Copula”. In: *Hudson and Thames* (May 10, 2021).

[50] Leo C. van Rijn. “Sediment Transport, Part I: Bed Load Transport”. In: *Journal of Hydraulic Engineering* 113.9 (1987), pp. 1189–1190.

[51] Ludovica Sartini, Lorenzo Mentaschi, and Giovanni Besio. “Comparing different extreme wave analysis models for wave climate assessment along the Italian coast”. In: *Coastal Engineering* (Mar. 2015).

[52] Jorg Schneider. *Introduction to Safety and Reliability of Structures*. Vol. 5. Structural Engineering Documents, 1997.

[53] Cavicchia & von Storch. 2012, p. 2276.

[54] “SwanOne User Manual V1.3”. In: (April, 2018).

[55] U. Tomasicchio, K. Andah, and Gruppo nazionale per la difesa dalle catastrofi idrogeologiche. *Technical Instructions for the Design of Maritime Dikes*. 1996. URL: https://books.google.nl/books?id=iEkJjwEACAAJ.

[56] V. Tsimopoulou, W. Kanning, H.G. Voortman, H.J. Verhagen. *Probabilistic design of breakwaters in shallow, hurricane-prone areas*.

[57] Anthony Viselli et al. “Estimation of extreme wave and wind design parameters for offshore wind turbines in the Gulf of Maine using a POT method”. In: *Ocean Engineering* 104 (Aug. 2015), pp. 649–658. DOI: 10.1016/j.oceaneng.2015.04.086.

[58] WAFO-group. *WAFO - A Matlab Toolbox for Analysis of Random Waves and Loads - A Tutorial*. Math. Stat., Center for Math. Sci., Lund Univ. Lund, Sweden, 2000.

[59] M. van der Wal. “Heranalyse van M 1115 onderzoeksresultaten”. In: ().

[60] Port System Authority of the Western Ligurian Sea Port of Genoa. “Project dossier - OFFSHORE DAM IN THE PORT OF GENOA”. In: (Dec. 2020).

[61] Dane Wiebe, Hyoungsu Park, and Daniel Cox. “Application of the Goda Pressure Formulae for Horizontal Wave Loads on Elevated Structures”. In: *KSCE Journal of Civil Engineering* 18 (June 2014). DOI: 10.1007/s12205-014-0175-1.

[62] Yuhong Yang. “Can the strengths of AIC and BIC be shared? A confict between model identification and regression estimation”. In: *Biometrika* 92 (Dec. 2005), pp. 937–950. DOI: 10.1093/biomet/92.4.937.

A

Preliminary Wave Climate Analysis

This appendix provides a basic description of the wave climate in the Gulf of Genoa.

A.1. Data selection

This section discusses the data available of the Gulf of Genoa. There were buoys at two locations within the Gulf of Genoa; one at La Spezia, and one at Capo Mele. A third point is located at the center of the Gulf of Genoa, which will henceforth be referred to as simply 'Offshore Genoa'. The latter point did not have any buoy data. All three points do have hindcast data, provided by WavewatchIII. See A.1 for the exact location of all three points. Since the focus for now is primarily on describing the wave climate near Genoa, it was chosen to only discuss the buoy data. For an analysis of the bias and correction of WavewatchIII, see Chapter 2.

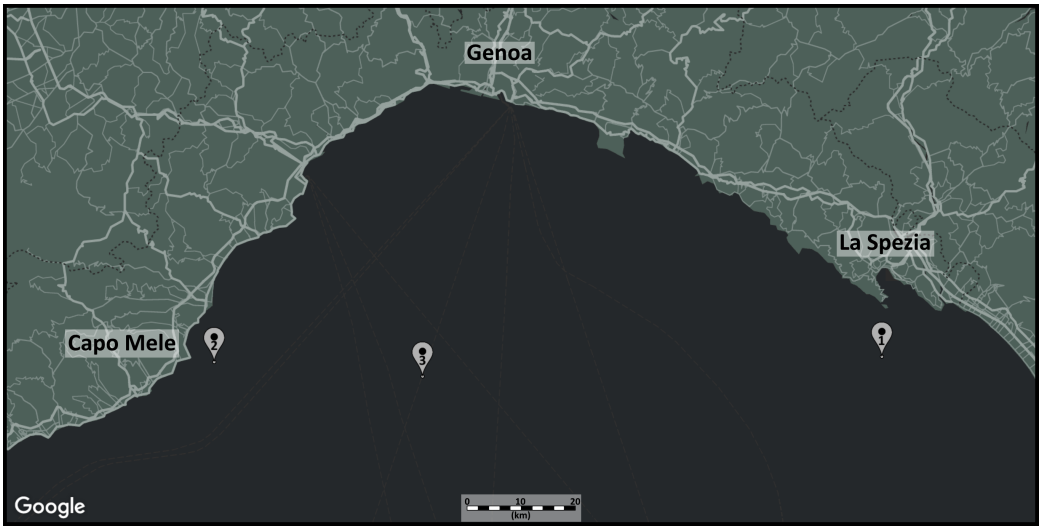

Figure A.1: Locations of the three datapoints[29].

Table A.1 features general information about the available datasets. Please note that the wave data measured at La Spezia consists of the records of three different buoys at nearly the same location. These buoys were measuring during different time periods with no overlap. This can be seen quite clearly in the timeseries in figure A.2. The first buoy measured only once per three hours, and with an accuracy of a single decimal. The second and third buoys measured once every hour, and with an accuracy of two decimals. For simplicity's sake, the records of these three buoys will be combined into a single long dataset.

Source	Location	Start	End	Measurement frequency	Amount of data	Decimals
La Spezia buoy RON 1989	1	1989-07-01 00:00:00	2001-01-01 00:00:00	Every 3 hours	31.373	1
La Spezia buoy RON 2002	1	2002-07-12 17:00:00	2006-09-12 06:00:00	Every hour	46.040	2
La Spezia buoy RON 2009	1	2009-12-27 15:30:00	2014-12-29 20:00:00	Every hour	80.679	2
La Spezia buoys (combined)	*1*	*1989-07-01 00:00:00*	*2014-12-29 20:00:00*	*∼Every hour*	*158.092*	*∼2*
WavewatchIII point 000367	2	1979-01-01 05:00:00	2018-12-31 23:00:00	Every hour	350.635	3
Capo Mele buoy	2	2012-02-23 09:00:0	2018-12-31 23:30:00	Every 30 min	81.818	2
WavewatchIII point 000354	3	2012-02-01 00:00:00	2018-12-31 23:00:00	Every hour	60.624	3
WavewatchIII point 000323	3	1979-01-01 05:00:00	2018-12-31 23:00:00	Every hour	350.635	3

Table A.1: The wave data used in this project, for locations 1 (La Spezia), 2 (Capo Mele) and 3 (Offshore Genoa).

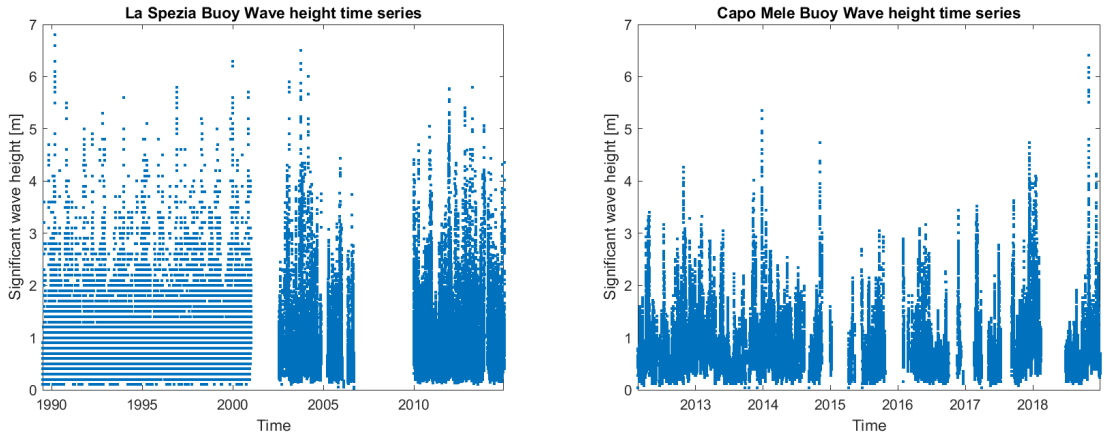

(a) La Spezia

(b) Capo Mele

Figure A.2: A time-series of the wave height data collected at points 1 and 2, La Spezia (left), Capo Mele (right).

A.2. Wave characteristics

This section focuses on how the most important parameters of the wave climate are distributed and correlated. A quick way to visualize the full dataset is through a plotmatrix. A plotmatrix is a structure of scatterplots and histograms. Inside the scatterplots the density of the datapoints is highlighted through color, where blue indicates sparse data and yellow indicates dense data. The plotmatrices of La Spezia and Capo Mele can be viewed in figure A.3. Directions were measured in degrees, clockwise from North.

The majority of waves are below 2 meters in height, with the mean wave being roughly 0.5 meters tall. On the histograms, it is difficult to see the distribution of waves beyond 3 meters in height. In the graphs of the exceedance distribution functions it is shown that waves far larger than 3m have occurred a few times in the buoy records. The extreme waves are the most relevant for probabilistic design. Appendix C shows an extreme value analysis through the Peak over Threshold method (PoT) for Capo Mele and La Spezia. There's a large concentration of waves with a height between 0 and 1m and a period between 2 and 5 seconds. Generally, there seems to be a positive relation between significant wave height and peak wave period. Though there is still a large difference in wave heights for larger periods. A large concentration of waves are fairly low (0.5m) and . The highest waves come from the South-West, with concentrations at 230 and 200 degrees respectively. This corresponds to the Balearic Sea, which is the largest open side of the Gulf of Genoa. The distribution of higher waves in the Capo Mele dataset is very scattered. There are higher waves (>3m) coming from almost every direction, even though such directions have a low density of waves. The highest waves are from an otherwise quite barren direction at 275 degrees, which is from the coastline.

Munk[31] classified wave types through a difference in wave periods. A period of the order of magnitude between 1 and 10 seconds corresponds to typical wind-generated waves. The periods of most waves in the dataset fall within this range. This indicates that the waves are mainly of a single type. The period of swell waves are typically at around 10 seconds[31], of which there were few in the dataset. From this it can be concluded that there is little presence of swell waves, and that by far most waves are locally-generated wind-waves. The Gulf of Genoa is relatively isolated from the rest of the Mediterranean Sea (see figure A.4). It does not allow for the fetch necessary for swell waves to occur within it. This is partly due to the blocking of the neighbouring lands; Tuscany, the islands of Elba and Corsica, Liguria and Côte d'Azur. The only open side of the Gulf of Genoa is the relatively small gap between the Balearic Islands and the Islands of Corsica and Sardinia, a gap of roughly 30 degrees when measured from Genoa. This region, also known as the Balearic Sea, is less than 1000km in width though. Waves generating from a storm within this region can arrive at the Gulf of Genoa within a few hours. Such a time-span is not enough for swell conditions to occur. It is likely these waves are still being driven by the same winds that generated them in the first place.

See figure A.5 for a wave rose of the buoy data. Both La Spezia and Capo Mele show a significant amount of waves coming from 230 and 210 degrees respectively. This corresponds to roughly the same place of origin: the Balearic Sea. This is also the direction that allows for the largest fetch for wind-waves. So, it should be expected that these waves are generally larger than those coming from other places. There are a few other smaller concentrations of wave directions present. La Spezia has a concentration of waves coming from around 175 degrees and one from around 10 degrees. The first corresponds to the gap between Corsica and Elba, which is also a direction that leads to the open sea (the Thyrrenian Sea), though it is far smaller than the Balearic Sea. The second one comes from a landward direction, likely generated due to land winds. Capo Mele shows two minor concentrations from 60 and 115 degrees. These come from within the Gulf of Genoa itself, likely generated from a local storm. This direction corresponds to the gap between the Tuscan Archipelago islands, towards the Tyrrhenian Sea.

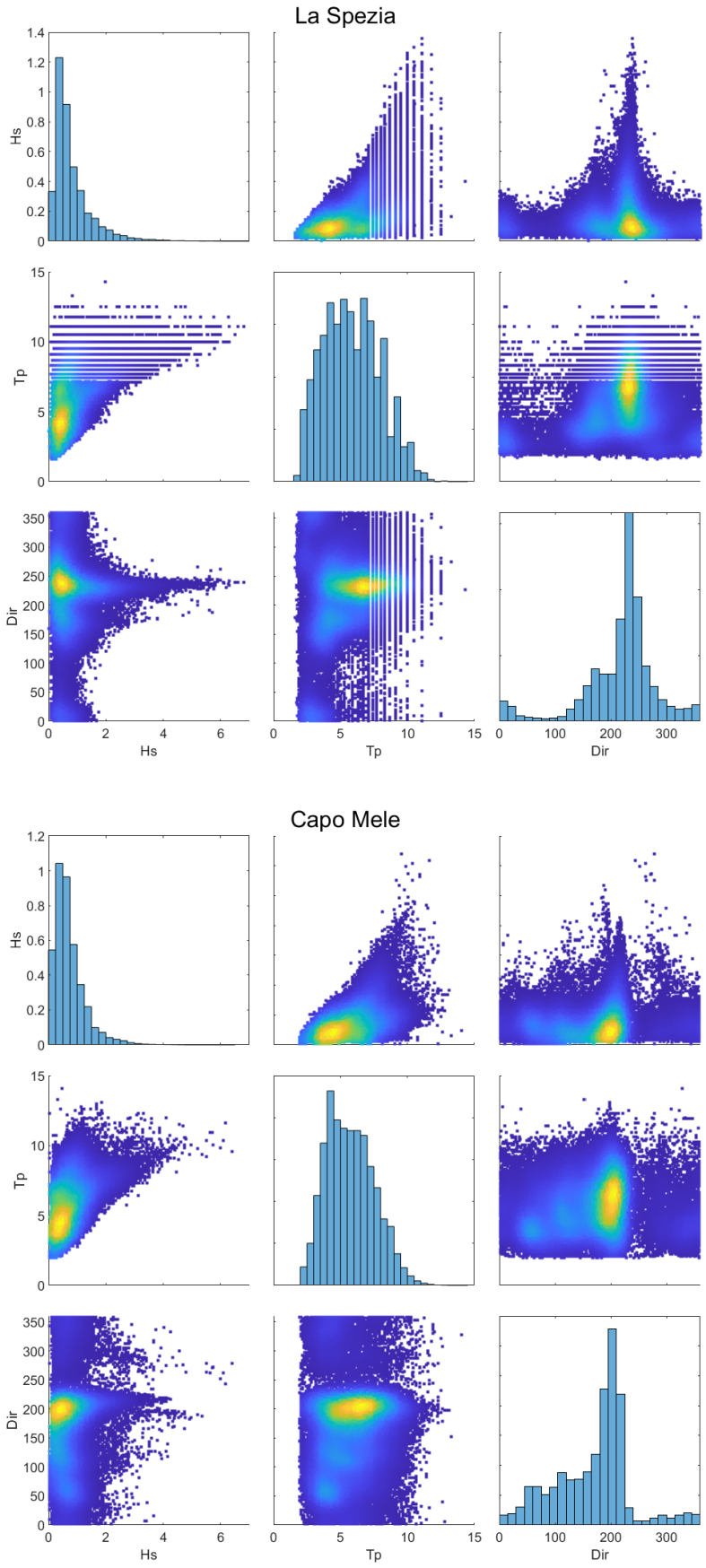

Figure A.3: Plotmatrix of La Spezia and Capo Mele.

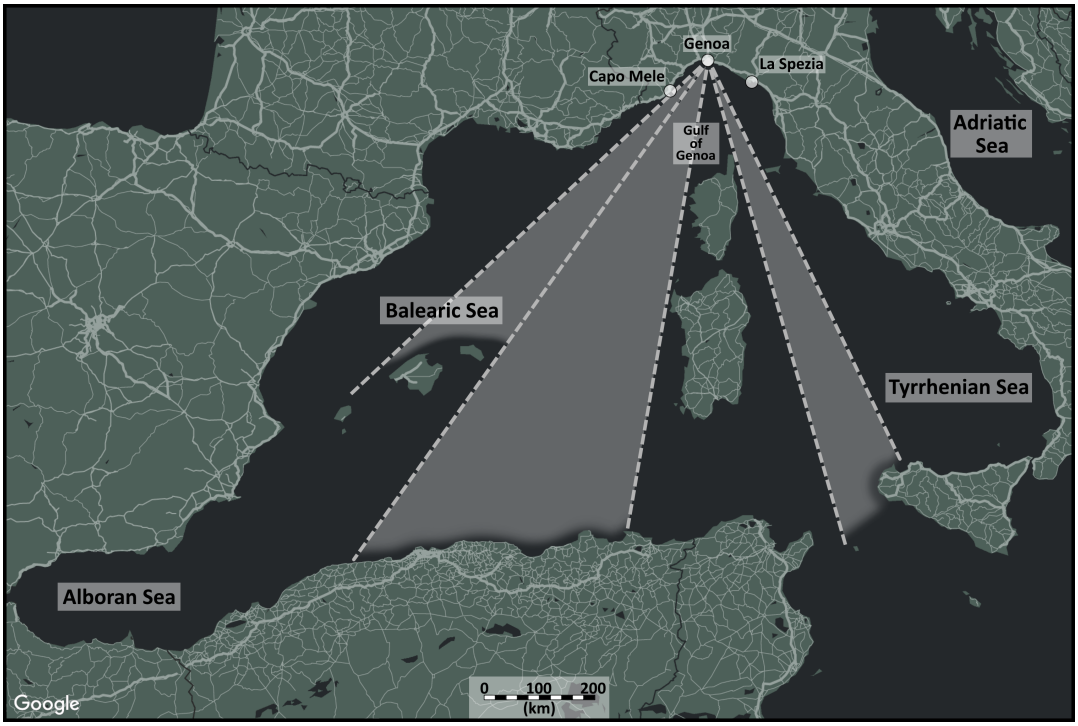

Figure A.4: The Western Mediterranean Sea[29].

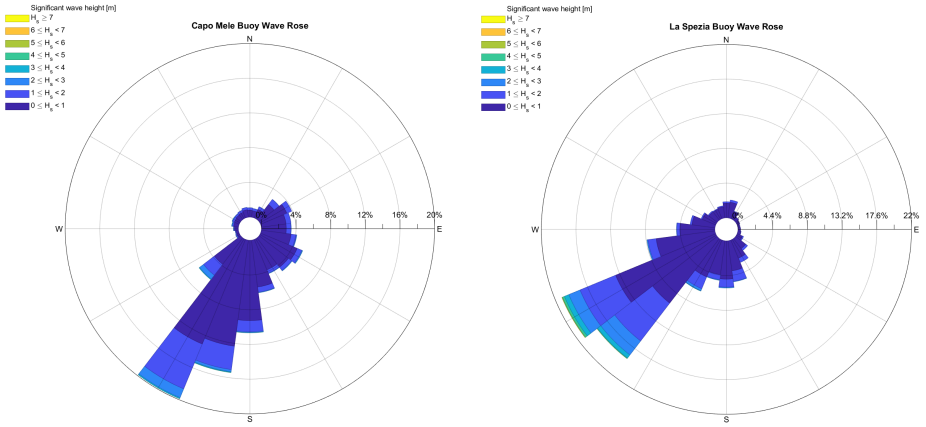

Figure A.5: Wave rose signifying the directional frequency and height of the waves. Made with Wind Rose by Daniel Pereira[20].

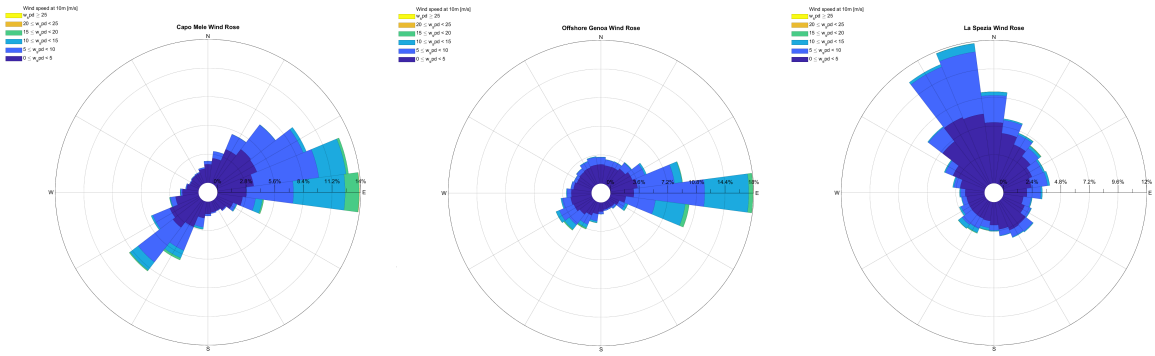

Figure A.6: Wind rose signifying the directional frequency and speed of the wind. Made with Wind Rose by Daniel Pereira[20].

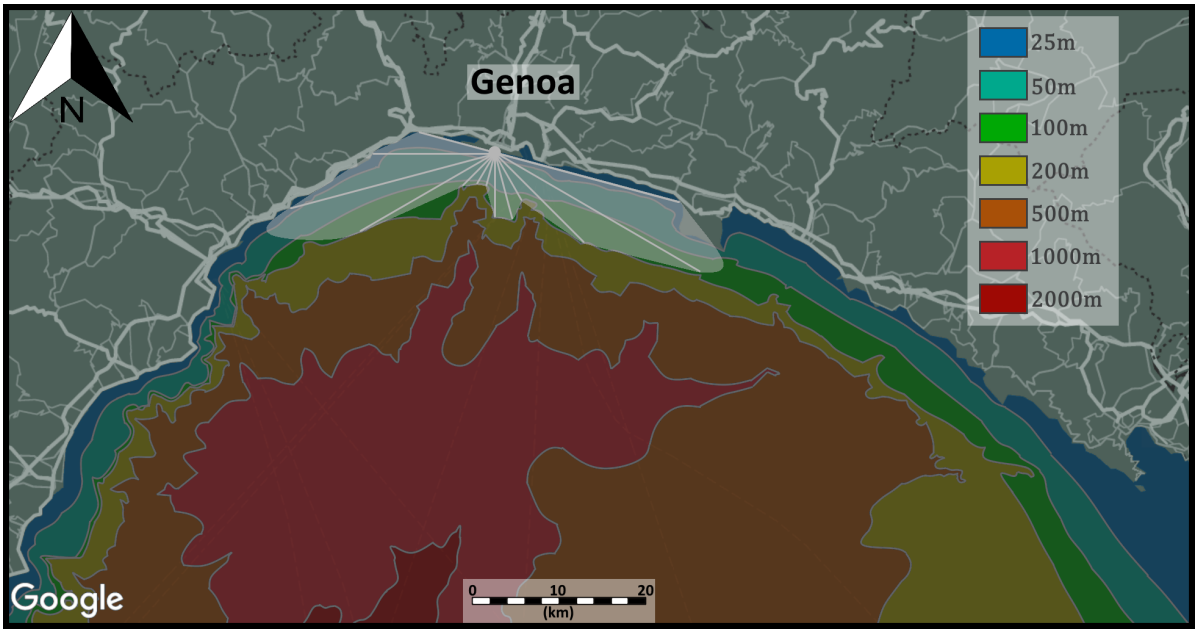

Figure A.7: Bathymetry of the Gulf of Genoa.

Wind is often the greatest contributor to the generation of waves. For accurately describing the wave climate, the corresponding winds should also be taken into account. Wind data was only available from the hindcast model WavewatchIII. Figure A.6 shows wind roses of the three locations.

Figure A.7 shows the bathymetry of the Gulf of Genoa. There is a canyon close to the city of approximately 1-2 kilometer deep. Wind set-up and set-down are phenomena in which the water level tilts in the direction of the wind, as a balance between drag force and gravity. Wind set-up only occurs over relatively shallow water (less than 200m[12]), as at greater depths the water is able to flow away. Because of that, the fetch for wind set-up and wind set-down is limited to shallow waters. The white area in figure A.7 shows the extent of the fetch for wind set-up and set-down measured from the Port of Genoa.

B

Quantile Mapping

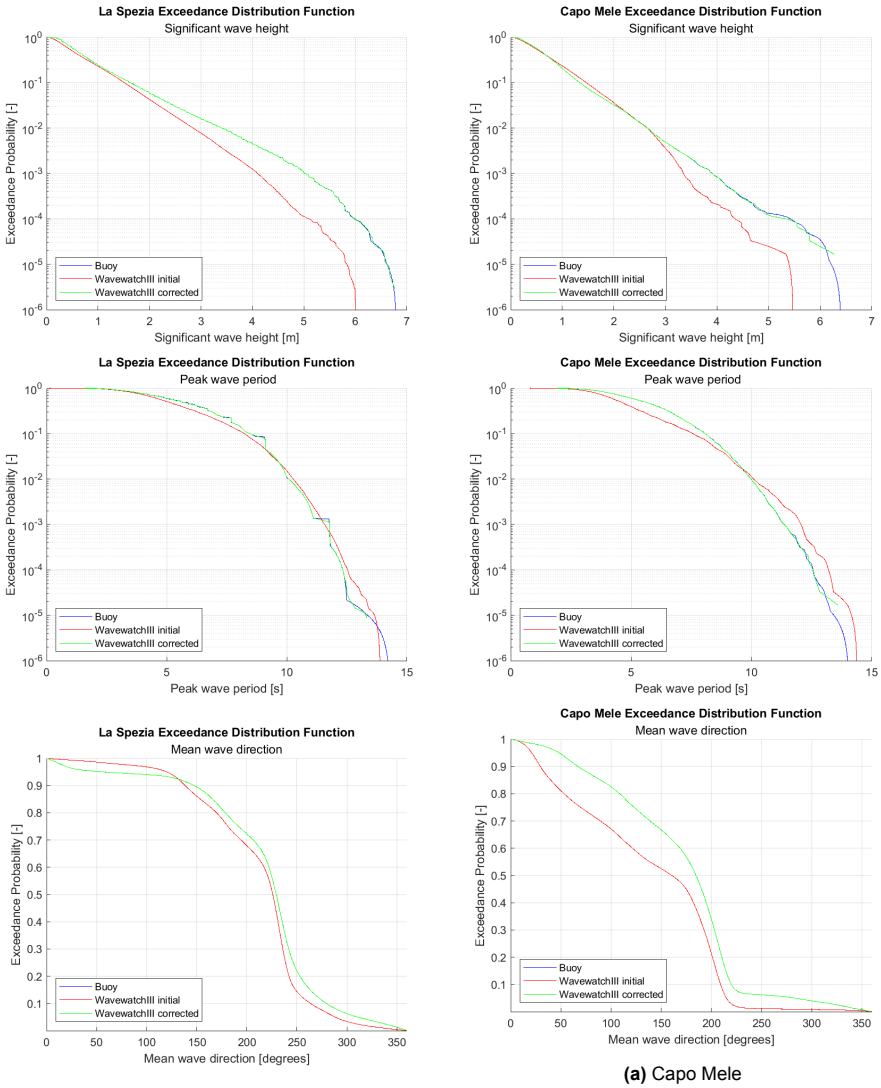

(a) Capo Mele

Figure B.1: The Exceedance Distribution Functions (EDF) of the data.

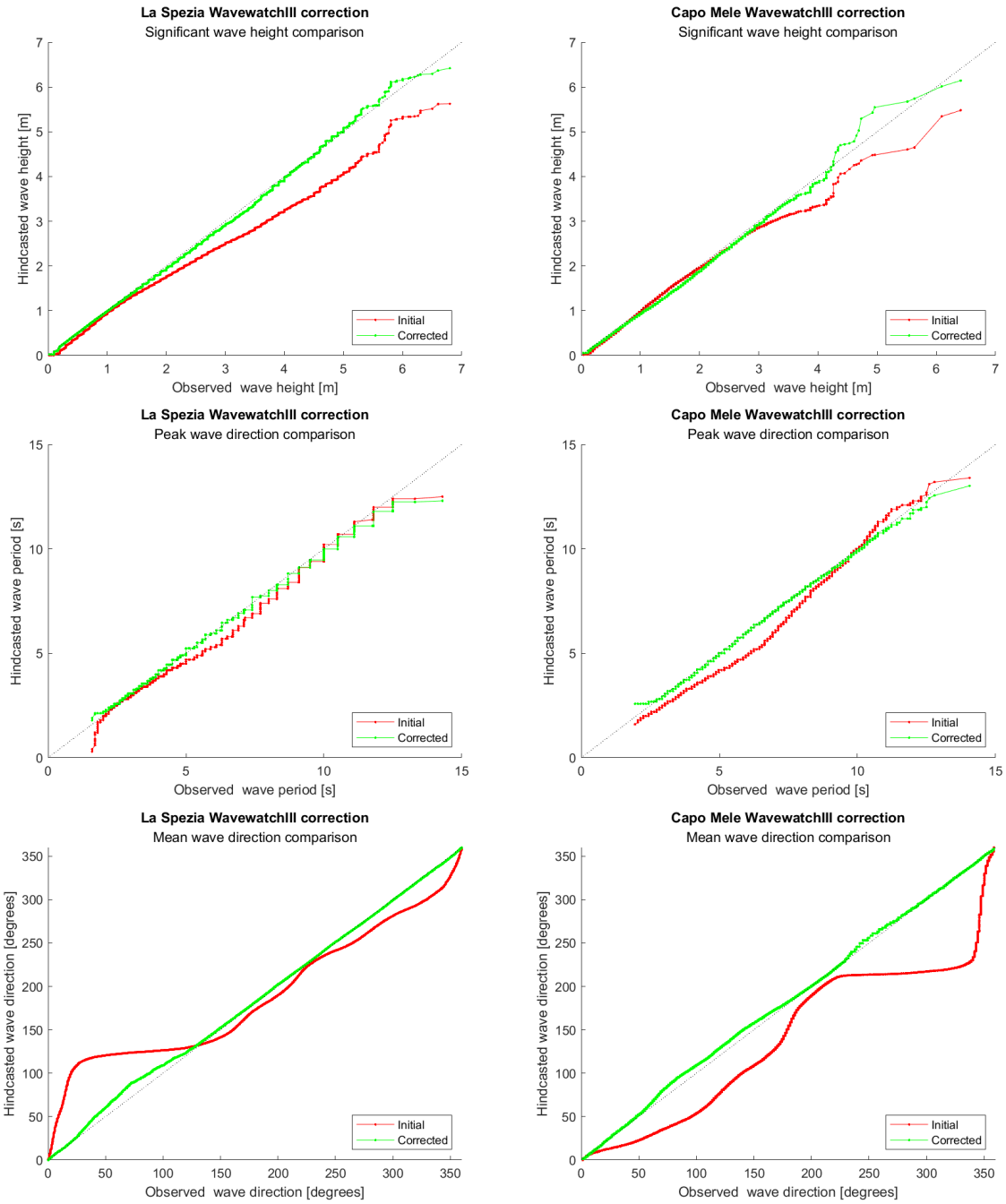

Figure B.2: A direct comparison of the hindcast data and the measured data of the buoys.

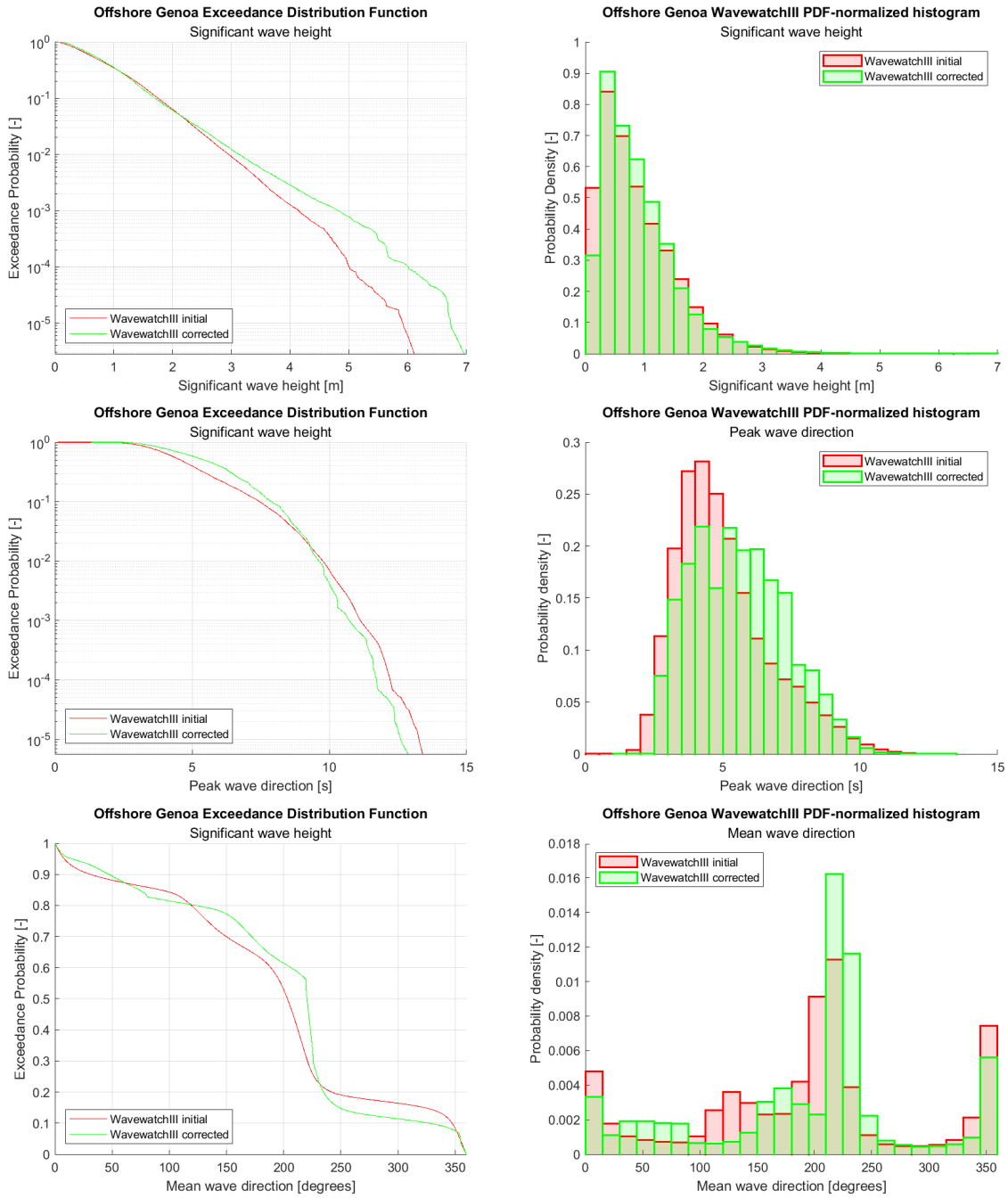

Figure B.3: The hindcast data for Offshore Genoa.

C

Extreme value analysis of La Spezia and Capo Mele

This Appendix features graphs and a brief analysis of the extremes of La Spezia and Capo Mele. For a more elaborate explanation of the methods applied and an analysis of Offshore Genoa, see Chapter 3. Only the buoy records are considered in this analysis. This analysis is made to assess the order of magnitude of the extremes in the region.

C.1. La Spezia

Name	Definition	Value [m]	Source
th1	μ + 1.4 σ	1.74	[57]
th2	μ + 1.9 σ	2.07	[57]
th3	$p_{97.5}$	2.66	[5]
th4	μ + 3 σ	2.80	[7]
th5	p_{99}	3.40	[5]
th6	$p_{99.5}$	3.91	[51]
th7	$p_{99.7}$	4.32	[38]

Table C.1: The thresholds considered the La Spezia buoy record.

Based on figures C.1 and C.2, the timelag was selected at 24 hours and the threshold 5.

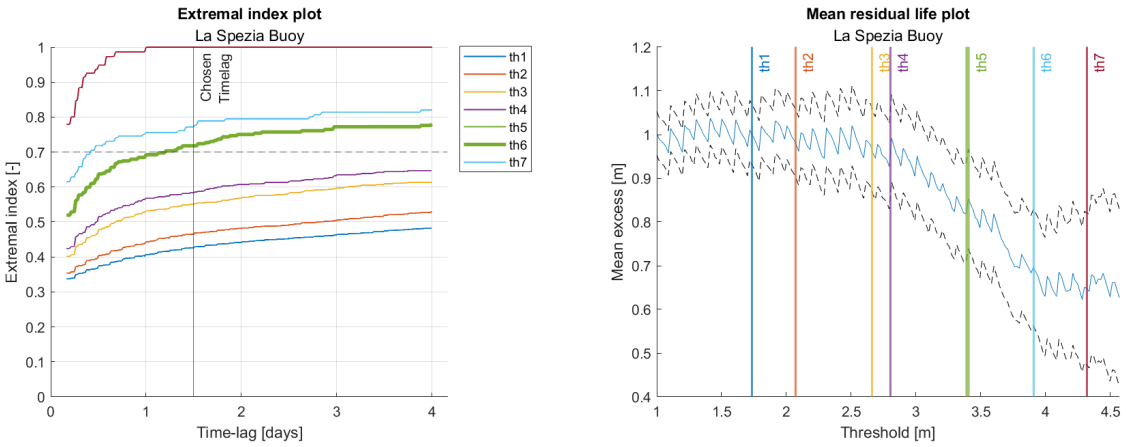

Figure C.1: Left: The Extremal Index for the considered thresholds over a varying time lag. Right: The Mean Residual Life plot.

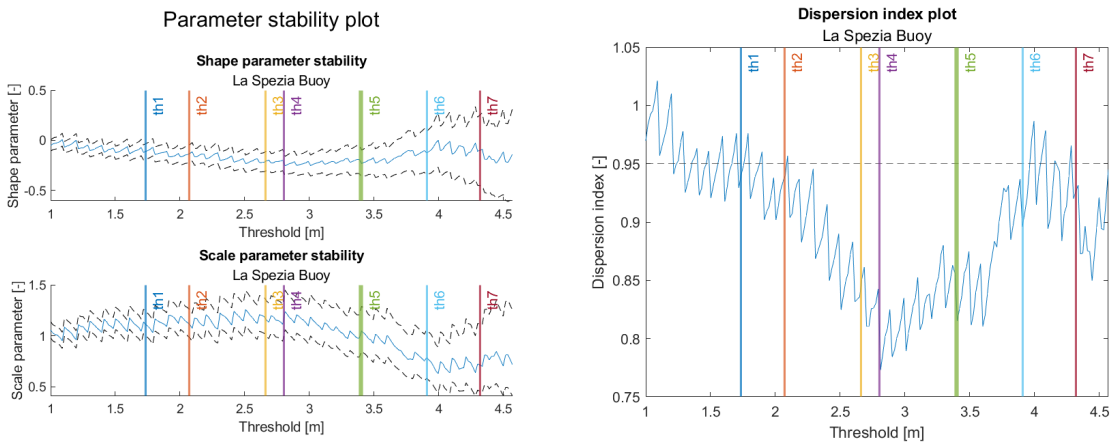

Figure C.2: Left: The GPD shape- and scale parameter stability plot. Right: The Dispersion Index plot.

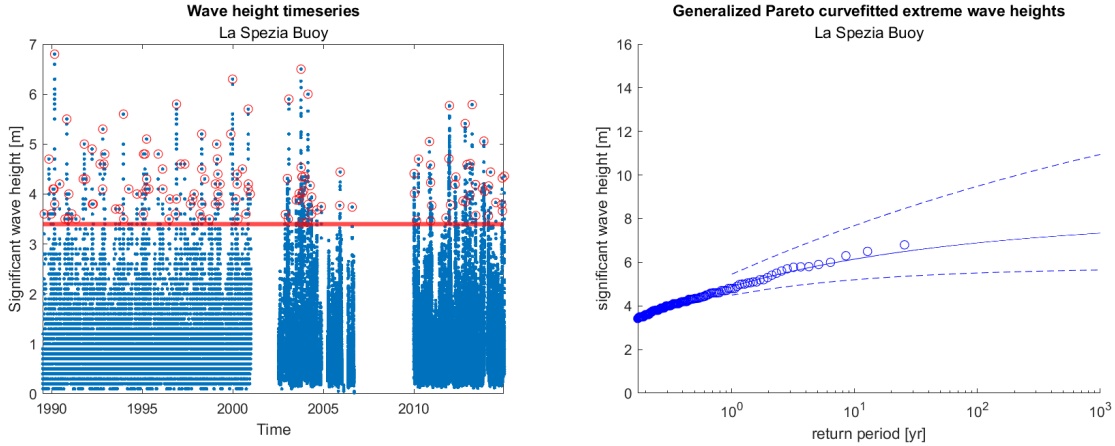

Figure C.3: Left: PoT method applied to the time-series. Right: The GPD curve fitted through the extreme values.

Return period [yr]	Predicted H_s L.B [m]	Predicted H_s [m]	Predicted H_s U.B [m]
10	5.18	6.10	7.59
25	5.35	6.47	8.41
50	5.44	6.70	8.97
100	5.51	6.89	9.48
250	5.58	7.09	10.10
500	5.62	7.22	10.54
1000	5.65	7.33	10.95

Table C.2: The predicted wave heights per return period based on an extreme value GPD fit.

The extreme value analysis yielded a total of 148 extremes, which meant about 5.8 storms per year. The La Spezia dataset was more comparable in length to Offshore Genoa than Capo Mele, at about 26 years. As a result, the GDP fit is more bounded to realistic values. The extreme value analysis of La Spezia yielded similar results to that of Offshore Genoa, though about 1 meter shorter. The buoy at La Spezia is located much closer to shore, which might mean wave height is limited due to breaking.

C.2. Capo Mele

Based on figures C.4 and C.5, the timelag was selected at 36 hours and the threshold 6.

The extreme value analysis yielded a total of 35 extremes, which means about 5.1 storms per year. As can be seen in figure C.6 and table C.4, the shortness of the Capo Mele dataset meant that estimates for the extreme wave heights were very imprecise. The 95% confidence interval was very

Name	Definition	Value [m]	Source
th1	μ + 1.4 σ	1.47	[57]
th2	μ + 1.9 σ	1.73	[57]
th3	$p_{97.5}$	2.19	[5]
th4	μ + 3 σ	2.31	[7]
th5	p_{99}	2.66	[5]
th6	$p_{99.5}$	3.01	[51]
th7	$p_{99.7}$	3.32	[38]

Table C.3: The thresholds considered for the Capo Mele buoy record.

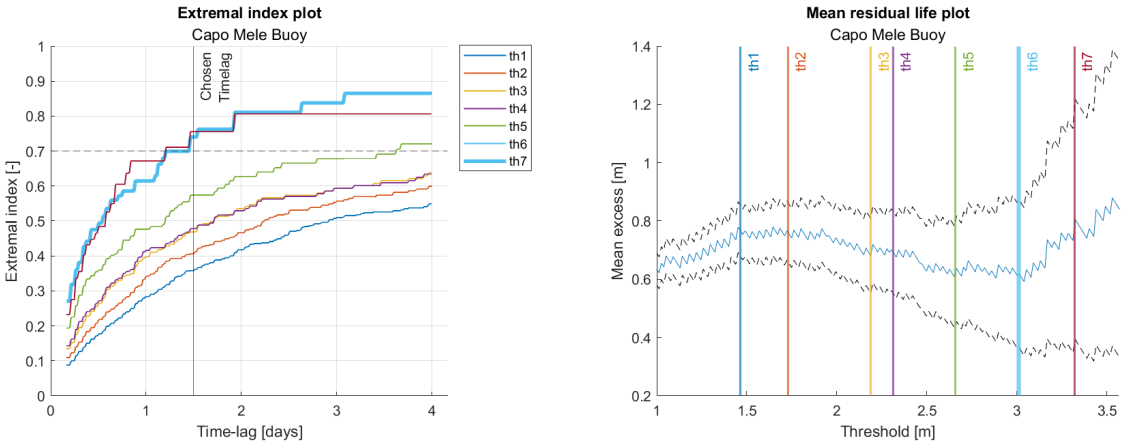

Figure C.4: Left: The Extremal Index for the considered thresholds over a varying time lag. Right: The Mean Residual Life plot.

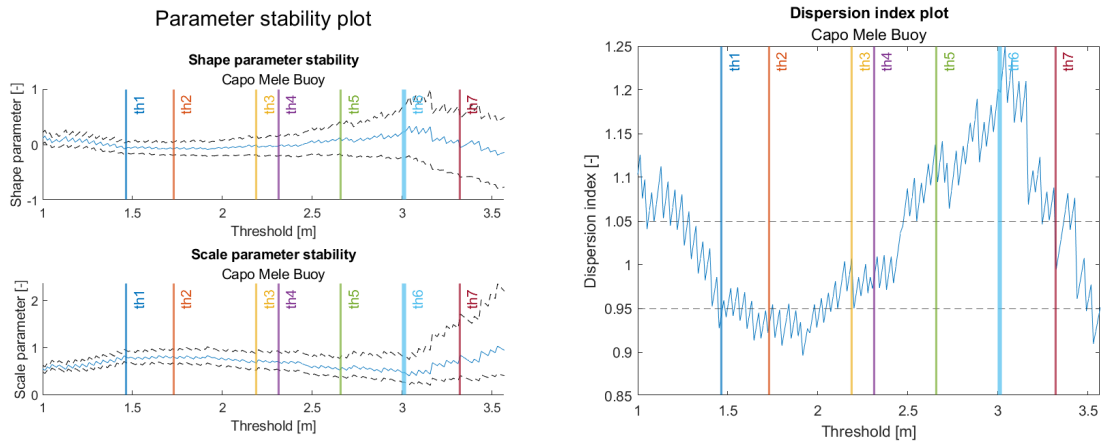

Figure C.5: Left: The GPD shape- and scale parameter stability plot. Right: The Dispersion Index plot.

wide, predicting completely unrealistic wave heights at the higher end. The timeseries of Capo Mele was only about 7 years long, which is simply too short for an extreme value analysis. This data is not advised to be used.

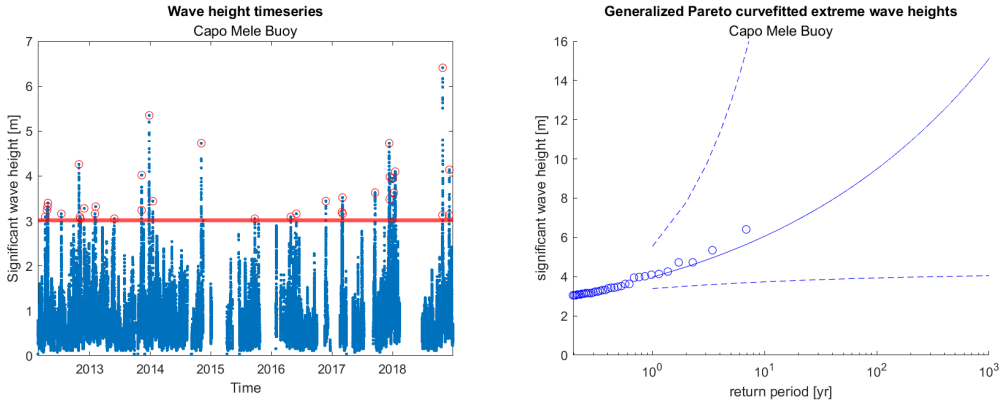

Figure C.6: Left: PoT method applied to the time-series. Right: The GPD curve fitted through the extreme values.

Return period [yr]	Predicted H_s L.B [m]	Predicted H_s [m]	Predicted H_s U.B [m]
10	3.72	5.94	18.23
25	3.82	7.17	33.45
50	3.89	8.24	52.77
100	3.93	9.47	83.26
250	3.99	11.39	152.43
500	4.02	13.11	241.17
1000	4.05	15.11	381.89

Table C.4: The predicted wave heights per return period based on an extreme value GPD fit.

D

SWAN loop matlab code

This appendix shows the matlab code for the SWAN loop, which was utilized to transform offshore waves to onshore waves. A description of the input parameters, how the code functions and results can be found in section 5.2.

```
%% SWAN loop procedure
clear;
clc;
close all;
tic;

%% loading the data
data = readtable('Offshore Data.txt');  % wave climate data
bm = readtable('Bathymetry.txt');       % bathymetry

Hs  =   data{:,1};  % wave height [m]
Tp  =   data{:,2};  % wave period [s]
Dir =   data{:,3};  % wave direction [deg], relative to the north
w_spd = data{:,4};  % wind speed [m/s]
w_dir = data{:,5};  % wind direction [deg], relative to the north

xs  =   bm{:,1};    % distance [m]
d   =   bm{:,2};    % depth [m]

%% calculation settings
coast_angle = 105;  % angle of the coastline [deg], clockwise to the north

% grid
ng = 100;           % amount of grid points desired
xend =  xs(end);    % end of the grid
dx = (xend)/ng;     % gridsize

% savepath for output data
savepath = 'C:\Users\Menno\OneDrive\Documenten\TU Delft Civiele
↪  Techniek\Thesis\Coding\';

%% generate project_001_bot.DAT
for i = 1:(ng+1)
    s(i) = dx*(i-1);
    botdat(i) = interp1(xs,-d,(i-1)*dx);
end
```

```
writematrix(botdat', 'project_001_bot.DAT')

%% direction check
if min(Dir) < coast_angle + 90 - 70 || max(Dir) > coast_angle + 90 + 70
    disp('Warning! Wave direction out of bounds! Calculation may not be accurate. Process halted.']
    return
end

%% SWAN loop
for ii=1:length(Hs)
try
prjfile = fopen('project_001.SWN', 'w');
A = [       "PROJECT 'project_001''A577' '1'",
            "MODE STATIONARY ONED",
            "SET DEPMIN=0.01 MAXMES=999 MAXERR=3 PWTAIL=4",
            "SET LEVEL 0",
            "SET CARTESIAN",
            "SETUP 0",
            strcat('CGRID REGULAR 0 0 0',{' '},num2str(xend),' 0.',{' '}, num2str(ng), ' 0 &');
            "CIRCLE 36 0.03 0.8 30",
            "BOUND SHAPE JONSWAP 3.3 PEAK DSPR POWER",
            strcat('INPGRID BOTTOM REGULAR 0 0 0',{' '},num2str(ng),' 0',{' '}, num2str(dx), ' 1');
            "READ BOTTOM 1. 'project_001_bot.dat '1 0 FREE",
            "!NPGRID CURRENT REGULAR 0 0 0 100 0 10 1",
            "!EAD CURRENT",
            strcat('BOUN SIDE W CONSTANT PAR',{' '},num2str(Hs(ii)),{' '},num2str(Tp(ii)),{' '},num2str(wrapTo360(Dir(ii)-90-coast_angle)),{' '},'2');
            "",
            strcat('WIND',{' '},num2str(round(w_spd(ii,1),1)),{' '},num2str(round(wrapTo360(w_dir(ii,1)-90-coast_angle),1)));
            "GEN3 KOMEN",
            "BREAK 1. 0.73",
            "FRIC JONSWAP",
            "TRIAD",
            "NUM ACCUR 0.02 0.02 0.02 98 15",
            "OUTPUT OPTIONS '%' TABLE 16 BLOCK 9 1000 SPEC 8",
            strcat("CURVE 'curve' 0 0",{' '},num2str(ng),{' '}, num2str(xend), ' 0');
            "Table 'curve' HEADER 'project_001.tab' XP YP HSIGN RTP TM01 TMM10 DIR &",
            "DSPR DEPTH SETUP",
            "POIN 'S0'1 .00",
            "SPEC 'S0' SPEC1D ABS 'project_001_point1.sp1'",
            "SPEC 'S0' SPEC2D ABS 'project_001_point1.sp2'",
            "POIN 'S1'56709 .00",
            "SPEC 'S1' SPEC1D ABS 'project_001_point2.sp1'",
            "SPEC 'S1' SPEC2D ABS 'project_001_point2.sp2'",
            "TEST 0 0",
            "COMPUTE",
            "STOP",
            ""];
fprintf(prjfile,'%s\n', A);
```

```
fclose(prjfile);

% perform the SWAN calculation
[status,cmdout] = system(['swanrun ' 'project_001']);
disp(['Succes! Calculation completed for iteration ', num2str(ii)])

% get results
result      =   txt2mat('project_001.tab');
HsEns(ii,:) =   result(:,3);
TpEns(ii,:) =   result(:,4);
Dir_new(ii) =   wrapTo360(result(end,7)+90+coast_angle);

% error catcher, in case the process fails display the iteration number
catch ME
    disp(['Something went wrong! Error occured at iteration ', num2str(ii)])
end
end

%% new data
Hs_on(ii)   =   result(end,3);
Tp_on       =   result(end,4);
Dir_on      =   wrapTo360(nonzeros(DirEns(:,end)));


%% save data
% Create a new table with the splines
newtable = table(Hs_on, Tp_on, Dir_on, w_spd, w_dir, 'VariableNames', {'Wave
↪  height','Wave period','Wave direction','Wind speed','Wind direction'} );

% Write data to text file
filename = [savepath, 'Onshore Data.txt'];
writetable(newtable, filename)

load handel
sound(y,Fs)
toc;
```

E

Monte-Carlo simulation MATLAB code

This appendix shows the MATLAB code for the Monte-Carlo simulation, which was utilized for the probabilistic design of the breakwater. It should be noted that this appendix only covers the most important segments. Input values, code used for plotting and segments that relied on custom MATLAB scripts of various sources are excluded from this appendix. Many parts of this code require MATLAB add-ons and toolboxes by MathWorks that should be installed beforehand. For information about input parameters, results and an explanation of the methodology applied, see Chapter 6.

E.1. MC_Main

The following lines of code is the main procedure utilized for the Monte-Carlo simulation. This involves a parallel loop-function which runs calculations for all 10 failure modes. The calculations for the failure modes themselves were written as separate functions each to limit the length of the main code.

The array *modes* allows the ability to skip the calculation of specific failure modes (0 meaning 'skip'). This was done so that the simulation didn't have to be repeated for all 10 failure modes if one wasn't interested in those.

```
%% Monte Carlo simulation
% main code

%% MC settings
numIterations = 150000;          % number of iterations of the simulation
Lifetime = 50;                   % structure design working life
nyr = 6.05;                      % expected events per year
modes = [1 1 1 1 1 1 1 1 1 1];   % toggle specific failure modes

%% Monte Carlo simulation
parfor ii = 1:numIterations
    % design wave height Hmax
    Hmax(ii) = HmaxFunction(h(ii),Hs(ii),H0(ii),L0(ii),slope);

    % caisson weight
    [~,W(ii)] = Weight(h_caisson,B_caisson,m,h_crown,h(ii),rho_c(ii),rho_s(ii)); % mass and weight caisson per m

    % wave pressures and forces according to Goda
    if modes(1) == 1 || modes(2) == 1 || modes(3) == 1 || modes(4) == 1 || modes(5) == 1
    [Pwc,U,Mp,Mu] = GodaPressure(Hmax(ii),L(ii),h(ii),beta(ii),rho_w,Rc(ii),h_wet(ii),d(ii),Bberm,B_caisson,slope);
    [Pwt,Mwt] = WaveTroughPressure(h_wet(ii),Hmax(ii),L(ii),rho_w);
```

```
    end

    % bearing capacity
    if modes(5) == 1
    pe = BearingCapacity(W(ii),U,Mu,Mp,t,B_caisson);
    end

    % required thickness of the toe protection
    if modes(6) == 1
    [t_cr] = ToeProtection(Hmax(ii),d(ii),h(ii));
    end

    % required weight of the berm armor
    if modes(7) == 1
    rho_r = normrnd(2650,50);   % avg. density of rubble [kg/m^3]
    [M_berm_cr] =
↪   BermScour(Hmax(ii),L(ii),beta(ii),h_wet(ii),Bberm,rho_r,rho_w,B_toe,m,100);
    end

    % bottom scour
    if modes(8) == 1
    [u_cr, u_r] = NoFilter(h(ii),dn50_bottom,Hmax(ii),Tp(ii),Delta);
    end

    % overtopping
    if modes(9) == 1
    q = Overtopping(Hs(ii),L(ii),beta(ii),h(ii),d(ii),Rc(ii),alpha,hr,Br);
    if Hs(ii) > 5
        qcr = 0.010;
    elseif Hs(ii) < 5
        qcr = 0.020;
    end
    end

    % transmission
    if modes(10) == 1
    Ht = Transmission(h(ii),d(ii),h_wet(ii),Rc(ii),Hs(ii));
    end

    % limit-state functions
    if modes(1) == 1
    R1(ii) = mu(ii)*(W(ii)-U);
    S1(ii) = Pwc;
    Z1(ii) = R1(ii) - S1(ii);               % shoreward sliding
    if Z1(ii) < 0
        nfail_1(ii) = 1;
    end
    end

    if modes(2) == 1
    R2(ii) = mu(ii)*(W(ii)-U);
    S2(ii) = Pwt;
    Z2(ii) = R2(ii) - S2(ii);               % seaward sliding
    if Z2(ii) < 0
        nfail_2(ii) = 1;
```

```
76      end
77      end
78
79      if modes(3) == 1
80      R3(ii) = (W(ii)*t-Mu);
81      S3(ii) = Mp;
82      Z3(ii) = R3(ii) - S3(ii);              % shoreward overturning
83      if Z3(ii) < 0
84          nfail_3(ii) = 1;
85      end
86      end
87
88      if modes(4) == 1
89      R4(ii) = (W(ii)*t-Mu);
90      S4(ii) = Mwt;
91      Z4(ii) = R4(ii) - S4(ii);              % seaward overturning
92      if Z4(ii) < 0
93          nfail_4(ii) = 1;
94      end
95      end
96
97      if modes(5) == 1
98      R5(ii) = pbc;
99      S5(ii) = pe;
100     Z5(ii) = R5(ii) - S5(ii);              % bearing failure
101     if Z5(ii) < 0
102         nfail_5(ii) = 1;
103     end
104     end
105
106     if modes(6) == 1
107     R6(ii) = t_toe;
108     S6(ii) = t_cr;
109     Z6(ii) = R6(ii) - S6(ii);              % toe instability
110     if Z6(ii) < 0
111         nfail_6(ii) = 1;
112     end
113     end
114
115     if modes(7) == 1
116     R7(ii) = M_berm;
117     S7(ii) = M_berm_cr;
118     Z7(ii) = R7(ii) - S7(ii);              % berm instability
119     if Z7(ii) < 0
120         nfail_7(ii) = 1;
121     end
122     end
123
124     if modes(8) == 1
125     R8(ii) = u_cr;
126     S8(ii) = u_r;
127     Z8(ii) = R8(ii) - S8(ii);              % bottom scour
128     if Z8(ii) < 0
129         nfail_8(ii) = 1;
130     end
```

```
    end

    if modes(9) == 1
    R9(ii) = qcr;
    S9(ii) = q;
    Z9(ii) = R9(ii) - S9(ii);               % overtopping
    if Z9(ii) < 0
        nfail_9(ii) = 1;
    end
    end

    if modes(10) == 1
    R10(ii) = Hcr;
    S10(ii) = Ht;
    Z10(ii) = R10(ii) - S10(ii);            % transmission
    if Z10(ii) < 0
        nfail_10(ii) = 1;
    end
    end

    % limit states combined probabilities
    % count failures together
    if Z1(ii)<0 || Z2(ii)<0 || Z3(ii)<0 || Z4(ii)<0 || Z5(ii)<0 % total destruction
        nfail_ULS(ii) = 1;
    end
    if Z6(ii)<0 || Z7(ii) <0 || Z8(ii)<0 % scour & armor instability
        nfail_RLS(ii) = 1;
    end
    if Z9(ii)<0 || Z10(ii) <0 % port agitation
        nfail_SLS(ii) = 1;
    end
end

%% Probability calculation
% probability per limit state per year
Pf_ULS_1yr = sum(nfail_ULS)/nyr;
Pf_RLS_1yr = sum(nfail_RLS)/nyr;
Pf_SLS_1yr = sum(nfail_SLS)/nyr;

% over lifetime
Pf_ULS_life(ii) = 1-nchoosek(Lifetime,0)*(1-Pf_ULS_1yr)^Lifetime;
Pf_RLS_life(ii) = 1-nchoosek(Lifetime,0)*(1-Pf_RLS_1yr)^Lifetime;
Pf_SLS_life(ii) = 1-nchoosek(Lifetime,0)*(1-Pf_SLS_1yr)^Lifetime;
```

E.2. MC_Hmax

```
function [Hmax] = MC_Hmax(hb,Hs,H0,L0,slope)
hb = hb + 5.*Hs.*slope;      % still water depth at 5Hs from breakwater [m]
theta = atan(slope);
hL0ratio = hb/L0;

beta0star = 0.052*(H0/L0)^-0.38 * exp(20*tan(theta)^1.5);
beta1star = 0.63*exp(3.8*tan(theta));
betamaxstar = max(1.65,0.53*(H0/L0)^-0.29 * exp(2.4*tan(theta)));
```

```

if hL0ratio < 0.2
    Hmax = max([min([(beta0star*H0 + beta1star*hb),betamaxstar*H0,1.8*Hs]),Hs]);
else
    Hmax = 1.8*Hs;
end

end
```

E.3. MC_Weight

```
function [M,W] = MC_Weight(h_caisson,B_caisson,B_bslab,h_crown,h_water,rho_c,rho_s)
g = 9.81;
rho_w = 1030; % density of seawater [kg/m3]

%% dimensions
N_compart = 6;
B_compart = 4.6;
h_compart = h_caisson - 2*0.7;

% bottom slab
h_bslab = 1.5;

% crown
h_cslab = 2;
h_cwall = h_cslab - h_crown;
B_cwall = 1.8*2;

%% Weight
M = rho_c*(h_caisson*B_caisson-N_compart*B_compart*h_compart + 2*B_bslab*h_bslab + h_cslab*B_caisson + h_cwall*B_cwall) + rho_s*(N_compart*B_compart*h_compart) - rho_w*(h_water*B_caisson + 2*B_bslab*h_bslab);
W = M*g;
end
```

E.4. MC_GodaPressure

```
function [Fh,Fu,Mh,Mu,WB] = MC_GodaPressure(Hmax,L,h,beta,rho_w,Rc,h_wet,d,Bberm,B_caisson,slope)
g = 9.81;
k = 2*pi/L;

% reliability factors
N = max(normrnd(2500,500),1000); % number of waves in a storm
rN = sqrt(log(1/N)/log(0.004));
rFh = rN*max(normrnd(0.90,0.25),0.1); % Goda horizontal force reliability factor
rMh = rN*max(normrnd(0.81,0.40),0.1); % Goda horizontal moment reliability factor
rFb = rN*max(normrnd(0.77,0.25),0.1); % Goda vertical force reliability factor
rMb = rN*max(normrnd(0.72,0.37),0.1); % Goda vertical moment reliability factor

% Goda method
eta = 0.75*(1+cosd(beta))*Hmax;
hb = h + 5*Hmax*slope;
```

```
hcstar= min([eta,Rc]);

alpha1 = 0.6 + 1/2*(2*k*h/sinh(2*k*h))^2;
alpha2 = min([(hb - d)/(3*hb)*(Hmax/d)^2, 2*d/Hmax]);
alpha3 = 1 - h_wet*(1 - 1/cosh(k*h))/h;

delta11 = 0.93*(Bberm/L-0.12)+0.36*(0.4-d/h);
delta22 = -0.36*(Bberm/L-0.12)+0.93*(0.4-d/h);

if delta11 > 0
    delta1 = 15*delta11;
else
    delta1 = 20*delta11;
end

if delta22 > 0
    delta2 = 3*delta22;
else
    delta2 = 4.9*delta22;
end

if delta2 > 0
    alphaIB = 1/(cosh(delta1)*sqrt(cosh(delta2)));
else
    alphaIB = cos(delta2)/cosh(delta1);
end

alphaIH = min(Hmax/d,2);
alphaI = alphaIH*alphaIB;
alphastar = max(alpha2,alphaI);
if alphaI > alpha2
    WB = 1;
else
    WB = 0;
end

p1 = 0.5*(1+cosd(beta))*(alpha1+alphastar*cosd(beta)^2)*rho_w*g*Hmax; % Tanimoto and
↪  Takahashi extension

p2 = alpha3*p1;
if eta > Rc
    p3 = p1*(1-Rc/eta);
else
    p3 = 0;
end
pu = 1/2*(1+cosd(beta))*alpha1*alpha3*rho_w*g*Hmax;

Fh = rFh*(1/2*(p1+p2)*h_wet + 1/2*(p1+p3)*hcstar);
Fu = rFb*(1/2*pu*(B_caisson));

Mh = rMh*(1/6*(2*p1+p2)*h_wet^2+1/2*(p1+p3)*h_wet*hcstar+1/6*(p1+2*p3)*hcstar^2);
Mu = rMb*2/3*Fu*(B_caisson);
end
```

E.5. MC_WaveTroughPressure

This function depends on two *.mat* files which contain a digitized version of figures 4.9 and 4.10 of *Random Seas and Design of Maritime Structures* by Prof. Goda[27].

```
function [Pe,Mwt] = MC_WaveTroughPressure(h_wet,Hs,L,rho_w)

% reliability factors
N = max(normrnd(2500,500),1000); % number of waves in a storm
rN = sqrt(log(1/N)/log(0.004));
rFh = rN*max(normrnd(0.90,0.25),0.1); % Goda horizontal force reliability factor
rMh = rN*max(normrnd(0.81,0.40),0.1); % Goda horizontal moment reliability factor

pe_data = load('wavetroughpressures.mat');
arm_data = load('WaveTroughArm.mat');

hLratiovalues1 = [0.05,0.07,0.10,0.14,0.2,0.3,0.4,0.5,0.6,0.8,1,2];

hLratio = h_wet/L;
HLratio = Hs/L;
[a,b] = min(abs(hLratio-hLratiovalues1));

hLratiovalues2 = [1,0.5,0.3,0.2,0.1];

[a2,b2] = min(abs(hLratio-hLratiovalues2));


if b == 1
    f = pe_data.f005;
elseif b == 2
    f = pe_data.f007;
elseif b == 3
    f = pe_data.f010;
elseif b == 4
    f = pe_data.f014;
elseif b == 5
    f = pe_data.f020;
elseif b == 6
    f = pe_data.f030;
elseif b == 7
    f = pe_data.f040;
elseif b == 8
    f = pe_data.f050;
elseif b == 9
    f = pe_data.f060;
elseif b == 10
    f = pe_data.f080;
elseif b == 11
    f = pe_data.f100;
elseif b == 12
    f = pe_data.f200;
end
Pe = rFh*f(HLratio)*Hs*h_wet*rho_w;

if b2 == 1
    f2 = arm_data.f1;
elseif b2 == 2
```

```
    f2 = arm_data.f05;
elseif b2 == 3
    f2 = arm_data.f03;
elseif b2 == 4
    f2 = arm_data.f02;
elseif b2 == 5
    f2 = arm_data.f01;
end
arm = h_wet*f2(HLratio);
Mwt = rMh*arm*f(HLratio)*Hs*h_wet*rho_w;

end
```

E.6. MC_BearingCapacity

```
function [pe] = MC_BearingCapacity(W,U,Mu,Mp,t,B)
We = (W-U);
Me = W*t-Mu-Mp;
te = Me/We;

if te < 1/3*B
    pe = (2/3)*(We/te);
elseif te > 1/3*B
    pe = (2*We/B)*(2-3*te/B);
end
end
```

E.7. MC_ToeProtection

This function depends on a *.mat* file which contains a digitized version of figure VI-5-53 of the *Coastal Engineering Manual*[23].

```
function [t_cr] = MC_ToeProtection(Hs,hb,hs,type)
ToeThicc = load('ToeProtecc.mat');

hbhs_ratio = hb/hs;

dim =   [2.5 1.5 0.8 6;
                3 2.5 1 15;
                4 2.5 1.2 25;
                5 2.5 1.2 25;
                5 2.5 1.4 37;
                5 2.5 1.6 42;
                5 2.5 1.8 48;
                5 2.5 2 53;
                5 2.5 2.2 58];

if type == 1 % trunk
tH_ratio = ToeThicc.f2(hbhs_ratio);
elseif type == 2 % head
tH_ratio = ToeThicc.f1(hbhs_ratio);
end

```

```
t_cr = 1.25*tH_ratio*Hs;
end
```

E.8. MC_BermProtection

```
function [M_berm_cr] = MC_BermProtection(Hs,L,beta,h_wet,Bberm,rho_r,rho_w,B_toe,m,n,CS)
Sr = rho_r/rho_w;
Hs = Hs/1.2;
alphaS = 0.45;

if CS == 1 % trunk
x = linspace(2*B_toe+m,Bberm,n);
for i = 1:length(x)
    kappa2(i) = max(alphaS*sind(beta)^2*cos(2*pi*x(i)/L*cosd(beta))^2,cosd(beta)^2*sin(2*pi*x(i)/L*cosd(beta))^
end
[kappa2,xp] = min(kappa2);
xdist = Bberm/n*xp;

% obliquely incident waves
kappa = (4*pi*h_wet/L)*kappa2;

Ns_berm = max(1.8,(1.3*((1-kappa)/(kappa^(1/3)))*h_wet/Hs + 1.8*exp(-1.5*(((1-kappa)^2/(kappa^(1/3)))*h_wet/Hs))));

elseif CS == 2 % head

if beta > 60
    tau = 2.5;
else
    tau = 1.4;
end

kappa3 = (4*pi*h_wet/L)*alphaS*tau^2;
Ns_berm = max(1.8,(1.3*((1-kappa3)/(kappa3^(1/3)))*h_wet/Hs + 1.8*exp(-1.5*(((1-kappa3)^2/(kappa3^(1/3)))*h_wet/Hs))));

end
% required armor mass of the breakwater
M_berm_cr = rho_r/(Ns_berm^3*(Sr-1)^3)*Hs^3;

clear Hs L beta h_wet Bberm rho_r rho_w L_toe n CS
end
```

E.9. MC_BedProtection

```
function [u_cr, u_r] = MC_BedProtection(h,dn50,H,Tp,Delta)
g = 9.81;
kr = 2*dn50;                % Nikuradse grain roughness

% waves onshore
c = sqrt(g*h);              % wave propagation speed [m/s]
```

```
L = c*Tp;                    % wave length [m]
k = (2*pi)/L;                % wave number [rad/m]
omega = (2*pi)/Tp;           % wave frequency [rad]
a = H/2;                     % wave amplitude

ab = a/(sinh(k*h));          % wave amplitude at bed
ub = omega*ab;               % wave velocity at bed

cf = min(0.237*(ab/kr)^(-0.52),0.3); % friction factor

u_r = sqrt((cf/2))*ub;      % wave-induced shear velocity at bed

% shields
Psi_c = normrnd(0.03,0.03*0.15);               % shields stability parameter
C = 18*log10(12*h/kr);
u_cr = sqrt(dn50*Psi_c*Delta*C^2);

end
```

E.10. MC_Overtopping

```
function [q] = MC_Overtopping(Hs,L,beta,h,d,Rc,alpha,hr,Br)
g = 9.81;
s = Hs/L;
gamma_beta = max([1-0.0062*beta,0.72]);
Hs = Hs*gamma_beta;

if Hs/h < 1/20
        % no influence of the foreshore, use eq 7.1
        q = normrnd(0.047,0.007)*exp(-(normrnd(2.35,0.23)*Rc/Hs)^1.3);
    else
        % foreshore influence present
        % intermediate or shallow water conditions
        if d/h > 0.6
            % Breakwater is of the vertical type
            if h^2/(Hs*L) < 0.23
                % breaking occurs
                if Rc/Hs < 1.35
                    % low freeboard, use eq 7.7
                    q = sqrt(g*Hs^3) * normrnd(0.011,0.0045)*(Hs/(h*s))^0.5 *
↪   exp(-2.2*Rc/Hs);
                else
                    % high freeboard, use eq 7.8
                    q = sqrt(g*Hs^3) * normrnd(0.0014,0.0006)*(Hs/(h*s))^0.5 *
↪   (Rc/Hs)^-3;
                end
            else
                % breaking does not occur, use eq 7.5
                q = sqrt(g*Hs^3) *
↪   normrnd(0.05,0.012)*exp(-normrnd(2.78,0.17)*Rc/(Hs));
            end
        else
            % Breakwater is of the composite type
            if h*d/(Hs*L) < 0.65
```

```
                % breaking occurs
                if Rc/Hs < 1.35
                    % low freeboard, use eq 7.15
                    q = sqrt(g*Hs^3) *
↪  1.3*(d/h)^0.5*normrnd(0.011,0.0045)*(Hs/(h*s))^0.5*exp(-2.2*Rc/Hs);
                else
                    % high freeboard, use eq 7.14
                     q = sqrt(g*Hs^3) *
↪  1.3*(d/h)^0.5*normrnd(0.0014,0.0006)*(Hs/(h*s))^0.5 * (Rc/Hs)^-3;
                end
            else
                % breaking does not occur, use eq 7.5
                q = sqrt(g*Hs^3) *
↪  normrnd(0.05,0.012)*exp(-normrnd(2.78,0.17)*Rc/(Hs));
            end
        end
end
q = max(q,0);

% bullnose
if alpha == 0 && hr == 0 && Br == 0
    kbn = 1;
elseif alpha < 90
    R0star = 0.25*hr/Br + 0.05*(1-hr/Rc);
    mstar = 0.98*sqrt(hr/Br) + 0.16*(1-hr/Rc);
    if Rc/Hs < R0star
        kbn = 1;
    elseif Rc/Hs < R0star + mstar
        kbn = 1-(0.8/mstar)*(Rc/Hs-R0star);
    elseif Rc/Hs > R0star + mstar
        kacc = 0.2-0.01*(Rc/Hs - R0star - mstar);
        if Rc/h < 0.6
            kbn = kacc;
        elseif Rc/Hs < 1.1
            kbn = 27*kacc*exp(-5.5*Rc/h);
        elseif Rc/h > 1.1
            kbn = kacc*0.02;
        end
    end
else
    kbn = 1.1;
end

kbn = max(kbn,0.05);

q = q*kbn;

end
```

E.11. MC_Transmission

```
function [Ht] = MC_Transmission(h,d,h_wet,Rc,Hs)
% Heijn
alpha = 0.35;
```

```
n = 2;
Heijnk = load('Heijn k.mat');
Rcd = Rc/d;
k = Heijnk.fitresult(Rcd);


Kt = sqrt((alpha*exp(-1/k*Rc/Hs)^n)^2 + (0.15*(1-h_wet/h))^2);

Kt = normrnd(Kt,0.015);

Ht = Hs*Kt;
end
```

F

Preliminary Monte-Carlo runs

Several design decisions were made for the design proposal given in Chapter 6. These decisions were based on the results of dozens of Monte-Carlo simulations for various designs. In this Appendix, a few of the design decisions and the associated Monte-Carlo simulations are highlighted to show the effect and the reason why these decisions were made. Obviously, this includes only a small subset of all the simulations that have been ran. All simulations shown here were run with data generated by the vine-copula model.

F.1. Bullnose

The following results show the influence the addition of the bullnose on the overtopping discharge. With the bullnose, a freeboard of 9 meters relative to the still water level sufficed the design criteria. Figure F.1 show the results of the same breakwater design without the bullnose:

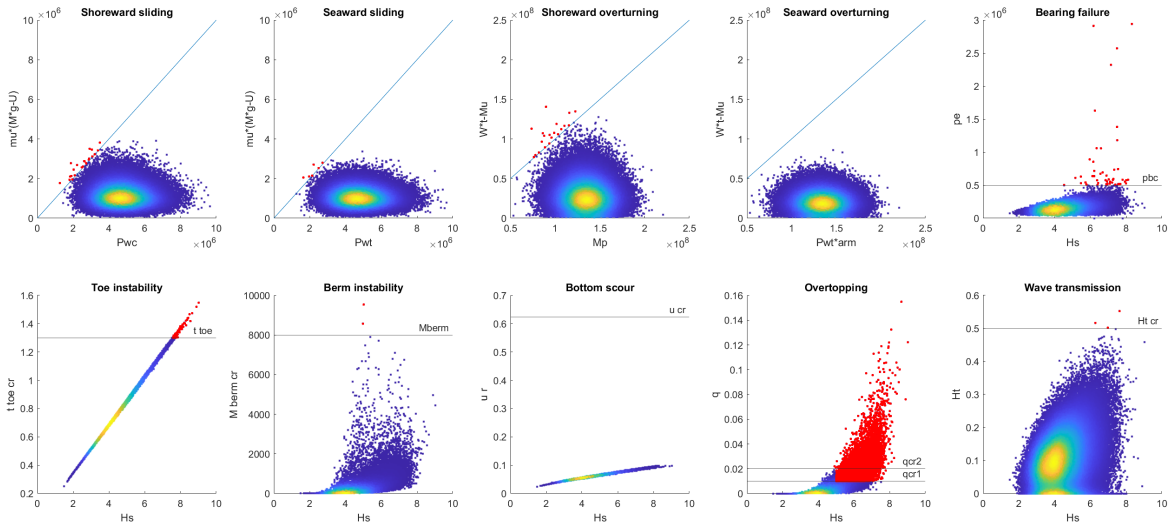

Figure F.1: Scatterplots of all 10 failure modes for the same breakwater design as proposed in figure 6.4, but without the bullnose.

Failure due to excessive overtopping discharge occurred 35 times as often without the bullnose, resulting in a probability of failure over the structure's lifetime of ~100%. So, without a bullnose, a higher freeboard is needed. Figures F.2 and F.3 show the results of freeboards of 10 meters and 11 meters respectively. Only with 11 meters, 2 meters more than with the bullnose, does the breakwater fulfill the design criteria for overtopping. Even though the bullnose is a small addition, it has a large impact on the performance of the breakwater. A bullnose is a feature than can greatly save construction material and reduce the structure dimensions. However, the addition of the bullnose introduces a new failure mode

Failure mode	Number of failures	$P_{f,yr}$	$P_{f,L}$
Shoreward sliding	23	0.09%	4.5%
Seaward sliding	6	0.02%	1.19%
Shoreward overturning	20	0.08%	3.92%
Seaward overturning	0	0%	0%
Bearing failure	49	0.2%	9.34%
Toe instability	130	0.52%	22.95%
Berm instability	2	0.01%	0.4%
Bottom scour	0	0%	0%
Wave overtopping	11406	45.62%	100%
Wave transmission	3	0.01%	0.6%
Limit-state			
ULS	79	0.32%	14.64%
RLS	132	0.53%	23.26%
SLS	11406	45.62%	100%

Table F.1: Results of 150.000 Monte-Carlo runs for no bullnose.

to the structure which was not considered in the design: the emergence of cracking in the bullnose structure. It is possible the wave-induced pressure distribution changes as a result of the bullnose. Wave making contact with the bullnose may induce forces significant enough to damage the crest of the structure, resulting in failure. The severity of this effect has not been analyzed.

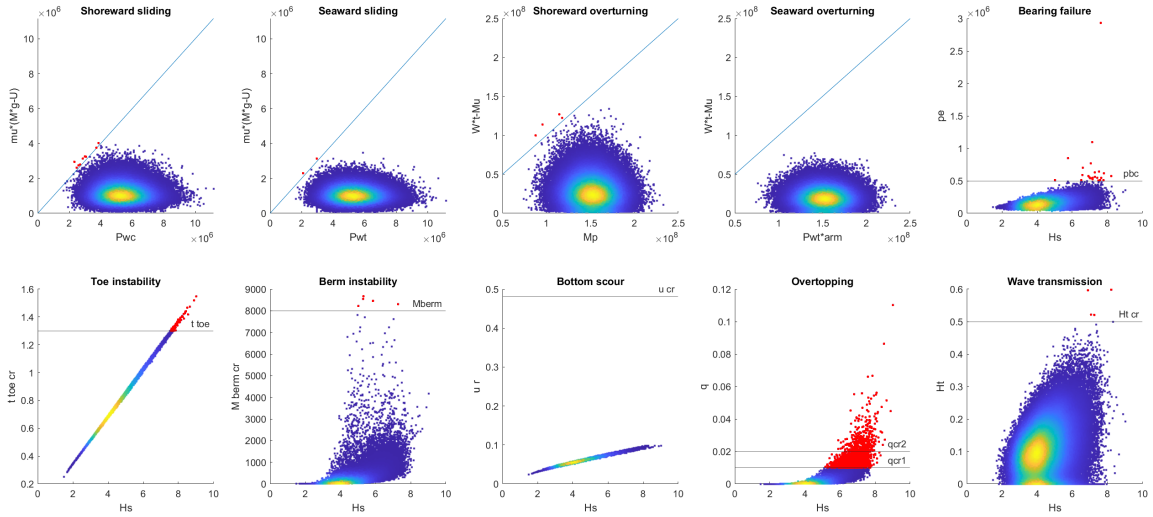

Figure F.2: Results for no bullnose and a freeboard of 10 meters.

Failure mode	Number of failures	$P_{f,yr}$	$P_{f,L}$
Shoreward sliding	9	0.04%	1.78%
Seaward sliding	2	0.01%	0.4%
Shoreward overturning	4	0.02%	0.8%
Seaward overturning	0	0%	0%
Bearing failure	24	0.1%	4.69%
Toe instability	130	0.52%	22.95%
Berm instability	5	0.02%	1%
Bottom scour	0	0%	0%
Wave overtopping	2239	8.96%	99.08%
Wave transmission	4	0.02%	0.8%
Limit-state			
ULS	33	0.13%	6.39%
RLS	135	0.54%	23.72%
SLS	2240	8.96%	99.08%

Table F.2: Results of 150.000 Monte-Carlo runs for no bullnose and +1 meter of freeboard.

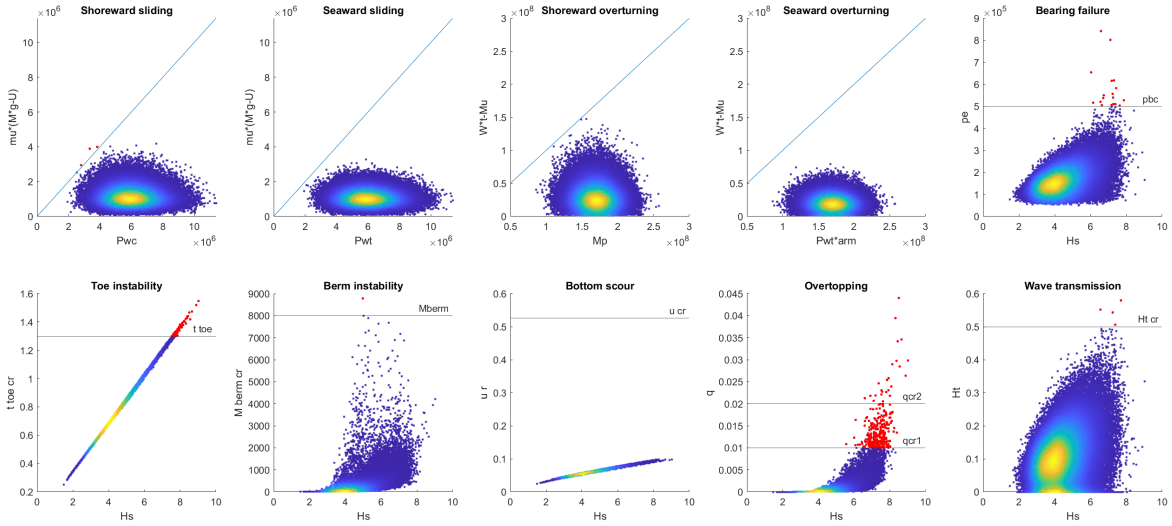

Figure F.3: Results for no bullnose and a freeboard of 11 meters.

Failure mode	Number of failures	$P_{f,yr}$	$P_{f,L}$
Shoreward sliding	3	0.01%	0.6%
Seaward sliding	0	0%	0%
Shoreward overturning	0	0%	0%
Seaward overturning	0	0%	0%
Bearing failure	18	0.07%	3.54%
Toe instability	130	0.52%	22.95%
Berm instability	1	0%	0.2%
Bottom scour	0	0%	0%
Wave overtopping	285	1.14%	43.63%
Wave transmission	4	0.02%	0.8%
Limit-state			
ULS	21	0.08%	4.11%
RLS	131	0.52%	23.1%
SLS	289	1.16%	44.09%

Table F.3: Results of 150.000 Monte-Carlo runs for no bullnose and +2 meters of freeboard.

F.2. Bottom slab

The bottom slab was a necessary addition for increasing the width of the structure while keeping its weight at a minimum. This helped prevent bearing failure, which was one of the most critical failures for the ULS condition. The bottom slab added 3 meters of width to either side of the breakwater, bringing the total width to 36 meters. The greater width allows the weight of the caisson to be spread over a larger area, lowering the maximum bearing pressure. Figures F.5, F.5 and F.5 show the result of the Monte-Carlo simulation for a bottom slab adding a width to either side of 2.5 meters and 2 meters respectively.

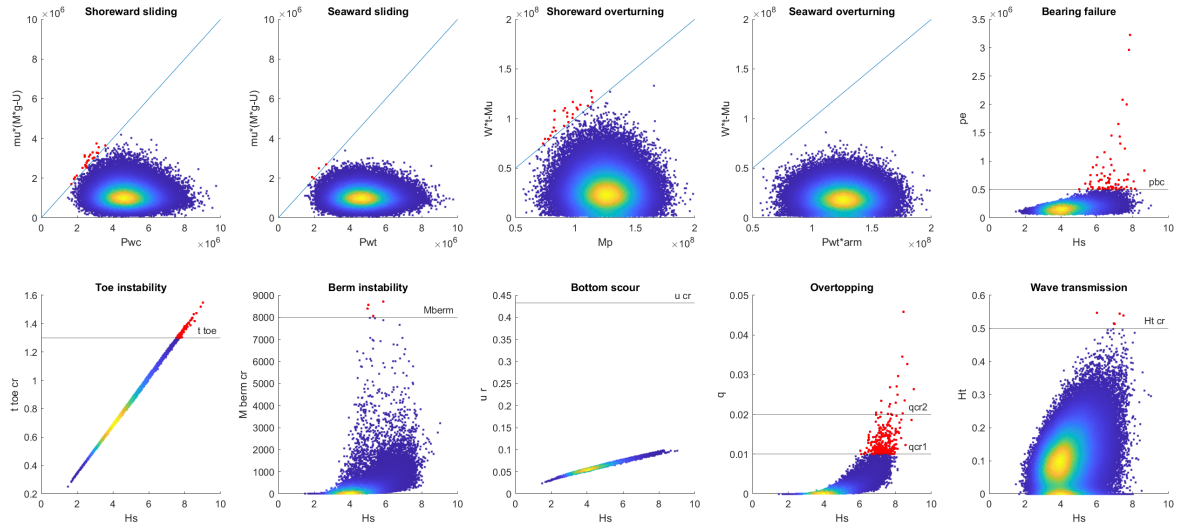

Figure F.4: Results for a bottom slab adding 2.5 meters width.

Failure mode	Number of failures	$P_{f,yr}$	$P_{f,L}$
Shoreward sliding	24	0.1%	4.69%
Seaward sliding	4	0.02%	0.8%
Shoreward overturning	27	0.11%	5.26%
Seaward overturning	0	0%	0%
Bearing failure	75	0.3%	13.95%
Toe instability	130	0.52%	22.95%
Berm instability	4	0.02%	0.8%
Bottom scour	0	0%	0%
Wave overtopping	295	1.18%	44.76%
Wave transmission	5	0.02%	1%
Limit-state			
ULS	101	0.4%	18.32%
RLS	134	0.54%	23.56%
SLS	299	1.2%	45.21%

Table F.4: Results of 150.000 Monte-Carlo runs for a bottom slab adding 2.5 meters width.

As can be seen, decreasing the width of the bottom slab has a large effect on the amount of occurrences of bearing failure. However, the extended width of the bottom slab does allow the possibility for a new failure mode which wasn't considered in design: cracks in the concrete slab as a result of wave-induced loading. It is possible a part of the relatively thin bottom slab breaks up, negating the additional width it is supposed to bring. An alternative way is to increase the width of the entire caisson, but this also increases the weight of the structure and does therefore not necessarily help against bearing failure.

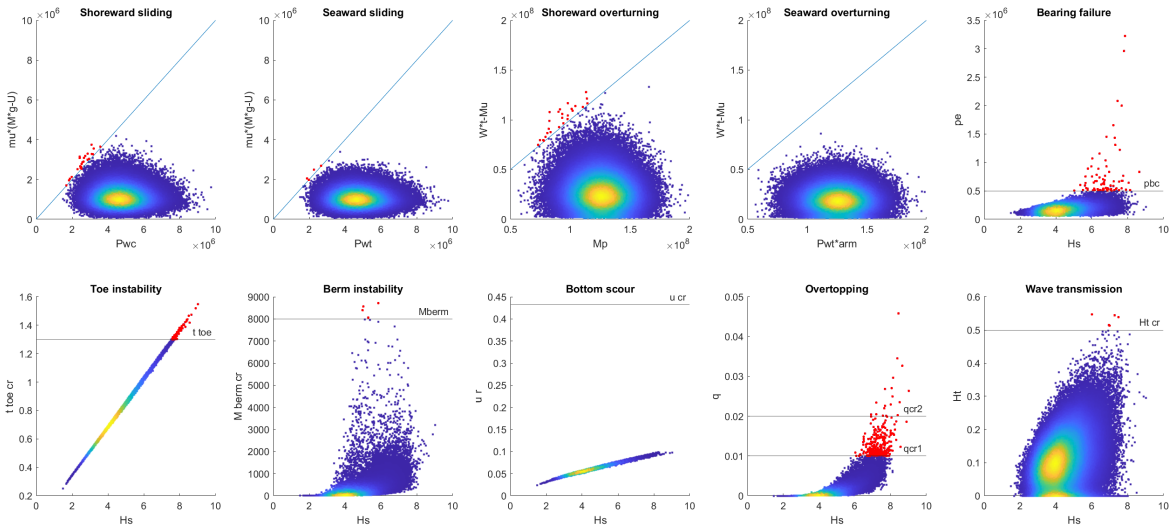

Figure F.5: Results for a bottom slab adding 2 meters width.

Failure mode	**Number of failures**	**$P_{f,yr}$**	**$P_{f,L}$**
Shoreward sliding	31	0.12%	6.02%
Seaward sliding	7	0.03%	1.39%
Shoreward overturning	75	0.3%	13.95%
Seaward overturning	0	0%	0%
Bearing failure	235	0.94%	37.64%
Toe instability	130	0.52%	22.95%
Berm instability	5	0.02%	1%
Bottom scour	0	0%	0%
Wave overtopping	299	1.2%	45.21%
Wave transmission	4	0.02%	0.8%
Limit-state			
ULS	279	1.12%	42.94%
RLS	135	0.54%	23.72%
SLS	301	1.2%	45.43%

Table F.5: Results of 150.000 Monte-Carlo runs for a bottom slab adding 2 meters width.

F.3. Rubble mound height

The proposed design in Chapter 6 had a rubble mound height of 8 meters. The purpose of the rubble mound foundation is to spread the weight of the structure over the seabed. A higher rubble mound means the caisson itself can be shorter. This reduces the weight of the caisson at the cost of a heavier foundation, reducing the cases of bearing failure. Yet decrease of the weight of the caisson is a double-edged sword, as a lighter caisson also suffers more from cases of sliding and overturning. Figures F.6 and F.7 show the results for rubble mound of 10 meters and 12 meters high respectively. The height of the caisson was reduced accordingly, keeping the freeboard the same in all cases. The occurrences of toe instability increased the most. This is not very alarming, however, as it can be counteracted by simply increasing the width of the toe protection. Nonetheless, the amount of cases of sliding and overturning have increased substantially. This is because a lighter caisson is easier to move, and is therefore more susceptible to these failure modes.

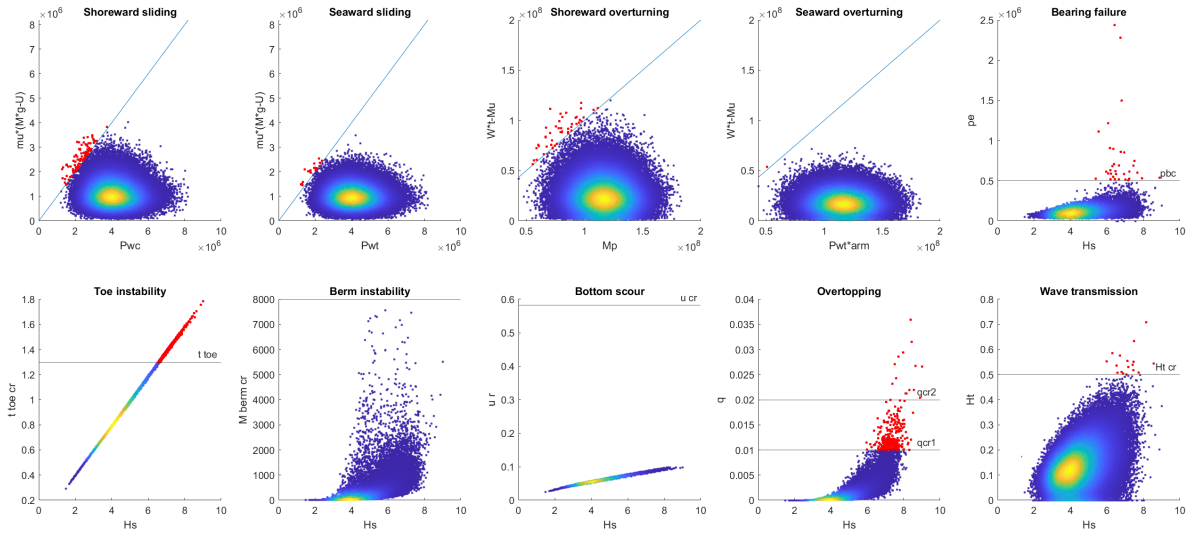

Figure F.6: Results for a rubble mound of 10 meters high.

Failure mode	Number of failures	$P_{f,yr}$	$P_{f,L}$
Shoreward sliding	95	0.38%	17.33%
Seaward sliding	19	0.08%	3.73%
Shoreward overturning	46	0.18%	8.8%
Seaward overturning	1	0%	0.2%
Bearing failure	33	0.13%	6.39%
Toe instability	3135	12.54%	99.88%
Berm instability	0	0%	0%
Bottom scour	0	0%	0%
Wave overtopping	301	1.2%	45.43%
Wave transmission	17	0.07%	3.34%
Limit-state			
ULS	159	0.64%	27.31%
RLS	3135	12.54%	99.88%
SLS	316	1.26%	47.06%

Table F.6: Results of 150.000 Monte-Carlo runs for a rubble mound of 10 meters high.

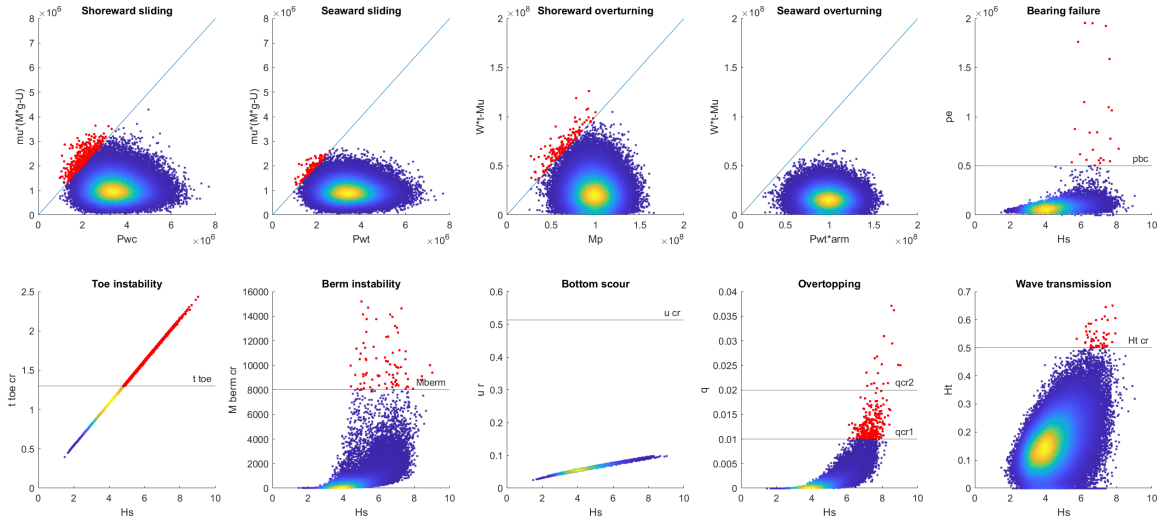

Figure F.7: Results for a rubble mound of 12 meters high.

Failure mode	Number of failures	$P_{f,yr}$	$P_{f,L}$
Shoreward sliding	403	1.61%	55.63%
Seaward sliding	92	0.37%	16.83%
Shoreward overturning	161	0.64%	27.61%
Seaward overturning	0	0%	0%
Bearing failure	23	0.09%	4.5%
Toe instability	41775	167.1%	100%
Berm instability	83	0.33%	15.32%
Bottom scour	0	0%	0%
Wave overtopping	288	1.15%	43.97%
Wave transmission	51	0.2%	9.71%
Limit-state			
ULS	584	2.34%	69.33%
RLS	41780	100%	100%
SLS	332	1.33%	48.75%

Table F.7: Results of 150.000 Monte-Carlo runs for a rubble mound of 12 meters high.

F.4. Concrete crown

The concrete crown is a large prefabricated concrete slab with a wall on one side. The purpose of this structure is to decrease the weight of the caisson while keeping the freeboard the same. A heavy caisson suffers more from bearing failure. Figure F.8 shows the results of the Monte-Carlo simulation for a breakwater with no concrete crown. This breakwater has the same freeboard and a bullnose as the design proposed in Chapter 6. As can be seen, greater weight of the structure means it is more resistant to sliding and overturning. Yet bearing failure has increased substantially, making the reduction in weight a necessity.

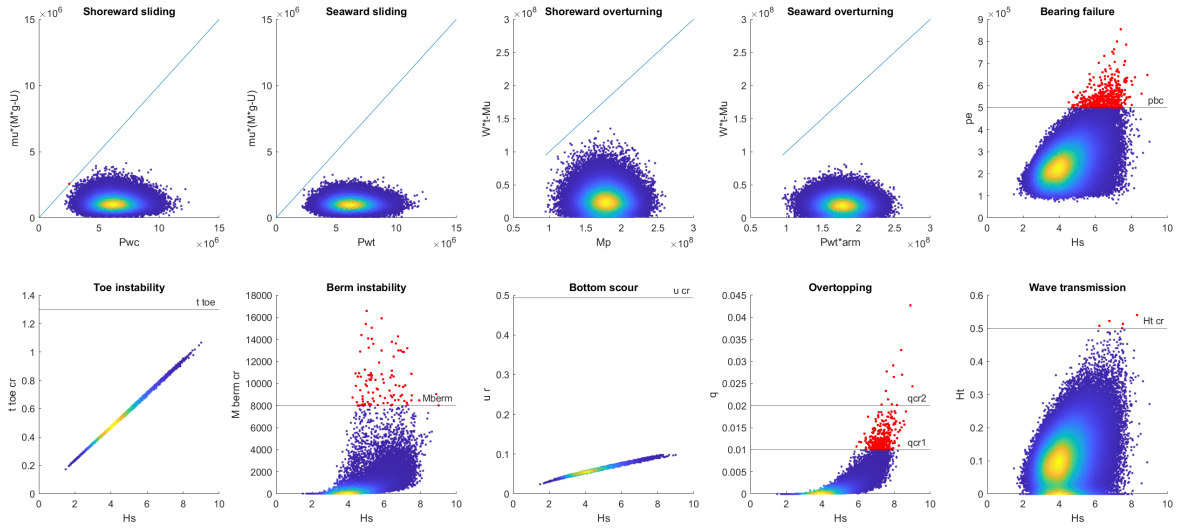

Figure F.8: Results for no concrete crown.

Failure mode	Number of failures	$P_{f,yr}$	$P_{f,L}$
Shoreward sliding	1	0%	0.2%
Seaward sliding	0	0%	0%
Shoreward overturning	0	0%	0%
Seaward overturning	0	0%	0%
Bearing failure	483	1.93%	62.3%
Toe instability	0	0%	0%
Berm instability	95	0.38%	17.33%
Bottom scour	0	0%	0%
Wave overtopping	306	1.22%	45.98%
Wave transmission	5	0.02%	1%
Limit-state			
ULS	484	1.94%	62.37%
RLS	95	0.38%	17.33%
SLS	310	1.24%	46.41%

Table F.8: Results of 150.000 Monte-Carlo runs for no concrete crown.